U-Pb, O and Lu-Hf isotope ratios of detrital zircon from Ghana, West-African Craton – Formation of juvenile, Palaeoproterozoic crust

Bára Dröfn Kristinsdóttir

Dissertations in Geology at Lund University,
Master's thesis, no 374
(45 hp/ECTS credits)

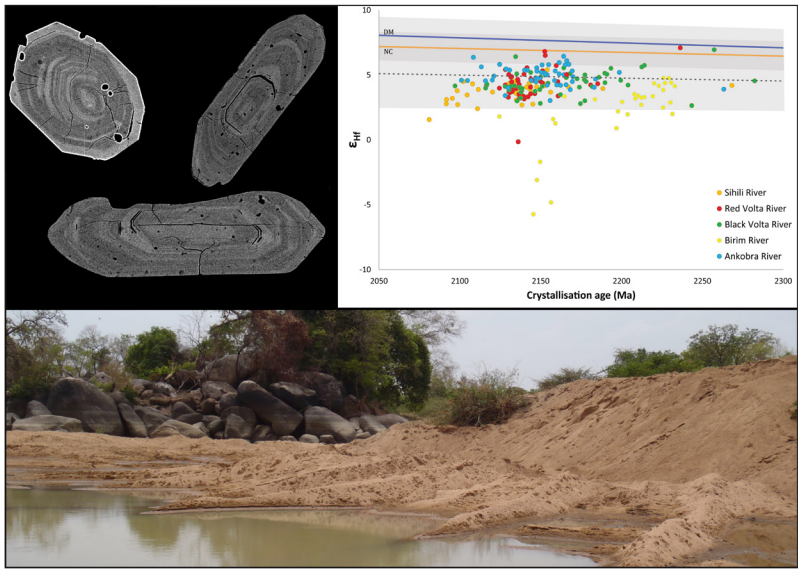

Department of Geology
Lund University
2013

U-Pb, O and Lu-Hf isotope ratios of detrital zircon from Ghana, West African Craton - Formation of juvenile Palaeoproterozoic crust

Master's thesis

Bára Dröfn Kristinsdóttir

Department of Geology
Lund University

2013

Contents

Cover Picture: Sihili river (Anders Scherstén), BSE images of detrital zircon and diagram describing the relationship between ε_{Hf} and crystallisation ages of the detrital zircon.

U-Pb, O and Lu-Hf isotope ratios of detrital zircon from Ghana, West African Craton - Formation of juvenile Palaeoproterozoic crust

BÁRA DRÖFN KRISTINSDÓTTIR

Kristinsdóttir, B.D., 2013: U-Pb, O and Lu-Hf isotope ratios of detrital zircon from Ghana, West African Craton - Formation of juvenile Palaeoproterozoic crust. *Dissertations in Geology at Lunds University*, No. 374, 54 pp. 45 hp (45 ECTS credits).

Abstract: Detrital zircon were sampled from five rivers in Ghana and they were analysed *in situ* for U-Th-Pb, O and Lu-Hf isotopes. Based on the analyses, their U-Pb crystallisation ages, $\delta^{18}O$ isotope ratio, ε_{Hf} and Hf-model ages were determined. This provides information about the origin and crustal evolution of the Palaeoproterozoic bedrock in Ghana. The U-Pb crystallisation ages of the zircon mainly range from 2.2-2.1 Ga, with an older zircon subset of ~2.22 Ga making up a large fraction of the Birim river sample (southeastern Ghana). These ages coincide with previously reported ages of volcanic and plutonic rocks in Ghana. Majority of the zircon have positive ε_{Hf} (0.9 -7.1) and relatively short residence time, indicating that they crystallised from juvenile magmas. Four zircon from the Birim river sample, that crystallised at ~2.15 Ga, do however have negative ε_{Hf} and Archean model ages, suggesting substantial contribution from an Archean crust. Oxygen isotope ratios indicate that influences from reworked supracrustal rocks were minor during the initial stages of magmatic activity, with zircon having $\delta^{18}O>6.5$ being rare before ~2.17 Ga. A correlation is observed between younger crystallisation ages and increased proportion of zircon with elevated $\delta^{18}O$, which might point towards a maturing arc system. Modelling based on ε_{Hf} and $\delta^{18}O$ of the zircon indicates that the contribution from an Archean crust to the magmas was generally less than 10%. Several zircon, particularly from the Ankobra river population, have elevated $\delta^{18}O$ and juvenile ε_{Hf}, indicating rapid reworking of juvenile crust.

Oxygen isotope ratios, crystallisation and Hf-model ages of detrital zircon have been used to evaluate the degree of addition of juvenile material to the crust and to model crustal growth throughout the geological record. Hf -model ages of the zircon that are reported here fall within a period when reworking of crust exceeds additions of new crust, as indicated by the detrital zircon record. This does not agree with the juvenile nature of the Birimian crust. Adding the data reported here to a dataset that was used for a previously established crustal growth model, has limited effect on the shape of the crustal growth curve, but suggests that the extent of reworking and recycling might be slightly overestimated in the Proterozoic.

Keywords: Detrital zircon, Ghana, West African Craton, Hf-Model ages, Crustal growth.

Supervisor: Anders Scherstén

Bára Dröfn Kristinsdóttir, Department of Geology, Lund University, Sölvegatan 12, SE-223 62 Lund, Sweden. E-mail: barakristins@gmail.com

U-Pb, O och Lu-Hf isotopförhållanden i detrital zirkon från Ghana, Västafrikanska kratonen - bildande av ny paleoproterozoisk skorpa

BÁRA DRÖFN KRISTINSDÓTTIR

Kristinsdóttir, B.D., 2013: U-Pb, O och Lu-Hf isotopförhållanden i detrital zirkon från Ghana, Västafrikanska kartonen - bildande av ny paleoproterozoisk skorpa. *Examensarbeten i geologi vid Lunds universitet*, Nr. 374, 54 sid. 45 hp.

Sammanfattning: Detrital zirkon provtogs från fem floder i Ghana och U-Th-Pb, O och Lu-Hf isotoper analyserades *in situ*. Utifrån analyserna beräknades U-Pb kristallisationsåldrar, $\delta^{18}O$, εHf och Hf-modellåldrar, vilket ger information om ursprung och utveckling av den paleoproterozoiska berggrunden i Ghana. Zirkon U-Pb kristallisationsåldrar varierar huvudsakligen mellan 2,2 och 2,1 Ga, med en äldre delmängd av ~2,22 Ga zirkon som utgör en stor del av det prov som togs i Birimfloden (sydöstra Ghana). Åldrarna sammanfaller med tidigare rapporterade åldrar för vulkaniska och djupbergarter i Ghana. Majoriteten av zirkonerna har positiva εHf (0,9-7,1) och relativt kort krustal residenstid, vilket indikerar att de kristalliserade från juvenila magmor. Fyra zirkoner från Birimfloden med åldrar kring ~2,15 Ga, har dock negativa εHf och Arkeiska modellåldrar, vilket tyder på ett betydande bidrag från en Arkeisk skorpa. Syreisotopförhållanden indikerar att inblanding av suprakrustala bergarter var mindre under de inledande skedena av magmatismen, och inga zirkoner med $\delta^{18}O > 6.5$ förekommer innan ~2.17 Ga. Yngre kristallisationsåldrar korrelerar med ökad andel av zirkon med förhöjd $\delta^{18}O$, vilket kan peka mot ett mognande öbågesystem. Modellering baserad på εHf och $\delta^{18}O$ av zirkon indikerar att bidraget från en Arkeisk skorpa var generellt mindre än 10%. Flera zirkoner, särskilt från Ankobrafloden, har förhöjda $\delta^{18}O$ och juvenil ε_{Hf}, vilket indikerar snabb omarbetning av en juvenil sedimentär skorpa.

Syreisotopförhållanden, kristallisations- och Hf-modellåldrarna för detritala zirkoner har använts för att utvärdera graden av juvenilt material till jordskorpan och att modellera jordskorpans globala tillväxt över geologisk tid. Hf-modellåldrar av zirkon som redovisas här kristalliserade under en period som dominerats av omarbetning av skorpa, såsom indikeras av den globala detritala zirkondatabasen. Detta är i motsats till Birimianskorpans juvenila karaktär. De nya data som rapporteras här har lagts till ett globalt dataset som användes för att etablera en tillväxtmodell för kontinentalskorpan. Effekten på jordskorpans tillväxtkurva är begränsad, men tyder på att omfattningen av omarbetning av kontinentalskorpan tidigare verskattas något för Proterozoikum.

Nyckelord: Detrital zirkon, Ghana, Västafrikanska kratonen, Hf-Model åldrar, jordskorpans tillväxt.

Bára Dröfn Kristinsdóttir, Geologiska institutionen, Lunds universitet, Sölvegatan 12, 223 62 Lund, Sverige. E-post: barakristins@gmail.com

1 Introduction

The continental crust is a database that stores the longest rock record of the Earth's crustal and tectonic evolution. Ability to decode these records provides an opportunity to obtain insight into the early Earth processes. Continental crustal growth has been of interest to scientists for several decades. The geochemical signature of the continental crust indicates that subduction zone magmatism is an important site of juvenile continental crust addition (i.e. formation; Hawkesworth & Kemp 2006), and begs the question how long subduction processes have been operating on the Earth. Growth of the continental crust will occur when the preservation of the juvenile crust formation exceeds the mass lost by recycling to the mantle (Table 1). Estimates of mass fluxes (i.e. crust generation and crust recycling) at modern subduction zones indicate that similar amount of crustal material is recycled into the mantle every year as is generated (Scholl & von Huene 2009). Based on these values, modern day conditions at subduction zones cannot easily explain the growth of the continental crust throughout the history of the Earth and the volume of continental crust observed today.

Global compilations of zircon U-Pb age data indicate that zircon crystallisation ages form fairly well defined peaks (e.g. Condie 1998; Campbell & Allen 2008; Hawkesworth et al. 2010). This apparent periodicity in crust formation has been correlated with crust accretion and supercontinent assembly (Campbell & Allen 2008). The trend might however not be due to periods of increased addition of material to the crust, associated with supercontinent amalgamation, but rather caused by variations in preservation of crust in altering tectonic settings (Hawkesworth et al. 2010). Furthermore, zircon crystallisation ages do not necessarily represent addition of material to the crust. They can indicate stabilization of the crust when less dense, intermediate to acidic rock is formed, since zircon commonly form in silica saturated magma and is therefore rarer in basaltic than acidic rocks. Zircon model ages describe when magma separated from the mantle and might therefore yield a better representation of continental crustal growth. However, when juvenile magma is mixed with ancient sediments or is formed through melting of a heterogeneous crust, it will have a mixed model age in accordance with the components that are involved (Arndt & Goldstein 1987).

Table 1. Definitions of common terms used in crustal growth

Term	Description
Crust generation	Addition of juvenile material to the crust
Crustal reworking	Internal remelting of continental crust within the continental crust
Crustal recycling	Return of continental crust back to the mantle (i.e. loss of crust) through e.g. subduction
Crustal growth	Crust formation > Crust recycling, which leads to increasing continental crust mass/volume

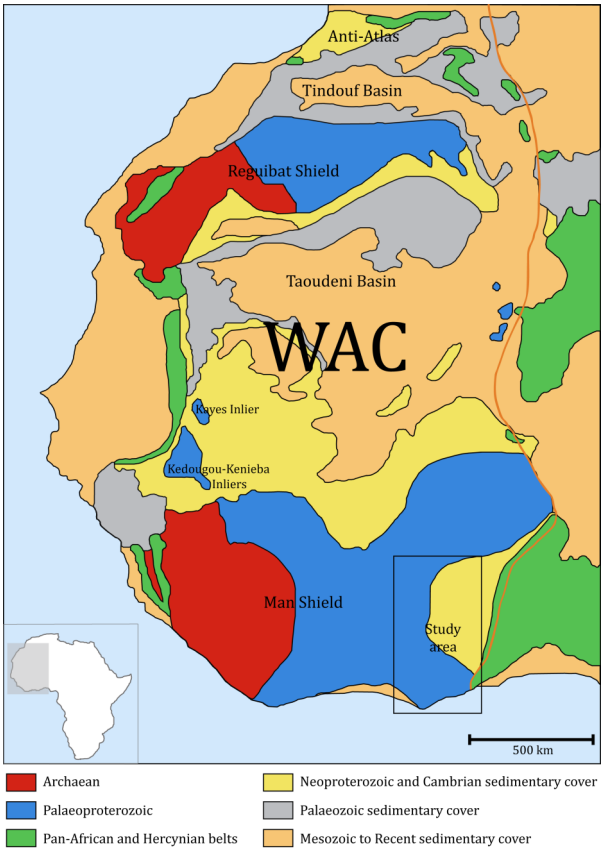

Fig. 1. Major geological units of the West African Craton (WAC). Orange line marks the eastern border of the craton as interpreted from geophysical data. Modified from Ennih & Liégeois (2008).

When linking zircon model ages to periods of crust formation, it is important to distinguish between zircon derived from magma that has preserved its mantle isotopic properties and those derived from magma formed from mixed sources. The Hf-model ages of the first group indicate additions of new magma to the crust, while the Hf-model age of the second group is based on an average value of different sources and is therefore supposedly not an indicator of periods of crustal growth. Zircon is able to preserve its original oxygen isotope composition under conditions such as high temperature metamorphism (Valley et al. 1994; Peck et al. 2003; Page et al. 2007), hence has its oxygen isotope composition been used to separate mantle-like zircon from zircon that crystallised from magma containing a reworked component (Kemp et al. 2006; Pietranik et al. 2008; Lancaster et al. 2011; Dhuime et al. 2012).

Several different models have been published describing continental crustal growth throughout the

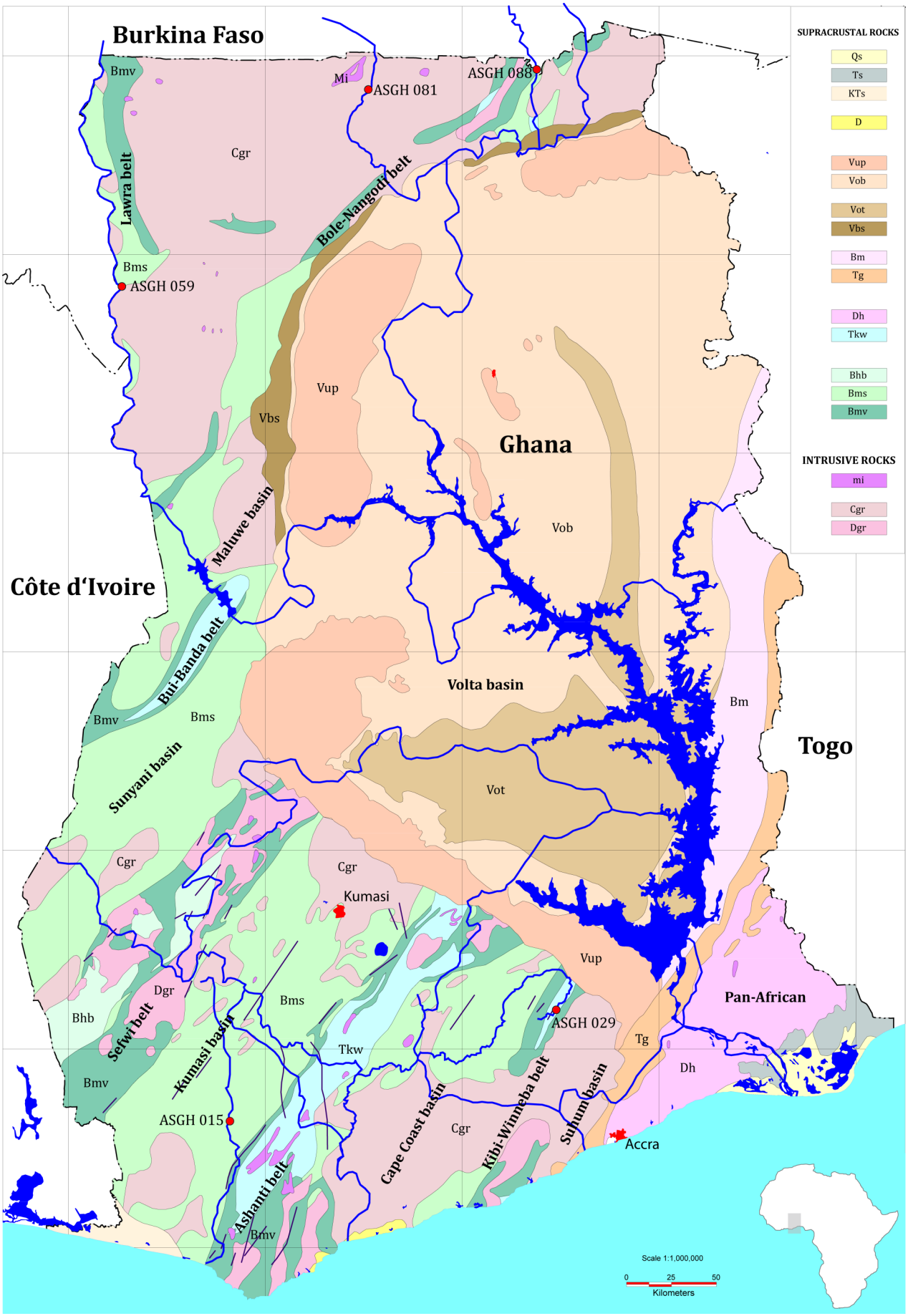
Burkina Faso
Ghana
Côte d'Ivoire
Togo
Bmv
Mi
ASGH 081
ASGH 088
Cgr
Lawra belt
Bole-Nangodi belt
Bms
ASGH 059
Vup
Vbs
Maluwe basin
Vob
Bui-Banda belt
Volta basin
Bm
Sunyani basin
Vot
Kumasi
Dgr
Sefwi belt
Bhb
Kumasi basin
Tkw
ASGH 029
Tg
Pan-African
Dh
Cape Coast basin
Kibi-Winneba belt
Suhum basin
Accra
ASGH 015
Ashanti belt
SUPRACRUSTAL ROCKS
Qs
Ts
KTs
D
Vup
Vob
Vot
Vbs
Bm
Tg
Dh
Tkw
Bhb
Bms
Bmv
INTRUSIVE ROCKS
mi
Cgr
Dgr
Scale 1:1,000,000
0
25
50
Kilometers

geological history. These vary from a fast growing continental crust in the Archaean (Fyfe 1978; Armstrong 1981; 1991) to a more stable crustal growth throughout the geological record (Reymer & Schubert 1984; Allégre & Rousseau 1984; Belousova et al. 2010). Combination of Hf-model ages and oxygen isotope ratios of detrital zircon indicates that additions of juvenile components to the crust were dominating during the Archaean, but at ~3.1 Ga the proportion of zircon with non mantle-like oxygen isotopic signature increased as compared to zircon that crystallised from magma with mantle-like signature (Dhuime et al. 2012). This indicates that reworking of crust became more prominent after ~3.1 Ga .

The Birimian bedrock of Ghana (~2.15 Ga) belongs to the West African Craton (Fig. 1) and is a part of an area that has been interpreted as being formed through voluminous, juvenile magmatism (Boher et al. 1992). With its juvenile signature (Boher et al. 1992; Taylor et al. 1992; Doumbia et al. 1998; Gasquet et al. 2003) and relatively narrow age range (Lompo 2009 and references therein), the Birimian has been suggested to be an example of a rapid crustal growth event (e.g. Abouchami et al. 1990; Boher et al. 1992). The growth of the Birimian crust took place during a period which seems to be dominated by a relatively high reworking rate as indicated by the detrital zircon record (Dhuime et al. 2012). The proposed juvenile nature of the Birimian crust is therefore in stark contrast with the apparently low production of juvenile crust in the Palaeoproterozoic. The aim of this thesis is to evaluate the extent of juvenile crust formation of the Palaeoproterozoic crust in Ghana through analysis of detrital zircon from five rivers that run through Ghana and southern Burkina Faso. The results are put into context with a previously established model of continental crustal growth based on oxygen isotope ratios and crystallisation and Hf-model ages of detrital zircon (Dhuime et al. 2012).

2 Geological settings

2.1 The West African Craton (WAC)

The bedrock of Ghana belongs to the West African Craton (WAC), which covers a wide area that ranges from Morocco and Algeria in north, to Liberia, Côte d'Ivoire, and Ghana in the south. The WAC is bound towards east and west by Pan-African and Hercynian (Variscan) orogenic belts (Fig. 1) (Ennih & Liégeois 2008). The Man shield is the southernmost part of the WAC and is separated from the Reguibat shield in north by the Taoudeni basin (Ennih & Liégeois 2008). Both the Man and the Reguibat shields are made up of a western Archaean nuclei and a Palaeoproterozoic basement to the east (e.g. Abouchami et al. 1990). Further north, the Reguibat shield and Anti-Atlas belt are separated by the Tindouf basin. The Anti-Atlas belt contains Palaeoproterozoic inliers and is suggested to form the northernmost part of the WAC (Ennih & Liégeois 2008).

Palaeoproterozoic (~2.15 Ga), Birimian rocks of the Baoulé Mossi domain are abundant in the eastern part of the Man shield. They are separated from the western, Archaean (~2.7 Ga) domain by the Sassandra fault (Abouchami et al. 1990 and references therein). Alternating volcanic, greenstone belts and metasedimentary basins represent the Birimian rocks of the Man shield (e.g. Milési et al. 1992; Abouchami et al. 1990). Midway between the Archaean domains of the Man and the Reguibat shields, the Kedougou-Kenieba and Kayes inliers are found within the Taoudéni basin. The inliers are made up of Palaeoproterozoic rocks indicating that the Taoudéni basin overlies Birimian bedrock (Boher et al. 1992). The lithology and ages recorded in the bedrock of the São Luis craton in South America correlate with data from the Man shield (Feybesse et al. 2006; Klein et al. 2005) and it has been suggested that these two cratons formed a single unit in the Palaeoproterozoic during the emplacement of the Birimian bedrock (e.g. Feybesse et al. 2006).

Fig. 2. (On left page) Geological map of Ghana compiled by Watts, Griffit and McQuat Ltd, Lakewood Colorado, USA. Description of legends is as follows. *Phanerozoic to recent*: **Qs** – Quaternary, alluvial and lake sediments, unconsolidated. **Ts** – Tertiary, continental clastic sedimentary rocks. **KTs** – Cretaceous-Tertiary, Eocene, marine sedimentary rocks. **D** – Devonian, Sekondian and Accraian Units, sandstone and subordinate shale. **Vup** – Lower Palaeozoic, Upper Voltaian. Molasses deposits, mainly sandstone. **Vob** – Eocambrian, Obosum Beds. Shale and mudstone. *Precambrian*: **Vot** – Late Proterozoic, Oti Beds. Sandstone. **Vbs** – Late Proterozoic, Basal Sandstone. Sandstone. **Bm** – Late Proterozoic, probably 650-500 Ma, Buem Tectonic Unit. Mafic volcanic rocks, shale, jasper and sandstone. **Tg** – Late Proterozoic, Togo Series. Quartzite, sandstone and phyllite. **Dh** – Early Proterozoic, 2200-1800 Ma, Dahomeyan Units. Felsic and mafic gneiss, schist, and migmatite; reactivated Birimian rocks. **Tkw** – Early Proterozoic, 2130-2115 Ma, Tarkwaian Units. Conglomerate, quartzite and phyllite. **Bhb** – Early Proterozoic, probably 2184-2135 Ma, Metamorphosed Sedimentary Facies. Metamorphosed and metasomatised shale, tuff, and greywacke. **Bms** – Early Proterozoic, 2184-2135 Ma, Sedimentary Facies. Volcaniclastic rocks, greywacke, and argillite. **Bmv** – Early Proterozoic, >2180 Ma, Volcanic Facies. Basaltic flows, volcaniclastic and subvolcanic rocks. *Intrusive rocks*: **mi** – Precambrian-Mesozoic, possibly Pan African, Mafic intrusives. Gabbro, dolerite, norite and serpentinite. **Cgr** – Precambrian, Eburnean Orogeny, 2115-2088 Ma, Cape Coast or Basin Granitoids. Tonalite to peraluminous granite. **Dgr** – Precambrian, Eburnean Orogeny, 2180-2170 Ma, Dixcove or Belt Granitoids. Tonalite to granodiorite.

2.2 Birimian bedrock of Ghana

Evenly spaced volcanic belts and sedimentary basins that trend in a NE-SW direction dominate the Palaeoproterozoic basement of Ghana (Fig. 2) (Leube et al. 1990; Hirdes et al. 1996). An exception of this is the Larwa belt in northwestern Ghana which trends N-S (Leube, et al. 1990). The volcanic belts are represented by bimodal volcanism where tholeiitic basalts are common in the lower part of the belts but calc-alkaline andesitic, rhyolitic, and dacitic lavas and tuffs become more abundant in the upper part. Volcaniclastic sediments, hyaloclastites and pillow lavas are sometimes present (Leube et al. 1990; Abouchami et al. 1990; Sylvester & Attoh 1992; Milési et al. 1992). Volcaniclastic rocks, greywackes, argillitic rocks and chemical sediments are the main rock types forming the metasedimentary Birimian basins (Leube et al. 1990).

Felsic intrusions of different generations are found within the basins and belts. Towards north, their proportion in the volcanic belts increases due to more uplift and greater erosion (Leube et al. 1990). The intrusions have been divided into four suites; the Winneba, Cape Coast (basin type), Dixcove (belt type) and Bongo (K-rich) granitoids. The Dixcove type granitoids are mainly found within the volcanic belts. They are plutons of metaluminous, hornblende-bearing granitoids that are unfoliated and lack compositional banding. Granites (*sensu strictu*) constitute a minor part of these intrusions, which are dominated by tonalites and granodiorites (Eisenlohr & Hirdes 1992; Leube et al. 1990). The Cape Coast type granitoids are mainly found within the metasedimentary basins. They tend to form larger plutons of peraluminous granodiorites and granites with biotite as the main mafic mineral. Foliation is commonly present and is defined by the orientation of minerals and compositional banding with alternating biotite-poor and biotite-rich bands (Leube et al. 1990; Eisenlohr & Hirdes 1992). The Bongo type granitoids are potassium-rich, granitic intrusions with porphyroblasts of alkali feldspar (Leube et al. 1990). The Winneba type granitoids are granitic to granodioritic in composition (Leube et al. 1990) and are the only intrusions in Ghana that seem to have an Archaean component (Taylor et al. 1992). The Birimian bedrock is partially, unconformably overlain by Tarkwaian sediments (Milési et al. 1992). These are an erosional product of Birimian rocks, containing clasts of similar lithological units as the surrounding Birimian terrains (Eisenlohr & Hirdes 1992). The sediments were deposited between 2135 Ma and 2097 Ma ago (Davis et al. 1994; Oberthür et al. 1998).

According to a geodynamic model proposed by Feybesse et al. (2006) the initial tectonic and magmatic activity that formed the Birimian bedrock in Ghana, started at ~2.35 Ga with a deposition of banded iron formations and plutonic activity. This was followed by the formation of extensive, juvenile, basic to ultrabasic crustal segments between 2.25 and 2.17 Ga. Emplacement of monzogranite between 2.16 and 2.15 Ga marks the first formation of continental crust and was followed by opening of the basins and deposition of greywacke and flysch-type sediments within them between 2.15 and 2.10 Ga.

The Eburnean orogeny affected the Birimian terrain between ~2.13 and 2.00 Ga (Feybesse et al. 2006). Observed mineral assemblages of Birimian rocks indicate that peak metamorphism occurred within the greenschist facies during the Eburnean, but amphibolite facies mineral assemblages are present close to the felsic intrusions (Leube et al. 1990; Eisenlohr & Hirdes 1992; Hirdes & Davis 1998). Geothermobarometric examinations made on rocks from the Ashanti belt by John et al. (1999), indicate however that Birimian rocks underwent a clockwise P-T path with amphibolite facies peak metamorphism (500-650°C and 5-6 kbar) and were retrogressed through greenschist facies. Mineral assemblages and mineral relicts (phengite and chlorite) in metamorphic rocks from the Fada N'Gourma area in Burkina Faso indicate that metamorphism reached blueschist facies conditions (400-450°C and 10-12 kbar) during the Eburnean orogeny (Ganne et al. 2012). This has to be confirmed and further research is needed to support the blueschist facies metamorphism.

2.3 Birimian bedrock - evolution

Various hypotheses have been proposed regarding the tectonic environment of the emplacement of the Birimian bedrock. The general juvenile isotopic nature of the bedrock (Boher et al. 1992; Taylor et al. 1992; Doumbia et al. 1998; Gasquet et al. 2003) has led some scientists to propose that volcanism took place in distance from any continental crust (e.g. Abouchami et al. 1990). However, the Winneba belt granitoids in south-eastern Ghana record an Archaean reworked component having Nd-model ages around 2.6 Ga (Taylor et al. 1992). Furthermore, Feybesse et al. (2006) suggested that the formation of Lake Superior type banded iron formations in the beginning of the emplacement of Birimian terrains and the presence of diamondiferous fields in southeastern Ghana might indicate that they were formed in close vicinity to a continent.

Leube et al. (1990) suggested an intracontinental rift setting for the Birimian. However, it is likely that such a setting would leave a continental crustal imprint on the Birimian rocks which does not agree with their juvenile nature (Boher et al. 1992; Taylor et al. 1992; Doumbia et al. 1998; Gasquet et al. 2003). Abouchami et al. (1990) analysed slightly depleted light rare earth elements (LREE) patterns from the majority of the Palaeoproterozoic rocks belonging to the Man shield. The Ti enrichment of the rocks is situated between common values of Mid Ocean Ridge Basalts (MORB) and Island-Arc Basalts (IAB), they have relatively low concentrations of Nb, and radiogenic Sm-Nd values. This led Abouchami et al. (1990) to propose a model where the Birimian bedrock was formed by magmatic activity in relation to a mantle plume, forming an oceanic plateau in a short period of

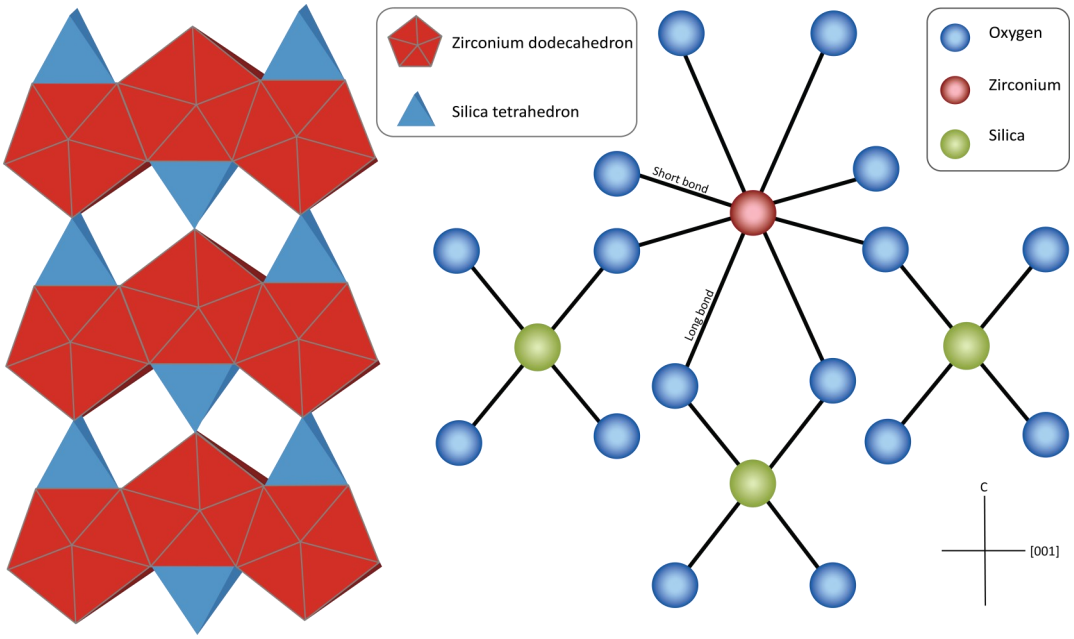

Fig. 3. Zircon is made up of Zr^{4+} (red), Si^{4+} (green) and O^{2-} (blue) ions. Each zirconium ion is linked to eight oxygen ions, forming a ZrO_8 dodecahedron. The zirconium dodecahedra are linked together on the edges forming chains (red pentagons). They share their corners and edges with silica tetrahedra (blue triangles), forming the zircon crystal structure. Figure modified from Kolesov et al. (2001) and Finch & Hanchar (2003).

time. Some of the rocks that were analysed by Abouchami et al. (1990) showed LREE enrichment and characteristics of island arc rocks. However, due to the small number of rocks that held these features, it was assumed that they were not representative for the Birimian bedrock. Boher et al. (1992) further developed this model, where the mantle plume activity was proposed to have been followed by subduction as well as local calc-alkaline island arc magmatism on the thickened crust, and formation of sedimentary troughs in between the volcanic belts. The terrain was then accreted to an Archaean continent resulting in the generation of granitic magmas by partial melting of the metamorphosed basalts.

Sylvester & Attoh (1992) suggested that the successions of tholeiitic mafic lavas, calc-alkaline felsic lavas and tuffs, along with flysch turbidites that are represented in the volcanic belts in the eastern Man shield, resembled modern, immature island arcs. This was supported by provenance analysis made by Asiedu et al. (2004) where major and trace element geochemistry of metagreywackes and metapelites in southern Ghana pointed towards a young, undifferentiated arc terrane. Rocks within the volcanic belts tend to form three distinct groups based on their trace element chemistry, basalts with flat to slightly depleted LREE patterns, basalts and basaltic andesites enriched in LREE over heavy rare earth elements (HREE), and andesites and dacites with greater LREE enrichment (Sylvester & Attoh 1992; Dampare et al. 2008). The first group resembles the rocks analysed by Abouchami et al. (1990), but these form only a part of the volcanic belts. The enrichment in large-ion lithophile (LIL) elements over high field strength (HFS) elements of the remaining rocks, indicate that they formed in an island arc environment (Sylvester & Attoh 1992; Soumaila et al. 2004; Dampare et al. 2008).

3 Zircon

3.1 Isotopes in zircon

Zircon ($ZrSiO_4$) is an accessory mineral that forms mainly in silica saturated melts (Hoskin & Schaltegger 2003). It is a tetragonal, orthosilicate composed of ZrO_8 dodecahedra that form chains by sharing their edges, and SiO_2 tetrahedra that share corners and edges with the ZrO_8 chains (Fig. 3). Elements such as Hf, U, Th and the REE, to which Lu belongs to, can be incorporated into the crystal lattice in various amounts (e.g. Mahood & Hildreth 1983; Fujimaki 1986; Heaman et al. 1990; Rubatto 2002). This can both take place through simple substitution and a coupled substitution (Hoskin & Schaltegger 2003). Si^{4+} can be replaced by P^{5+}, particularly in association with REE substitution for Zr^{4+} in order to balance out the difference in charge between the REE (+3) and the zirconium ion (Hanchar et al. 2001; Belousova et al. 2002). The total amount of REE in zircon is relatively low, commonly ranging between 1500 and 2000 ppm (Hoskin & Schaltegger 2003). In igneous zircon, HREE are generally more abundant than LREE (Heaman et al. 1990; Hoskin & Ireland 2000; Belousova et al. 2002; Hoskin et al. 2000). This is partially based on the smaller ionic radius of the HREE compared to the LREE, and therefore an ionic radius more similar to the 0.84Å radius of Zr^{4+} (Hoskin & Schaltegger 2003; Hoskin & Ireland 2000; Belousova et al. 2002). Two REE anomalies are commonly pre-

sent in zircon; a positive cerium anomaly and a negative europium anomaly (Hoskin & Ireland 2000; Hoskin et al. 2000; Belousova et al. 2002; Hoskin & Schaltegger 2003). Ce is found both as a trivalent (1.14Å) and tetravalent ion (0.97Å) (Shannon 1976) making Ce^{4+} more compatible in the zircon than Ce^{3+}. Eu can appear as a divalent ion with an ionic radius of 1.25Å (Shannon 1976), which reduces its compatibility. The negative Eu anomaly of zircon has also been attributed to partitioning of Eu^{2+} into plagioclase (Belousova et al. 2002).

Hafnium ions (0.83Å) (Shannon 1976) are a common substitute for Zr^{4+} in zircon due to their identical charge and similar ionic radius. Hafnium is generally more abundant in zircon than the REE (Harley & Kelly 2007) and can often be recorded on a weight percentage scale rather than a ppm scale (Fujimaki 1986; Belousova et al. 2002; Hoskin & Ireland 2000). Uranium (U^{4+}) and thorium ions (Th^{4+}) have an ionic radius of 1.0 and 1.05 Å respectively (Shannon 1976), making both of them slightly larger than the zirconium ion. U and Th can be incorporated in substantial amounts into the crystal lattice of zircon by a simple substitution with Zr^{4+} (Hoskin & Schaltegger 2003). Pb^{2+} has a yet larger ionic radius of 1.29 Å (Shannon 1976) and a charge that differs from the one of Zr^{4+}, making it less compatible in zircon and generally being represented in much smaller amounts than U and Th (Hoskin et al. 2000; Belousova et al. 2002). Under more oxidized conditions, lead can be present as a tetravalent ion with an ionic radius of 0.94Å (Shannon 1976), which would make it more compatible in zircon than Pb^{2+}. However, the oxidation state of most metamorphic and igneous processes does not facilitate the formation of Pb^{4+}, making it unlikely for zircon to grow in the presence of substantial amounts of Pb^{4+} (Watson et al. 1997). Kramers et al. (2009) suggested that the robustness of the U-Pb system in zircon during high-temperature metamorphism and anatexis might be explained by that radiogenic lead is tetravalent, making it more stable in the zircon crystal structure than the divalent common lead.

Pure zircon and zircon containing small amounts of trace elements is not very susceptible towards changes in response to external variations of temperature and pressure (Harley & Kelly 2007). Zircon does not break down to its Zr- and Si-oxides until it is exposed to temperatures in excess of 1690°C at 1 atm (Finch & Hanchar 2003). The refractory nature of zircon, the slow diffusion rate of elements within the

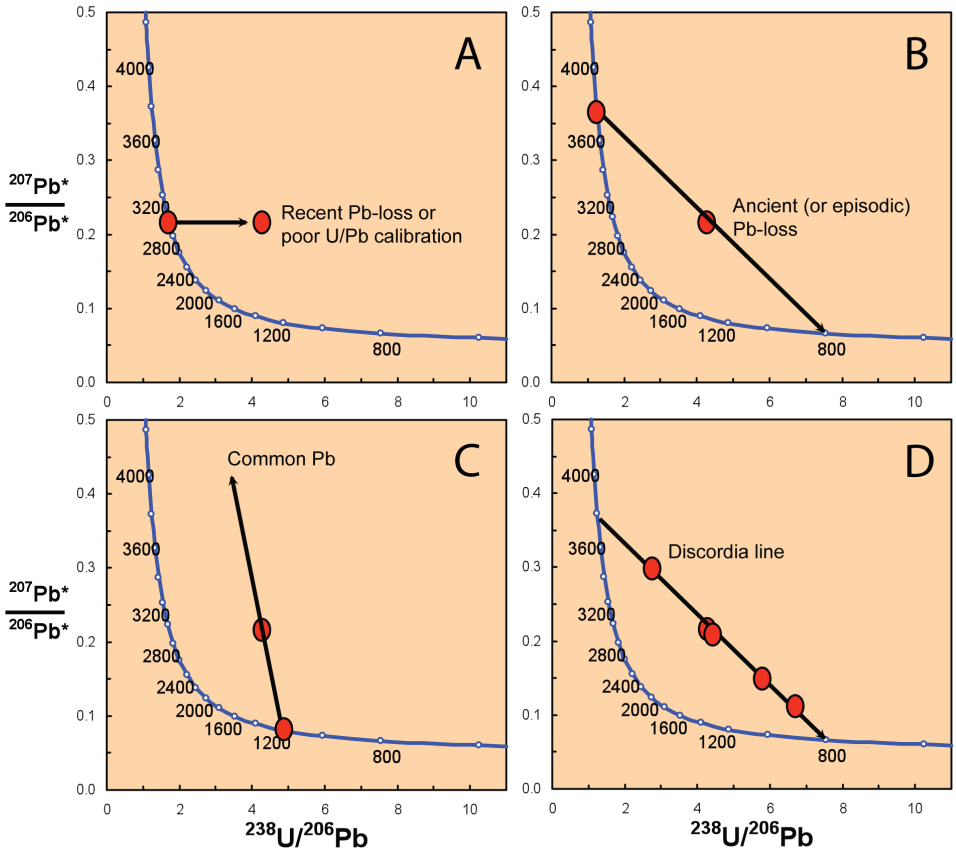

Fig. 4. Tera-Wasserburg diagrams showing trends of: A) Recent lead-loss or poor U/Pb calibration causing the grain to be displaced vertically on the diagram. B) Ancient or episodic Pb-loss. C) Addition of common lead that has a higher $^{207}Pb/^{206}Pb$ than the zircon. D) Discordia line defined by several discordant zircon that were affected to different extent by the same event. Upper intercept represents the crystallisation age of the zircon and the lower intercept gives the age of the event that caused disturbance of the U-Th-Pb system of the zircon.

mineral, its high blocking temperature (Cherniak & Watson 2003) and ability to incorporate various trace elements (Hanchar & van Westrenen 2007; Harley & Kelly 2007), makes zircon a good candidate for various geological researches (e.g. Heaman et al. 1990; Belousova et al. 2002; Pietranik et al. 2008; Belousova et al. 2010; Dhuime et al. 2012). It can grow in stages, forming layers that represent a certain phase in the history of the zircon (Corfu et al. 2003). As such, it can provide information about several events by using microbeam techniques to analyse each layer of the zircon individually.

3.2 U-Pb system in zircon

The U-Pb system in zircon has been used for several decades in geochronology (Davis et al. 2003). It is based on the decay of ^{238}U and ^{235}U to the stable isotopes of ^{206}Pb and ^{207}Pb. These decays are comprised of several intermediate steps where each step involves the formation of a radioactive isotope with a short lifetime as compared to the final step of each system. This property of the decay series makes it possible to simplify the age calculations by using only a single decay constant to represent the decay of uranium to lead. The calculation is described by the following equation (Harley & Kelly 2007):

$$^{206}Pb^{*}/^{238}U = e^{\lambda^{238}t} - 1 \qquad \text{(Eq. 1)}$$

Where $^{206}Pb^{*}$ is the amount of radiogenic ^{206}Pb formed through decay of ^{238}U within the mineral, λ^{238} is the decay constant of ^{238}U to ^{206}Pb and t is time. Same equation is applied to the $^{235}U \rightarrow ^{207}Pb$ system, using the λ^{235} decay constant. Even though lead is not readily incorporated into the zircon crystal lattice during its crystallisation, corrections might have to be made to calculate the true value of radiogenic ^{206}Pb and ^{207}Pb that formed within the crystal, before applying the measured values to the equation (Ireland & Williams 2003).

A common way to present U-Pb dating results is to use a concordia diagram, which is a trajectory that describes how $^{206}Pb/^{238}U$ and $^{207}Pb/^{235}U$ ratios change with time according to their decay constants (Wetherill 1956), or by using an inverse concordia diagram that is based on measured and corrected $^{207}Pb/^{206}Pb$ and $^{238}U/^{206}Pb$ ratios (Fig. 4) (Tera and Wasserburg, 1972).

An advantage of the U-Pb system is that it is based on two independent decay systems. Both systems should give the same age of a grain that has remained as a closed system and therefore plot on the concordia. The grains that do not fall on the concordia are described as discordant. Their discordance has been attributed to mobilization of U and Pb isotopes in association with circulation of fluids or low-grade metamorphism (Mezger & Krogstad 1997 and references therein), but can also be attributed to poor U/Pb calibrations and the presence of common lead. When several zircons are analysed from a single rock that has been affected by metamorphism or fluids, values might fall out of the concordia curve but still define a line on the diagram. If a best fit through the analyses cuts the concordia twice, the upper intercept can be interpreted as the crystallisation age of the rock while the lower intercept represents the age of an event causing the change in the U-Pb isotopic system (Fig. 4D). Care must though be taken when interpreting ages represented by discordant zircon since discordance might involve multiple processes (Mezger & Krogstad 1997).

3.3 Oxygen isotopes in zircon

Oxygen is an important element in the majority of all minerals. There are three stable oxygen isotopes, ^{16}O (99.76%), ^{17}O (0.04%), and ^{18}O (0.20%). All three isotopes show similar chemical behaviour but mainly due to their difference in mass (^{18}O is 12.5% heavier than ^{16}O), they fractionate between phases (Rollinson 1993). The deviation in the measured oxygen ratio of a substance, from a standard is signified as $\delta^{18}O$ (‰) and is calculated according to the following equation (Rollinson 1993):

$$\delta^{18}O = \left(\frac{^{18}O/^{16}O_{Sample}}{^{18}O/^{16}O_{Standard}} - 1\right) \cdot 10^{3} \qquad \text{(Eq. 2)}$$

Where $^{18}O/^{16}O_{Sample}$ is the measured oxygen isotope ratio of the sample and $^{18}O/^{16}O_{Standard}$ is the standardized oxygen isotope ratio, which commonly is the Standard Mean Ocean Water (SMOW) (Baertschi 1976).

Zircon grains that crystallise from mantle derived magmas tend to record a rather narrow range of $\delta^{18}O$ values (Eiler 2001; Valley et al. 2005) falling

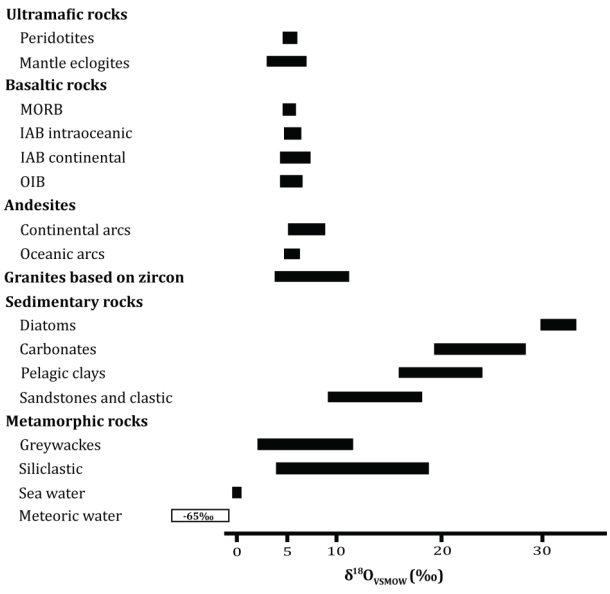

Fig. 5. Common $\delta^{18}O$ of various rock types. Most igneous rocks tend to have a relatively narrow spread falling close to values recorded in mantle rocks. A yet wider spread is recorded in sedimentary and metamorphic rocks, with the sedimentary rocks commonly being substantially enriched in ^{18}O. Meteoric and sea water are the main components depleted in ^{18}O. Figure modified from Bindeman (2008).

close to 5.3±0.3‰ (Valley et al. 1998). Low-temperature alteration of rocks, at or close to the surface of the Earth often raises the $\delta^{18}O$ value of sediments. Interaction between water and rock at higher temperatures can however lead to depletion in ^{18}O of the rock. This results in a difference in the oxygen isotope ratio of altering rock types (Fig. 5) (Rollinson 1993).

For zircon to serve as a proper indicator of the $\delta^{18}O$ of the magma from which it crystallised, it has to be able to preserve its original isotopic composition. It has been demonstrated that the diffusion rate of oxygen in zircon is slow (Watson & Cherniak 1997; Cherniak & Watson 2003) and analyses made on igneous zircon from high-grade metamorphic terrains indicate that non-metamict zircon tend to preserve their original oxygen isotope ratio even though having been exposed to high temperature conditions (Valley et al. 1994; Peck et al. 2003; Page et al. 2007).

3.4 Lu-Hf system in zircon

The radioactive isotope ^{176}Lu decays to ^{176}Hf by a β-emission with a $\lambda^{176}Lu$ decay constant of 1.867 x 10^{-11} yr^{-1} (Scherer et al. 2001; Söderlund et al. 2004). Lu and Hf are both incompatible in most basaltic rock-forming minerals such as olivine, pyroxene, and plagioclase, with Hf being more incompatible than Lu. In addition, Lu tends to reside in garnets while Hf is incompatible (Rollinson 1993). During partial melting of the upper mantle, Hf enters the melt more readily than Lu leading to contrasting Lu/Hf of the residual mantle and the melt. The process of partial melting discriminates between elements with different chemical properties, but due to the small relative mass difference, it does not discriminate between different isotopes of heavy elements such as Hf (Winter 2010). The $^{176}Hf/^{177}Hf$ ratio of the melt and the upper mantle at the time of formation of the melt is therefore identical. With time ^{176}Lu decays to ^{176}Hf, changing the $^{176}Hf/^{177}Hf$ of both the crust (melt) and the mantle. Since the mantle is enriched in Lu/Hf, its $^{176}Hf/^{177}Hf$ ratio will rise more rapidly than the $^{176}Hf/^{177}Hf$ of the crust with its lower Lu/Hf.

Because of the small differences in Hf isotope ratios between different rock types and reservoirs, a common way to denote variations in $^{176}Hf/^{177}Hf$ ratios of rocks is to calculate their ε_{Hf} value. This is done by comparing the measured ratio of a sample to the chondritic uniform reservoir (CHUR) reference value. CHUR values are based on analyses made on chondritic meteorites, which are thought to represent the composition of silicate earth (Bouvier et al. 2008). The epsilon notation represents the deviation in parts per 10.000 from the CHUR standard and is calculated as follows:

$$\varepsilon_{Hf} = \left(\frac{^{176}Hf/^{177}Hf_{Sample}}{^{176}Hf/^{177}Hf_{CHUR}} - 1 \right) \cdot 10^4 \qquad \text{(Eq. 3)}$$

Where $^{176}Hf/^{177}Hf_{sample}$ is the measured hafnium isotope ratio of the sample and $^{176}Hf/^{177}Hf_{CHUR}$ is the reference ratio. Zircon incorporates lutetium in much smaller amounts than hafnium (Harley & Kelly 2007), resulting in a very low $^{176}Lu/^{177}Hf$. The $^{176}Hf/^{177}Hf$ of the zircon therefore stays nearly constant over time, making it record a value close to the initial value of the magma that it crystallised from. Age corrected zircon $^{176}Hf/^{177}Hf$ are usually within error of the measured $^{176}Hf/^{177}Hf$ even if the grain is several billion years old. Zircon crystallising in equilibrium with juvenile magmas tend to be represented by positive ε_{Hf} values, falling close to the mantle source values. Zircon that crystallises in equilibrium with ancient, reworked magmas do however show a value more dissimilar to the mantle source value at the time of their formation.

3.5 Model ages

3.5.1 What is a model age?

Model ages vary from crystallisation ages of rocks and minerals. Instead of giving information about their time of crystallisation, model ages represent when the magma that the minerals crystallised from, separated from the mantle. When working with model ages, one has to be aware that melting of a heterogeneous crust or incorporation of sediments into magma sources, results in magma that is a mixture of two or more components. The retrieved model age will then represent a mixed value from the sources (Arndt & Goldstein 1987). Oxygen isotopes in zircon have been used to discriminate between zircon that grew in magma with mantle-like $\delta^{18}O$ and those containing a reworked component represented by zircon with $\delta^{18}O$ falling outside the mantle range (Kemp et al. 2006; Pietranik et al. 2008). Zircon grains that belong to the former group are thought to be derived from magmas that were formed by melting of a single source component and therefore have model ages representative of when material was added to the crust. Model ages of the latter group are based on an average value of the components contributing to the magma and do therefore not indicate when material was added to the crust.

Two systems have mainly been used to determine model ages with respect to continental crust growth, the Sm-Nd system and Lu-Hf system. This study uses the Hf-model ages. Discussion will therefore focus on the Lu-Hf system, although these systems are in essence working in the same way. Hf model ages can be calculated from rock or mineral samples where the $^{176}Lu/^{177}Hf$ and $^{176}Hf/^{177}Hf$ have been determined. The mineral zircon is particularly useful as it has high concentrations of Hf and very low $^{176}Lu/^{177}Hf$. Measurements can be made on a single zircon mineral by microbeam U-Pb dating and Lu-Hf isotope analysis (e.g. this thesis). Lu-Hf analysis on zircon has become a growing subject in more recent years with numerous papers being published in the past decade (Lackey et al. 2005; Kemp et al. 2006; Pietranik et al. 2008; Wang et al. 2009; 2011; Iizuka et al. 2010; 2013; Lancaster et al. 2011; Dhuime et al. 2012; Næraa et al. 2012; Roberts et al. 2013).

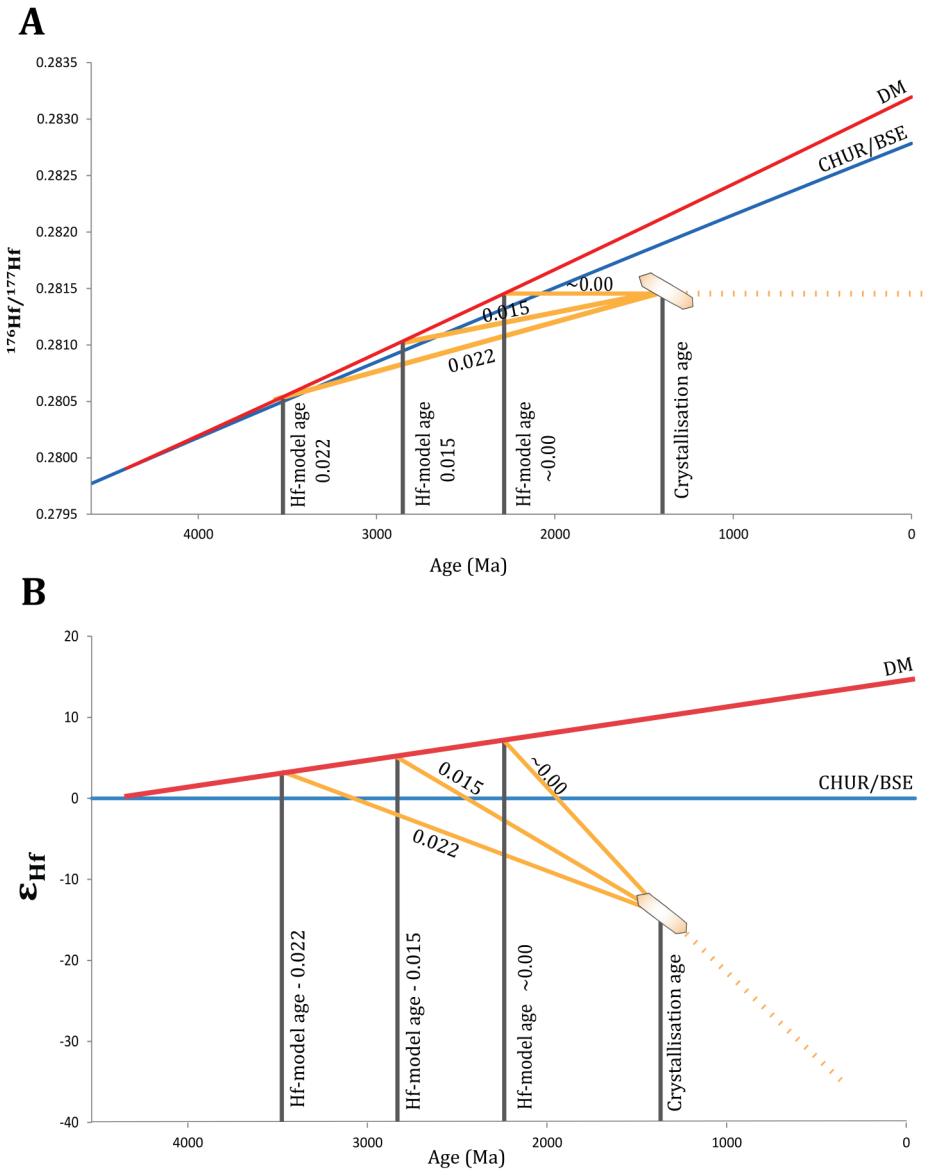

Fig. 6. Hf enters the melt more readily than Lu during partial melting, leading to lower $^{176}Lu/^{177}Hf$ ratio of the melt than the residue. If assuming that the depleted mantle (DM) (red) and continental crust (orange) are complimentary, where the depleted mantle corresponds to the residue and the continental crust to the melt, extraction of continental crust from the mantle will result in an enrichment in $^{176}Lu/^{177}Hf$ of the mantle. CHUR (blue) is a common reference material used to represent the bulk composition of the silicate Earth and is based on analyses on chondrites (Bouvier et al. 2008). Since there are small variations in the $^{176}Hf/^{177}Hf$ between different rock types and reservoirs (Fig. 6A), it is commonly represented as an ε_{Hf} value (Fig. 6B). The ε_{Hf} value describes the deviation of reservoirs from the reference material, in this case CHUR. ^{176}Hf is formed through β-decay of ^{176}Lu and due to the greater Lu/Hf ratio of the mantle, the $^{176}Hf/^{177}Hf$ of the DM increases more rapidly than of both the continental crust and CHUR, leading to positive ε_{Hf} of the DM. Zircon incorporates minor amounts of Lu resulting in its nearly constant $^{176}Hf/^{177}Hf$ and rapidly lowered ε_{Hf} (dashed orange lines).

Two stage Hf-model ages calculations assume that the zircon bearing magma was formed through a two stage process. The first stage involves partial melting of the mantle forming primitive magma and the second stage either involves fractional crystallisation or partial melting of a mantle derived magma. In order to calculate the Hf-model age of zircon, its present day $^{176}Lu/^{177}Hf$ and $^{176}Hf/^{177}Hf$ are measured. These values, combined with its known crystallisation age and the decay constant of ^{176}Lu, allow for a calculation of its $^{176}Hf/^{177}Hf$ at the time of crystallisation. Next step involves determining when the $^{176}Hf/^{177}Hf$ of the magma was equal to the DM, which corresponds to the time when it separated from the DM. This part of the calculations requires the $^{176}Lu/^{177}Hf$ of the magma. However, it cannot be determined from analyses on the zircon and is therefore often assumed based on average values of crustal rocks. Two evolutionary trends of crustal rocks are presented on the diagrams (orange), one represents mafic crust (0.022) (Amelin et al. 1999 and references therein) and the other average crust (0.015) (Griffin et al. 2002). An even younger model age would be retrieved if only using the measured value of $^{176}Lu/^{177}Hf$ in the zircon (orange line, ~0.00), which is often negligible. Considerable difference in calculated model ages would be acquired by using those three values, but this difference is enhanced by the long residence times represented on the figures and is much lower in zircon representing shorter residence times (Wang et al. 2009).

Considerable deviations between analyses that were done to determine the decay constant of ^{176}Lu (e.g Gehrke et al. 1990; Nir-El & Lavi 1998; Grinyer et al. 2003) hampered the usage of the Lu-Hf isotopic system in the beginning. A nearly identical decay constants of ^{176}Lu based on analysis of terrestrial samples that was reported by Scherer et al. (2001) and Söderlund et al. (2004) is now generally accepted. Difficulties in the analytical procedures of Hf due to its low ionization efficiency (Patchett & Tatsumoto 1980) did also limit the usage of Lu-Hf analysis until the emergence of multicollector inductively plasma mass spectrometry (MC-ICP-MS). More effective techniques that required smaller sample sizes have become available in recent years (Salters 1994; Amelin et al. 1999), making Lu-Hf analysis on zircon more accessible.

3.5.2 Model age calculations

Model ages are calculated according to the following equation (Rollinson 1993):

$$T_{DM}^{Hf} = \frac{1}{\lambda^{176}_{Lu}} \ln\left[\frac{^{176}Hf/^{177}Hf_{Sample} - {}^{176}Hf/^{177}Hf_{DM}}{^{176}Lu/^{177}Hf_{Sample} - {}^{176}Lu/^{177}Hf_{DM}} + 1\right] \quad \text{(Eq. 4)}$$

Where λ^{176Lu} is the decay constant for ^{176}Lu to ^{176}Hf, $^{176}Hf/^{176}Hf_{Sample}$ and $^{176}Lu/^{176}Hf_{Sample}$ are measured values from sample and $^{176}Hf/^{176}Hf_{DM}$ and $^{176}Lu/^{176}Hf_{DM}$ are calculated values based on the reference material, which the magma is assumed to have separated from. A commonly used reference material is the depleted mantle (DM) or chondritic uniform reservoir (CHUR) (Rollinson 1993). Dhuime et al. (2011a) pointed out that modern island arc magmas tend to plot slightly lower than the DM on a ε_{Hf} diagram. Based on their observations they suggested a new reference model, which was called new crust (NC).

Zircon is presumably rare in magmas formed directly through partial melting of the mantle and it is therefore likely that at least two stages are required before the crystallisation of most zircon, affecting the Hf-model age calculations based on zircon. The first stage involves a formation of magma derived from the mantle and the second stage either involves partial melting of that magma after its solidification, forming a zircon bearing rock, or fractional crystallisation of the mantle derived magma. If assuming partially melted mafic protolith, the $^{176}Hf/^{177}Hf$ alters according to the $^{176}Lu/^{177}Hf$ of the magma during the first stage, while during the second stage the $^{176}Hf/^{177}Hf$ alters according to the $^{176}Lu/^{177}Hf$ of the zircon (Fig. 6). Since zircon contains minor amounts of ^{176}Lu its $^{176}Hf/^{177}Hf$ ratio will experience little changes after the crystallisation of the zircon, resulting in minor corrections due to post-crystallisation decay of ^{176}Lu to ^{176}Hf. The melt has a higher $^{176}Lu/^{177}Hf$ than the zircon where silicic rocks record an average of around 0.009 (Amelin et al. 1999 and reference therein) and basic and intermediate rocks commonly have a higher ratio (Fig. 7). As the $^{176}Lu/^{177}Hf$ of the precursor is not recorded in the zircon, a proper ratio has to be assumed for the calculations commonly lying within the values of crustal rocks.

3.6 Detrital zircon

Working with detrital zircon gives an opportunity to explore a larger surface of area than by sampling rocks and therefore to retrieve more easily a general picture of the rocks found within the upstream catchment area of a sampled river. Furthermore, due to its resistance and refractory nature, zircon can be the only relicts of a body of rock that has been weathered down and eroded away, providing information that otherwise would have been lost (Wilde et al. 2001; Kemp et al. 2010; Cavosie et al. 2005). Detrital zircon has been used in provenance studies where the age of the youngest zircon population in the sediment is interpreted to record the maximum age of sedimentation and as an indicator of the validity of proposed palaeaogeographic reconstruction (Fedo et al. 2003).

Detrital zircon populations can be made up of zircon belonging to several events and from a large area. Analysing only a group of zircon with certain morphology and colour can cause biases where zircon that only belong to a single event are analysed. Fedo et al. (2003) addressed the difference between choosing zircon for analyses in a quantitative and a qualitative manner. When doing it qualitatively, equal amounts of zircon of all morphologies and colours that are present in the sample are analysed, independent on the proportion of each group within the sample. During quantitative analysis it is however sought to preserve the proportion between zircon groups in the analysed population, as it is in the whole sample. For quantitative analysis to be statistically significant a fairly large number

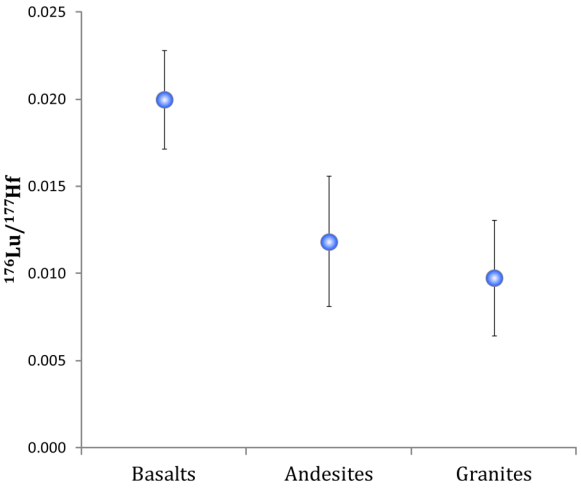

Fig. 7. $^{176}Lu/^{177}Hf$ is generally higher in basic rocks than in more silica rich rocks. Average values for basalts, andesites and granites were calculated using data from GERM reservoir database (GERM 2013) giving values of 0.020±0.003 (1σ), 0.012±0.004 (1σ) and 0.010±0.003 (1σ) respectively. These values are in agreement with previously determined average values of crustal rocks (Griffin et al. 2002; Amelin et al. 1999 and references therein).

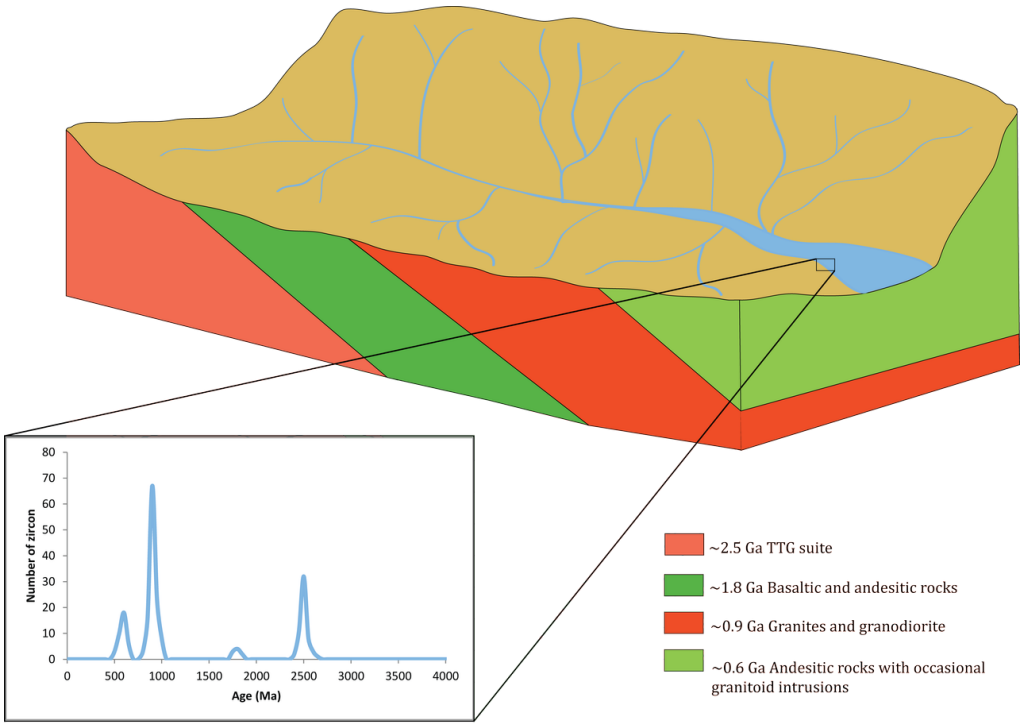

Fig. 8. Schematic figure of a catchment area of a single river system. The bedrock is made up of rocks of different lithologies formed at ca. 2.5 Ga, 1.8 Ga, 0.9 Ga and 0.6 Ga. Due to small amount of zircon formed in the ~ 1.8 Ga basaltic and andesitic rocks, the 1.8 Ga is underrepresented in the detrital zircon population sampled close to the river mouth. The Archaean TTG contains abundant zircon but due its age, the 2.5 Ga peak is not as prominent as the 0.9 Ga peak.

of zircon has to be analysed (Fedo et al. 2003). Quantitative analysis might therefore detect events represented by only few zircon grains that might be overseen in a qualitative analysis due to their rarity. Comparison between different age groups will though only be meaningful using qualitative analysis since quantitative analysis does not take into account the proportion between zircon groups in the whole sample (Fedo et al. 2003). Modelling made by Vermeesh (2004) indicates that to be 95% certain of detecting every age fraction that comprises more than 5% of the total zircon population, at least 117 grains need to be analysed.

Several factors can contribute to biases in the detrital zircon record (Fig. 8). Zircon grows mainly in silica saturated magmas (Hoskin & Schaltegger 2003), which makes silica under-saturated rocks underrepresented in the detrital zircon record (Fedo et al. 2003). Iizuka et al. (2010) analysed over 1000 detrital zircon from Mississippi, Congo, Yangtze and Amazon rivers and compared their average Hf-model ages to previously reported Nd-model ages of the sediments. The Hf- and Nd-model ages correlated rather well, apart from the Amazon river where average Nd-model ages were around 1.1 Ga younger than the average Hf-model ages. This difference they attributed either to a greater resistance of Lu and Hf isotopes in zircon than of Sm and Nd in other minerals, or that the Hf-model ages failed to record Cenozoic magmatism in the Amazon area that is mainly represented by basaltic to basaltic-andesite rocks. However, just as Hf-model ages are controlled by zircon, Nd-model ages can be largely controlled by the mineral monazite when it is present in the sediments (Garçon et al. 2011). Monazite bearing, silicic rocks might therefore be overrepresented in Nd-model ages.

The age of the bedrock can affect its contribution to sediments where old bedrock located in distal areas from the sampling site can be underrepresented in the sedimentary record (Dhuime et al. 2011b). The K-factor is an erosion parameter that describes the relationship between the distribution of a source within a catchment area and its abundance in the sedimentary sample. To correct for the deviations caused by the age of the bedrock and to obtain values that better represent the average composition of the bedrock within the catchment area, a suitable K-factor can be applied to the dataset.

Another shortcoming of detrital zircon is that discordant data cannot be treated in similar fashion as discordant zircon grains collected from a body of rock. When a single discordant zircon is available it cannot be securely linked to other zircon in the dataset and therefore locating a lower and upper intercept cannot be used to determine the crystallisation age. A way to treat discordance is to set a certain discordance limit where all zircons with discordance greater than e.g. ±10% are omitted (Fedo et al. 2003).

Fig. 9. Sampling sites of the five zircon populations analysed in this thesis. A) Ankobra river (ASGH 015A). B) Birim river (ASGH 029D). C) Black Volta river (ASGH 059A). D) Sihili river (ASGH 081A). E) Red Volta river (ASGH 088B) (Photos by Anders Scherstén).

4 Methods

4.1 Sample collection

All samples were collected by Anders Scherstén. Samples ASHG 015A and ASGH 029D were sampled in 2009 but ASGH 059A, ASGH 081A, and ASGH 088B in 2011. ASGH 015A (Ankobra river) was sampled in an open pit gold mine filled with recently deposited river sediments rich in quartz pebbles (Fig. 9A). Around 15 litres of sediment or 3 full pans were panned down to half a kilogram. ASGH 029D (Birim river) was sampled from a heavy mineral separate produced by a gold production company (Fig. 9B). Sediment and water was poured into a trapezoidal container. The mixture flowed down from the container along a ramp segmented by steps. Each step contained aligned sponges that impeded the flow and thus separated the heavy minerals from the mixture. Heavy mineral separates were collected from the ramp and put into barrels. Several hundred grams of sample were collected from the heavy mineral separates in the barrels. ASHG 059A (Black Volta river) was sampled from Black Volta river by panning four full pans of sediment that was reduced to around 200 grams (Fig. 9C). ASHG 081A (Shili river) was sampled from the centre of the river by panning three pans of sediment. The sediment was sand-rich and deprived of pebbles (Fig. 9D). ASGH 088B (Red Volta river) was sampled from sandy patches in the middle of the river. Sampling was conducted during dry season leaving behind exposed sediment in the dried out river bed (Fig. 9E). Three pans of sand were panned and reduced to a half a kilogram of sediment.

4.2 Zircon separation and sample processing

Each sample was dried and sieved to remove the coarse-grained fractions. Heavy mineral separation was carried out at the Department of Geology, Lund University, using a Wilfey shaking table following a modified procedure of Söderlund & Johansson (2002).

Zircon grains were handpicked in water under a light microscope by Andreas Peterson and mounted on tape along with a zircon standard 91500 (Wiedenbeck et al. 2004). The grains were casted in epoxy and polished to expose their interior. Backscatter electron images (BSE) were captured with a Hitachi S-4300N electron microscope using standard SEM methods. The images showed the internal structures of the crystals and were used for guidance during analysis, to detect different zones of structurally complex zircon, and avoid inclusions and fractures where it was possible. Prior to Lu-Hf analysis, detailed transmitted and reflected light images where captured at Lund University using a Nikon Eclipse E400 POL equipped with a Lumenera Infinity 1-2 CB camera for photo micrographs. The images were used to accurately locate the pits from the previously conducted U-Pb and oxygen isotope analyses, before selecting a spot for the Lu-Hf analysis. This was done in order to try to overlap the Lu-Hf spot with the two pits.

4.3 U-Th-Pb and O analyses using SIMS

Secondary ion mass spectrometer (SIMS) U-Th-Pb and O analyses were carried out in October 2010 and January and May 2012, using a large geometry Cameca IMS1280 instrument at the Swedish Museum of Natural History. Standard descriptions of the methods that were used are found in Appendix I.

Secondary Ion Mass Spectometry (SIMS) is a technique that allows *in situ* analysis of elements or isotopes that make up a material. In SIMS a high-energy ion beam, commonly consisting of O, O_2 or Ce ions, is used to ablate atoms off the sample surface. During this process of sputtering, both neutral and charged atoms and molecules are formed, making up a secondary ion beam. The choice of element for the primary beam is mainly based on the elements that are being analysed (Cherniak et al. 2010). The secondary ions travel within a vacuum and are focused into a beam that is transferred to the analyser. The analyser and detector units resemble the ones that will be described for the LA-ICP-MS system in section 4.4.

Prior to conducting SIMS analyses on zircon, the zircon must be mounted in epoxy and polished down to reveal a cross-section through its interior. A standard zircon is most commonly mounted in the epoxy along with the other grains and is used for quality control during analyses. SIMS analyses most often exploit only a small fraction of the sample, ablating about 5 μm into the sample with the spot size usually ranging between 10 and 50 μm. This allows for multiple analyses on the same zircon grain although the precision of each analysis does not reach the precision of TIMS analyses (Ireland & Williams 2003).

In U-Th-Pb zircon analysis, several elements and isotopes are measured. ZrO_2 is measured to serve as a reference value to calculate the concentration of Pb, U and Th and to help locate the ^{204}Pb peak. Th is measured both for age determination and can also serve as an indicator of the growth settings (Ireland & Williams 2003); e.g. as an indicator of metamorphic processes since metamorphic zircon tends to have a low Th/U ratio (Rubatto 2002). ^{206}Pb, ^{207}Pb and ^{208}Pb are measured for age determination but ^{204}Pb helps determine the amount of common lead in the zircon. The three first mentioned lead isotopes are all radiogenic and form through decay of ^{238}U, ^{235}U and ^{232}Th. ^{204}Pb is non-radiogenic indicating that Pb became a part of the sample through other processes than the decay of radioactive isotopes. Measuring the intensity of ^{204}Pb in the sample can therefore help to determine the original amount of lead in the zircon (Ireland & Williams 2003).

Early U-Th-Pb analyses on zircon showed that U and Th had a tendency to form charged compounds with O, but Pb was mainly represented by Pb^+. The measured Pb^+/U^+ and Pb^+/Th^+ ratios did therefore not represent the true Pb/U and Pb/Th ratios of the sample (Williams 1998 and references therein). Two U species, U, UO, or UO_2, are therefore also measured since the ratio between uranium of different oxidation states can be used to determine the Pb^+/U^+ ratio of secondary ions (Ireland & Williams 2003).

4.4 Lu-Hf analyses using LA-ICP-MS

Lu-Hf analyses were carried out in July 2012 at the Advanced Analytical Centre at James Cook University in Townsville, Australia using a GeoLas 193-nm ArF laser and a Thermo-Scientific Neptune High resolution multi collector ICP-MS. Backscattered electron (BSE) images from a scanning electron microscope (SEM), along with transmitted and reflected light images were used to determine a proper location of the spot on each zircon. Where it was suitable, the Lu-Hf spot overlapped pits from both the U-Th-Pb and O isotope analysis. Spot sizes with a diameter of 31 μm, 42 μm and 58 μm were used. Standard description of the method that was used is found in Appendix I.

Laser Ablation Inductively Coupled Plasma Mass Spectrometry (LA-ICP-MS) is a technique that allows chemical analysis of a small amount of material from a solid sample. The technique requires two units; a laser unit and an ICP-MS. The sample is fitted in a sample chamber of the laser unit where it can be moved around to make it possible to position the laser target at the appropriate spot. A pulsed laser beam is used to ablate small amounts of the sample per pulse. The ablated material is transported by a carrier gas, most often He or Ar, through a tube into the Ar plasma of the ICP-MS (Cherniak et al. 2010). A combination of He and Ar has been shown to be successful in decreasing the detection limit and the background intensity of most elements. Helium carrier gas is then flushed over the sample in the sample chamber and is combined with argon gas downstream from the chamber on the way to the plasma (Günther & Heinrich 1999).

The temperature in the Ar plasma is around 8000 K and at such temperatures most atoms and mol-

ecules become ionised. The ions that are created in the plasma enter the mass analyser through a sampler cone, skimmer cone and electrostatic lenses, at which point, the ions are contained in a vacuum. Analysing the ions under vacuum conditions reduces the risk of ions colliding with one another. Contemporaneously with decreasing pressure upon entering the vacuum stage, the ablated sample is reduced to around 1% of its original size in the skimmer cone and the ion beam is focused with the electrostatic lenses prior to entering a mass analyser (Longerich & Diegor 2001).

Several analysers are available. Three systems will be briefly mentioned here. The Magnetic Sector analyser uses the behaviour of ions in a magnetic field to separate ions with different mass to charge ratios. Magnetic fields deflect the ions of the sample about a curved path. Heavier ions tend to be less deflected by the magnetic field than lighter ions, resulting in their separation according to mass. Quadrupole analysers are made up of four hyperbolic rods that are arranged in a square, with the rods lying parallel to one another. The particles that pass through the quadrupole are selected based on their mass to charge ratio by changing the voltage of the two pair of rods. That affects the trajectory of the ions causing some masses to pass through while others collide with the rods or escape between them (Longerich & Diegor 2001). In the Time of Flight analyser, ions are separated according to the time it takes them to travel along ~1 m long empty tube. The ions are accelerated into the tube giving them the same initial kinetic energy so that the velocity of each ion is based on its mass to charge ratio. Since the distance is a constant, travelling time will discriminate between ions of different masses (Kosler & Sylvester 2003).

In the detector unit, intensities of the analysed mass to charge ratios are measured either by pulse counting where the number of ions is counted, or by measuring the voltage generated by the ion beam current that hits the detector. Belonging to the second group are Faraday detectors that are often used for multi-collector mass spectrometry. Several cups can then be functioning at the same time where each cup of the detector catches ions with a specific mass to charge ratio (Longerich & Diegor 2001).

The mass of ions affects how effectively they are transferred through the system of mass spectrometers. To account for the mass bias and to obtain the true values of each isotope, corrections have to be applied to the measured values. This is done either by using external or internal corrections and applying an exponential or a power law to the measured values. External correction involves measuring a known isotopic ratio of a standard to account for how much the measurement deviates from the true ratio of the standard (Kosler & Sylvester 2003). Internal correction is based on that ratios between non-radiogenic isotopes are known. By measuring these isotopic ratios along with the isotopic ratios in question, a mass bias correction can be made. Better accuracy and precision is commonly attained in mass bias corrections by using a reference isotopic ratio with an average mass equal or similar to the unknown ratios (Vance & Thrilwall 2002).

5 Results

U-Th-Pb analyses were carried out on 258 spots in 254 detrital zircons collected from the river beds of Red Volta, Sihili, and Black Volta rivers in northern Ghana, and Ankobra and Birim rivers in southern Ghana (Fig. 2). Catchment areas of the rivers cover an extensive part of Ghana as well as southern and western Burkina Faso, and were selected to avoid input from the Neoproterzoic Volta basin (Fig. 10). Zircon U-Pb data were screened for precision and data with a 1σ error >30 Ma were rejected (Fig. 11a). In addition, data that is >10% discordant was also rejected (Fig. 11b). A total of 26 zircon grains were discarded using these criteria. Oxygen analyses were carried out on 191 of the zircon grains, from all sampling sites except for the Sihili river. Lu-Hf analyses were carried out on 226 grains where one analysis was omitted due to unstable signal of stable isotopic ratios during the analysis. Results from all analyses along with calculated ε_{Hf} values and model ages (T_{NC}) are listed in Appendix II and Tera-Wasserburg diagrams with all the zircon is found in Appendix III.

5.1 Description of samples

In the sample collected from Ankobra river (ASGH 015A), 58 zircon grains were analysed for U-Pb crystallisation ages, 50 for oxygen isotope ratios and 49 for Lu-Hf isotopes. Of the 58 U-Pb analyses, three were rejected due to discordance or lack of precision. Grains are between 100-200 μm long and have igneous zoning; some more faintly zoned than others (Fig. 12).

From Birim river (ASGH 029D), 40 zircon grains were analysed for U-Pb crystallisation ages, 39 for oxygen isotope ratios and 36 for Lu-Hf isotopes. Of the 40 U-Pb analyses, six were omitted due to discordance or lack of precision. Unzoned zircon are more abundant in this population than in the other populations but several grains have igneous zoning. Grains tend to be smaller than in the other populations with the long axis mostly ranging between 75-125 μm (Fig. 13).

From Black Volta river (ASGH 059A), 52 zircon grains were analysed for U-Pb crystallisation ages, 51 for oxygen isotope ratios and 47 for Lu-Hf isotopes. Of the 52 U-Pb analyses, six were omitted due to discordance or lack of precision. Grains are commonly 150-200 μm long. Both unzoned zircon and zircon with weak and distinct igneous zoning are present in the sample (Fig. 14).

From Red Volta river (ASGH 088B), 52 zircon grains were analysed for U-Pb crystallisation ages, 51 for oxygen isotope ratio and 46 for Lu-Hf isotopes. Of the 52 U-Pb analyses, two were omitted due to discordance or lack of precision. The size of the zircon is

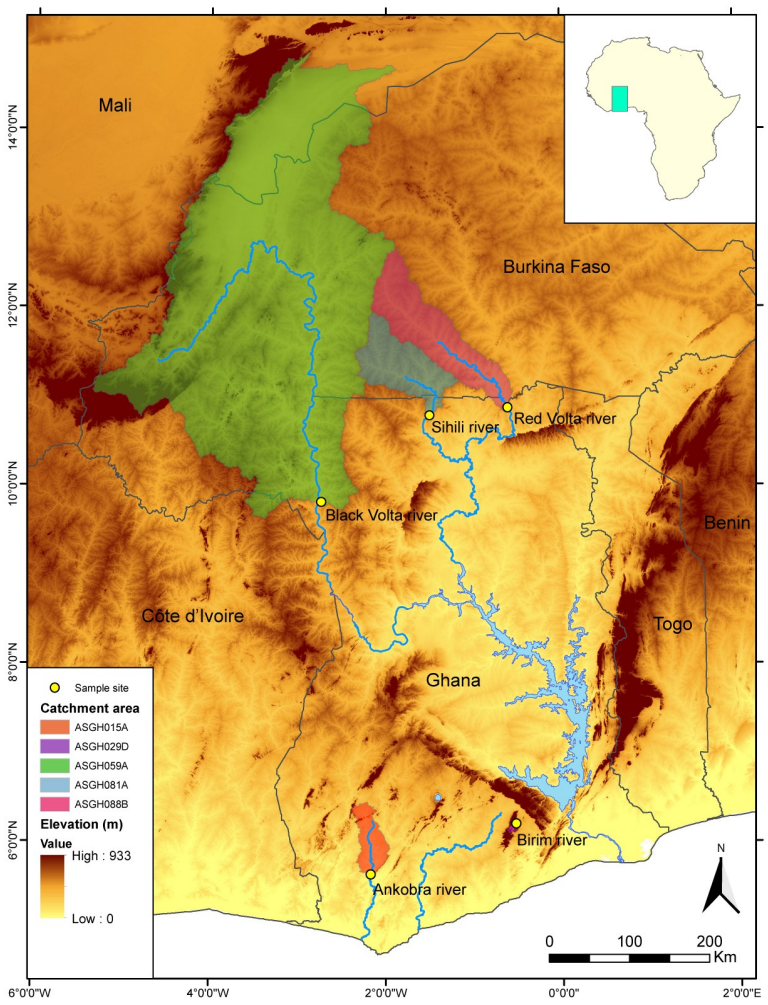

Fig. 10. Map showing the catchment areas of the five rivers, upstream of the sampling sites. Map was made by using a Digital Elevation Model (DEM). Black Volta river (ASGH 059A) has the most extensive catchment area of all the rivers, ranging over ~110.000 km^2 in Burkina Faso and northwestern Ghana. The areal distribution in the northernmost part of the catchment area might though be overestimated due to flat lying surfaces that make it more difficult to determine the flow direction of rivers and streams. Catchment areas of Red Volta (ASGH 088B) and Sihili (ASGH 081A) rivers range over ~7.200 km^2 and ~11.000 km^2 respectively and cover parts of Burkina Faso and northern Ghana. The catchment areas of Ankobra (ASGH 015A) and Birim (ASGH 029D) rivers lie within southern Ghana and cover areas of ~2500 km^2 and ~100 km^2 respectively (Map made by Mikael Grenholm).

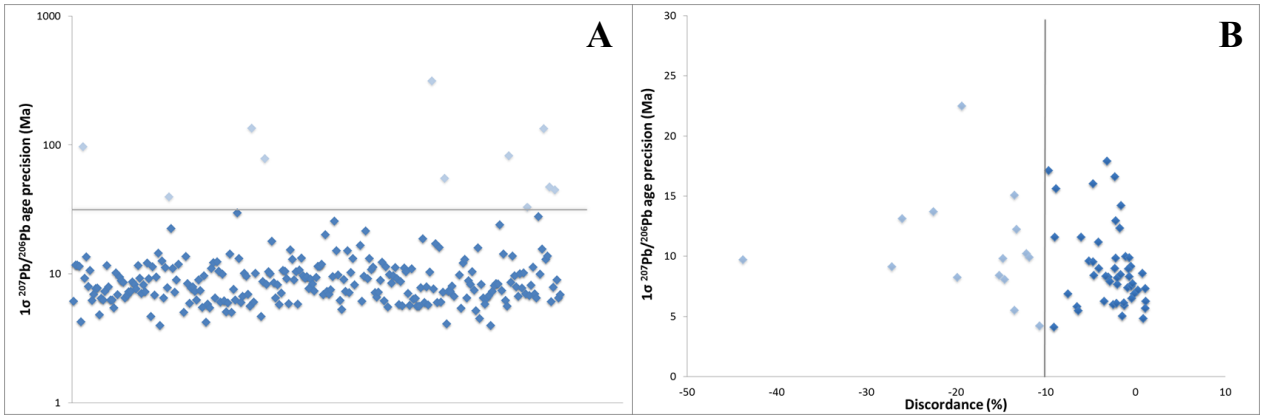

Fig. 11. A) All U-Th-Pb analyses yielding $^{207}Pb/^{206}Pb$ ages with a precision poorer than 30 Ma were rejected. Out of 258 analysed spots, 11 zircon were rejected based on this criterion. These are represented by the light blue diamonds, plotting above the 30 Ma boundary line. B) After precision filtering, all zircon having discordance greater than 10% were rejected. 15 zircons were eliminated based on this criterion. These are represented by the light blue diamonds to the left of the -10% discordance.

commonly in the range of 100-200 µm and nearly equal portions of unzoned and igneous zoned zircon are present in the sample (Fig. 15).

From Sihili river (ASGH 081A), 56 zircon grains were analysed for U-Pb crystallisation ages and 48 for Lu-Hf isotopes. No zircon was analysed for oxygen isotopes. Of the 56 U-Th-Pb analyses, nine were omitted due to discordance or lack of precision. As for the zircon from Red Volta river, most zircon range in size between 100-200 µm and nearly equal portions of unzoned and igneous zoned zircon are present in the sample (Fig. 16).

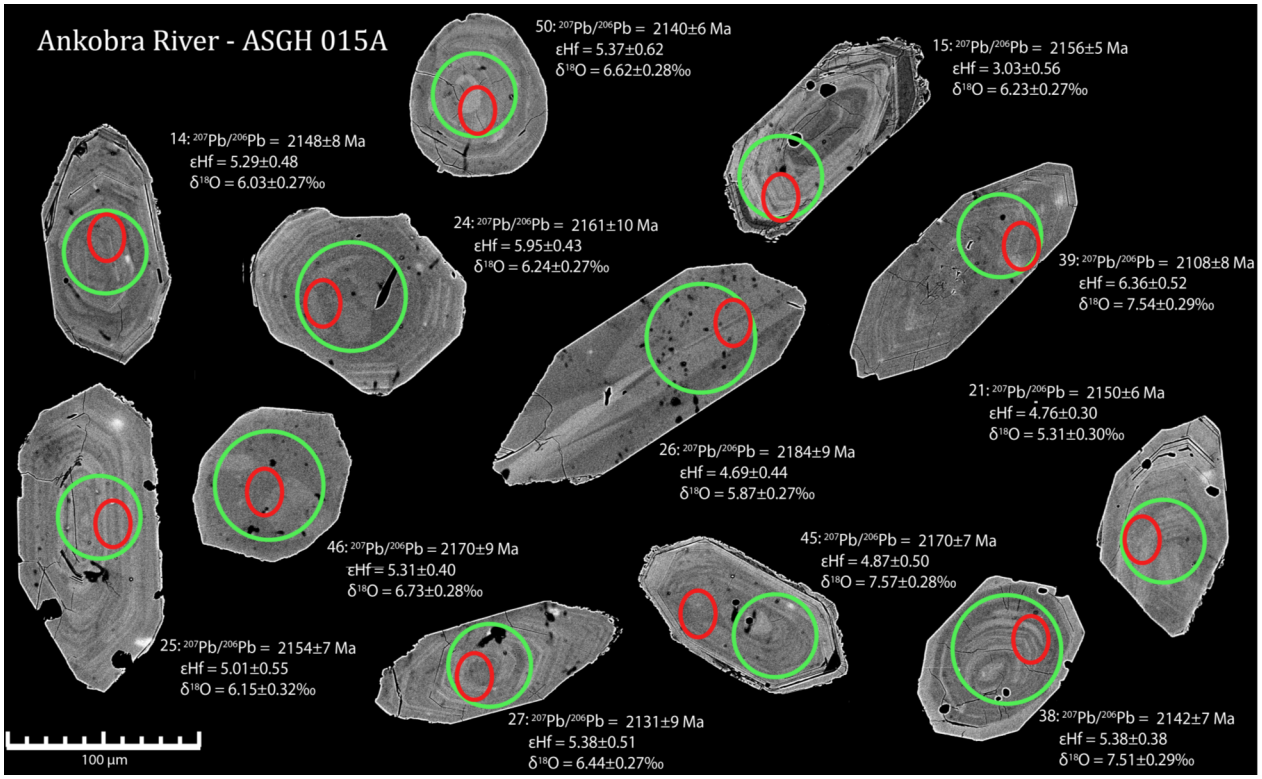

Fig. 12. BSE of detrital zircon from Ankobra river (ASGH 015A). Red ellipsoids mark the spot for U-Th-Pb analyses and green circles the spot location for Lu-Hf analyses.

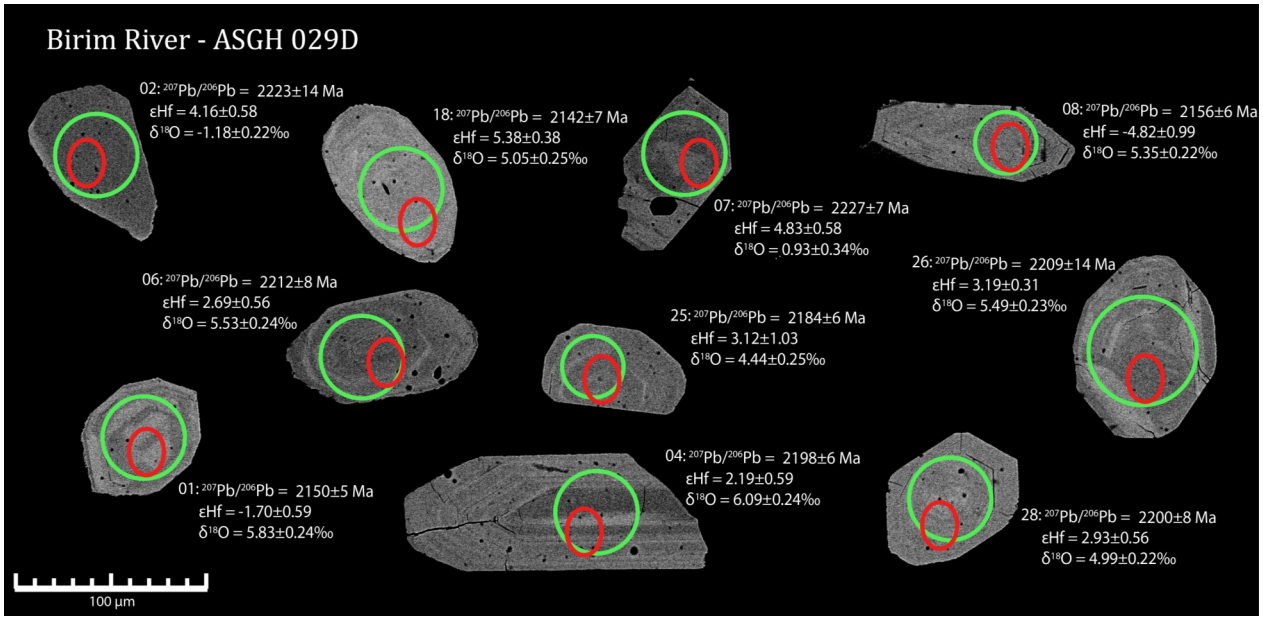

Fig. 13. BSE of detrital zircon from Birim river (ASGH 029D). Red ellipsoids mark the spot for U-Th-Pb analyses and green circles the spot location for Lu-Hf analyses.

Fig. 14. BSE of detrital zircon from Black Volta river (ASGH 059A). Red ellipsoids mark the spot for U-Th-Pb analyses and green circles the spot location for Lu-Hf analyses.

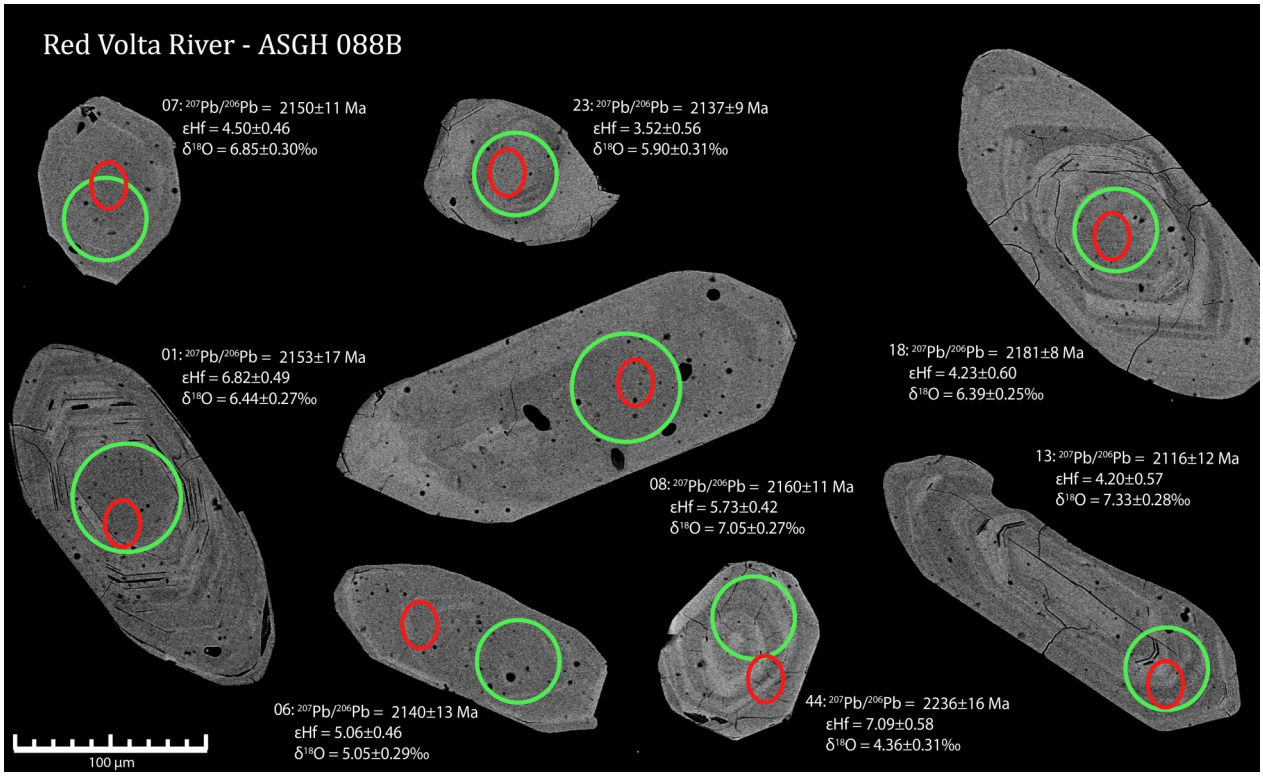

Fig. 15. BSE of detrital zircon from Red Volta river (ASGH 088B). Red ellipsoids mark the spot for U-Th-Pb analyses and green circles the spot location for Lu-Hf analyses.

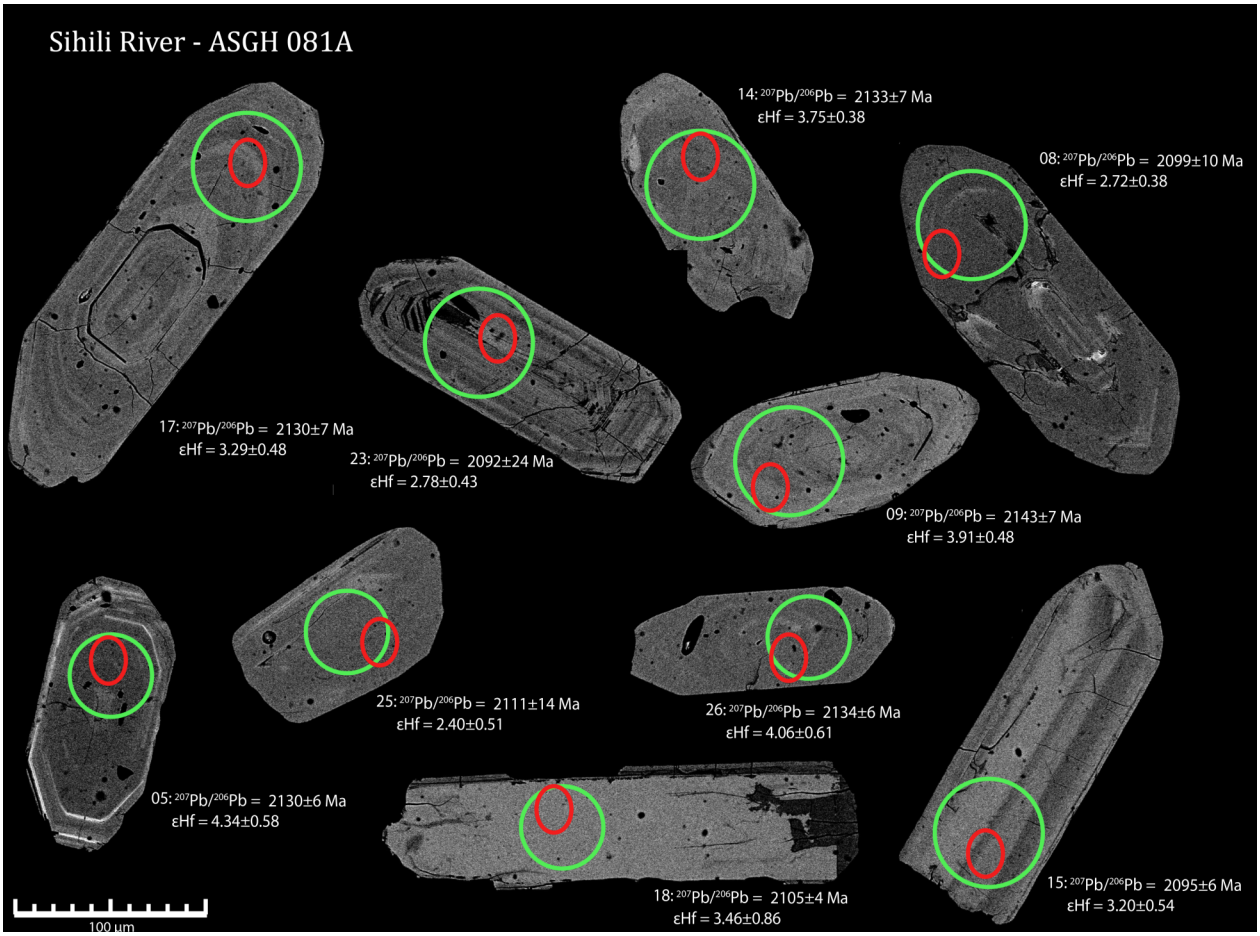

Fig. 16. BSE of detrital zircon from Sihili river (ASGH 081A). Red ellipsoids mark the spot for U-Th-Pb analyses and green circles the spot location for Lu-Hf analyses.

5.2 Crystallisation & model ages

The catchment area of Ankobra river lies mainly within the Kumasi basin in southwestern Ghana (Fig. 10). U-Pb crystallisation ages in the zircon population range between 2200±6 Ma and 2101±8 Ma. One crystal falls outside of this age span and is dated to 2263±12 Ma. They form a prominent peak at around 2150 Ma. Hf model ages were calculated in reference to NC values (Dhuime et al., 2011a) using a $^{176}Lu/^{177}Hf$ of 0.015 for the magma. In the Ankobra river sample they range from 2437 Ma to 2156 Ma and form a relatively flat curve with the greatest density between 2225 and 2325 Ma (Fig. 17).

The sampling site of the Birim river is located relatively close to the source of the river, resulting in a rather restricted catchment area within the Kibi-Winneba belt (Fig. 10). Another sample was collected downstream from the sampling site of the ASGH 029D sample, but that contained a large zircon fraction that is presumably derived from the Volta Basin, and was therefore disregarded in this study. The main zircon population has crystallisation ages ranging between 2233±10 Ma and 2124±30 Ma with a major peak at ~2220 Ma and a smaller one at ~2150 Ma (Fig. 17). Two additional grains are dated to 1494±6 Ma and 1883±6 Ma. Hf model ages mostly vary from 2572 Ma to 2352 Ma but one zircon has a model age of 1656 Ma and five zircons range between 2697 Ma and 2946 Ma. Model ages form a single peaked curve with the greatest density at ~2450 Ma (Fig. 17).

Black Volta river has the most extensive catchment area of the five sampling sites, ranging over a large area of western Burkina Faso and following the Lawra belt in Ghana (Fig. 10). Due to little difference in elevation in the northernmost part of the catchment area, the areal distribution of the northern part of the catchment area might be overestimated. The crystallisation ages of zircon from Black Volta river have a relatively wide age spread ranging between 2097±8 and 2282±6 Ma with marked peaks at ~2135 Ma and ~2170 Ma (Fig. 17). The scattered age distribution as compared to other detrital zircon populations might be a factor of the diversity of rock types close to the sampling site or larger catchment area. Most model ages fall between 2435 Ma and 2240 Ma with a prominent peak at around 2330 Ma. Two additional grains have distinctively younger and older model ages of 2174 Ma and 2500 Ma.

Catchment areas of Red Volta and Sihili rivers lie adjacent to one another in northern Ghana and southern Burkina Faso (Fig. 10). Both detrital populations peak at ~2130 Ma with an additional smaller

peak at ~2100 Ma in the Sihili population. Zircon from Red Volta river have crystallisation ages ranging between 2236±16 Ma and 2114±21 Ma with one zircon falling outside of this interval, having a crystallisation age of 2365±17 Ma. Hf model ages vary from 2387 Ma to 2164 Ma with one zircon having a distinctively older model age of 2589 Ma (Fig. 17). The main zircon population from Sihili river has crystallisation ages ranging between 2188±9 Ma and 2081±16 Ma with one distinctively older age of 2268±10 Ma (Fig. 17). Hf model ages range between 2437 Ma and 2254 Ma.

5.3 Hafnium - ε_{Hf}

A large portion of the zircons have positive ε_{Hf}, plotting relatively close to the New Crust (NC) evolutionary curve defined by Dhuime et al. (2011a) and rede-

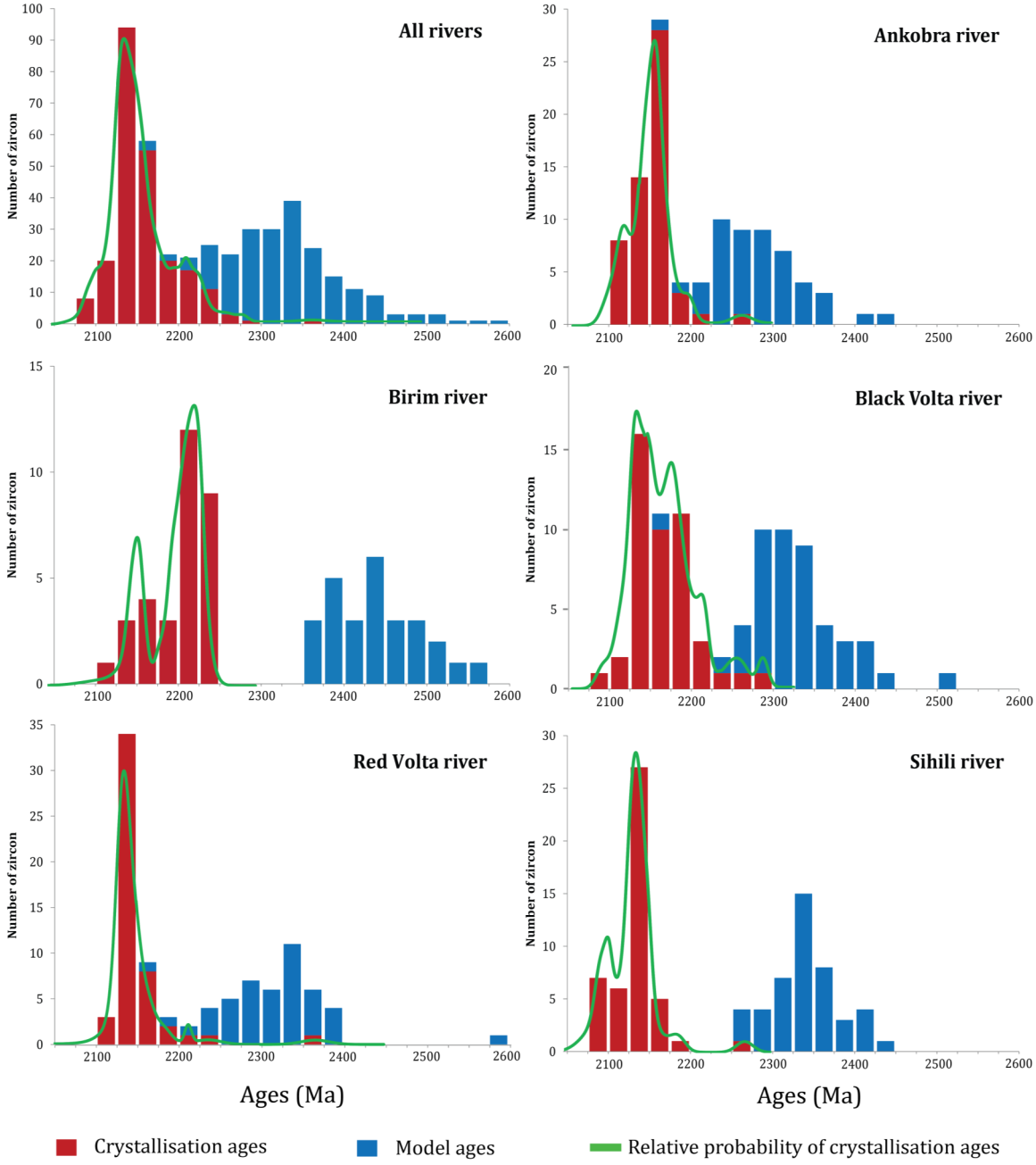

Fig. 17. Histogram showing the number of zircon with crystallisation ages (red) and model ages (blue) that belong to each 25 Ma age bracket, ranging from 2050 Ma to 2600 Ma. Model ages were calculated in reference to NC values (Dhuime et al. 2011a), using a $^{176}Lu/^{177}Hf$ of 0.015 for the magma. Two zircon grains from Birim river dated to 1494±6 Ma and 1883±6 Ma are not represented in the histograms. Model ages of five zircon grains from Birim river are not represented in the histogram, one with a model age of 1656 Ma and four with model ages ranging between 2697 Ma and 2946 Ma. Relative probability of crystallisation ages was calculated based on their $^{207}Pb/^{206}Pb$ ages and 1s errors using Isoplot 4.15 (Ludwig 2008).

fined here by anchoring ε_{Hf} = 0±1.1 to 4.5 Ga based on data from Næraa et al. (2012) (Fig. 18). The zircon population from Ankobra river has an ε_{Hf} signature lying between 3.0±0.6 and 6.4±0.4 and deviating from the NC values by an average of 2.04±0.73 (1σ) epsilon units, which yields an average protocrust residence time (here defined as the time between mantle model age and zircon crystallisation) of 129±46 Ma (1σ).

Similar ε_{Hf} values are recorded in the zircon populations from the Black Volta river, Red Volta river and Sihili river. Black Volta river zircon grains have an ε_{Hf} signature lying between 2.6±0.4 and 6.9±0.5 deviating from the NC values by an average of 2.55±0.96 epsilon units, which yields an average residence time of 161±60 Ma. Red Volta river zircon grains record ε_{Hf} signature lying between 3.2±0.7 and 7.1±0.6 with an additional zircon yielding ε_{Hf} of -0.1±0.5. The values deviate from the NC values by an average of 2.71±1.17 having an average residence time of 171±74 Ma. The zircon population from Sihili river has ε_{Hf} lying between 1.6±0.7 and 5.4±0.5 and deviates from the NC values by an average of 3.28±0.74 which gives an average residence time of 207±47 Ma. These values are somewhat higher than those recorded by the other three detrital samples and it is highlighted by the decoupling of crystallisation ages and model ages (Fig. 17).

Zircon grains collected from Birim river have a ε_{Hf} signature lying between -8.4±1.0 and 6.4±0.8, deviating from the NC values by an average of 4.92±3.33 epsilon units. This yields an average residence time of 310±209 Ma. The large standard deviation is in particular affected by five grains that yield ε_{Hf} lower than zero. The zircon population from Birim river is the one that plots furthest away from the new crustal values.

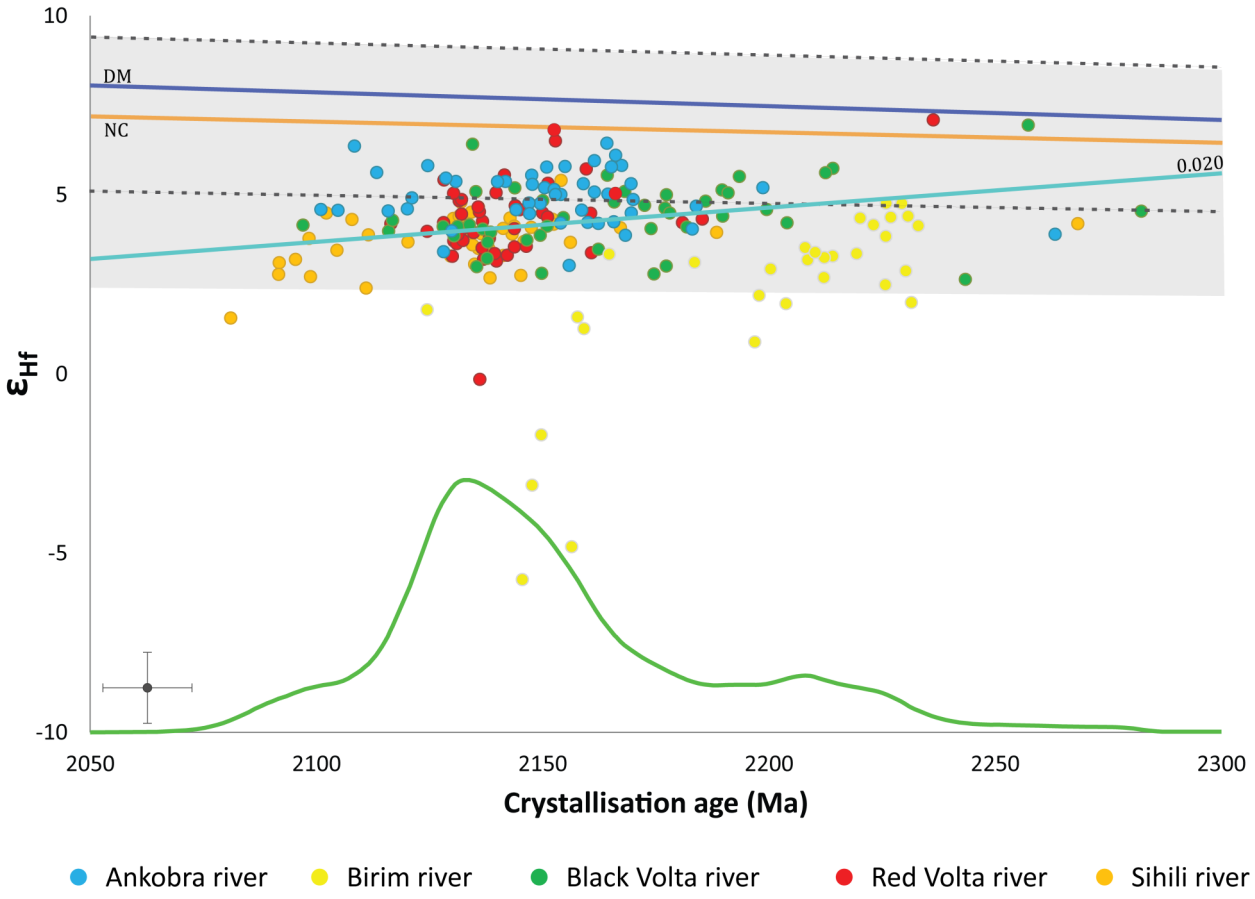

Fig. 18. NC (orange) evolutionary curve is calculated according to present day values (13.2±1.1) of island arc crust compiled by Dhuime et al. (2011a), assuming a ε_{Hf} = 0.0±1.1 at 4500 Ma based on Næraa et al. (2012). Slightly higher average ε_{Hf} of 13.3 for modern island arc crust was estimated by Iizuka et al. (2013) with a much greater scattering than represented in Dhuime et al. (2011a). The field of juvenile crust, according to estimates of Iizuka et al. (2013) is represented by the grey error envelope. However, the error towards lower value might be overestimated due to number of island arc magmas that yield an unusually low ε_{Hf} for juvenile magmas. If the lower error is estimated to be equal to the upper error, zircon that crystallised from juvenile, island arc magmas would fall within the field outlined by the dashed lines. Evolutionary curve of a crustal component that has $^{176}Lu/^{177}Hf$ of 0.020 and separated from the mantle at 2400 Ma is represented by the light blue line. Green curve describes the relative probability of crystallisation ages from Fig. 17. Two zircon that were analysed for Lu-Hf fall outside of the age span represented on the graph. These are two zircon from the Birim river population that have U-Pb crystallisation ages of 1494±6 Ma and 1883±6 Ma, and ε_{Hf} of 6.38±0.83 and -8.43±0.99 respectively. Error bars in the lower, left corner represent an ε_{Hf} error of ±1.0 epsilon unit and a crystallisation age error of ±10 Ma.

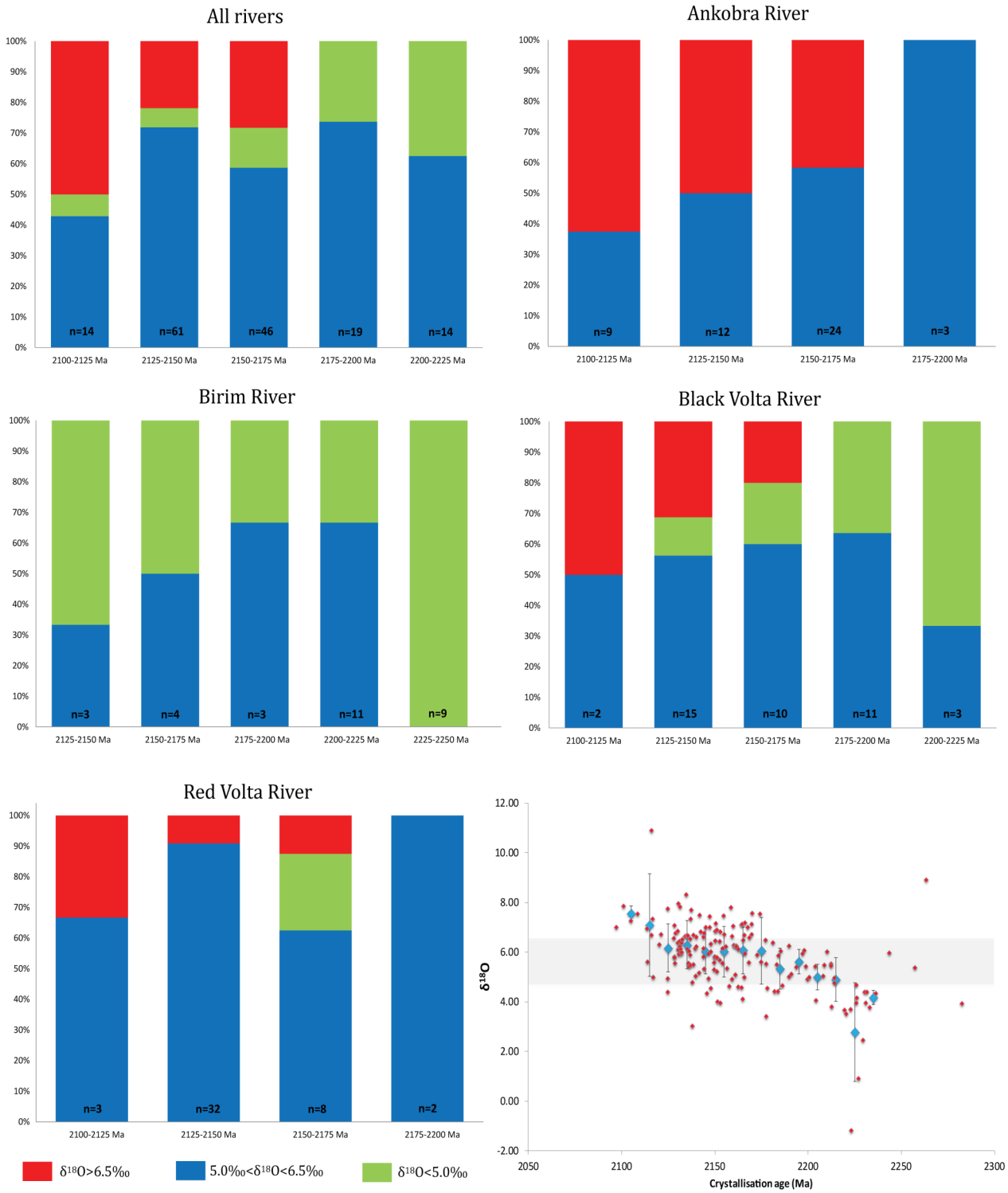

Fig. 19. Zircon grains are divided into three groups according to their $\delta^{18}O$. Zircon that crystallised in magmas with mantle-like oxygen isotope ratios have $\delta^{18}O$ ranging between 5.0‰ and 6.5‰ while those who have $\delta^{18}O$>6.5‰ are considered to have grown in melts containing supra-crustal material. Magmas that have been affected by light $\delta^{18}O$ meteoric water are presumably the reason for zircon with $\delta^{18}O$<5.0‰. The zircon population from Birim river is the only population that does not show any crustal reworking, while for the other three populations there is a stepwise increase in recycling of supra-crustal material from 2175 Ma to 2100. Low $\delta^{18}O$ zircon are most common in the Birim river population and tend to be represented by zircon older than 2150 Ma in the other populations. Bins based on two or more zircon (n≥2) are only shown. When crystallisation ages of the zircon are plotted against their $\delta^{18}O$ a correlation is seen between increased $\delta^{18}O$ and younger ages. Blue diamonds represent the average $\delta^{18}O$ for each 10 Ma, red diamonds represent individual zircon analysis and grey bar represents the field of mantle-like $\delta^{18}O$ values.

5.4 Oxygen – $\delta^{18}O$

Oxygen isotope analyses were carried out on four of the detrital populations, excluding the Sihili river population. The zircon grains are divided into three groups based on their $\delta^{18}O$ values. These groups are zircon with mantle-like $\delta^{18}O$ values ($5.0‰ \leq \delta^{18}O \leq 6.5‰$), zircon with heavy $\delta^{18}O$ signature ($\delta^{18}O < 6.5‰$) and zircon with light $\delta^{18}O$ signature ($5.0‰ < \delta^{18}O$).

Oxygen isotope ratios of zircon from Ankobra river vary between 5.31±0.30‰ and 8.92±0.31‰. Based on oxygen data, 54% of the zircon grains have, within error, mantle-like isotope values (<6.5‰) but no zircon with a $\delta^{18}O$ lower than 5.0‰ was recorded. Birim river zircon have oxygen isotope ratios between 0.93±0.34‰ and 6.09±0.24‰ with one exception of -1.18±0.22‰. 44% of the zircon have, within error, mantle-like isotope values and the remaining zircon have an oxygen isotope ratio lower than mantle-like values (>5.0‰). Zircon grains from Black Volta river have oxygen isotope ratios that vary between 3.02±0.16‰ and 8.32±0.18‰ with an additional grain having a $\delta^{18}O$ of 10.91±0.19‰. Based on oxygen data, 56% of the zircon have, within error, mantle-like isotope values, 20% have an oxygen isotope ratio greater than 6.5‰ and 24% lower than mantle-like values. Oxygen isotope ratios of zircon grains from Red Volta river vary between 3.96±0.25‰ and 7.33±0.28‰ with 83% of the zircon yielding, within error, mantle-like isotopic values, 10% have $\delta^{18}O$ greater than 6.5‰ and 6% lower than mantle-like values.

Apart from one zircon from Ankobra river dated to 2263±12 Ma, no zircon with a heavy oxygen isotope ratio is recorded in the zircon populations prior to ~2.17 Ga (Fig. 19) but the proportion of zircon with $\delta^{18}O > 6.5‰$ becomes more prevalent with younger crystallisation ages. This trend is particularly apparent in the populations from Ankobra and Black Volta rivers but is absent in the Birim river population (Fig. 19). Zircon grains with mantle affinities are found throughout age span as well as zircons with lower than mantle-like $\delta^{18}O$.

6 Discussion

6.1 Are crystallisation and model ages of the detrital zircon representative for their catchment areas?

When working with detrital zircon samples it is necessary to try to assess how representative the zircon populations are for the area from which they are collected. Crystallisation ages are repeated throughout the Baoulé Mossi domain in Ghana making it difficult to link detrital zircon to a certain basin or belt. However, most ages reported here lie within previously reported ages from the Birimian bedrock (Hirdes et al. 1992; Taylor et al. 1992; Davis et al. 1994; Oberthür et al. 1998; Hirdes & Davis 1998; Feybesse et al. 2006) indicating negligible contribution from other areas.

Two zircon grains from the Birim river sample have younger U-Pb ages than is commonly reported from Ghana. The Birim river flows along the Kibi belt towards NNE. Before it turns around and continues along the Cape Coast basin towards SW, it flows close to the Volta basin. Sediment from the Volta basin contains zircon derived from the Birimian bedrock as well as Archaean zircon that are assumed to be derived from the Archaean domains of the WAC. Zircon grains with crystallisation ages ranging between 1100 and 1900 Ma are also common in the Volta basin and are thought to be derived from cratons that were previously adjacent to the WAC, presumably the Amazonian craton (Kalsbeek et al. 2008). Sample ASGH 036A was collected from the Birim river, further downstream than sample ASGH 029D and was not analysed for Lu-Hf and O isotopes since it contained several zircon with U-Pb ages that do not coincide with ages of the Birimian bedrock. These U-Pb zircon ages do however coincide with zircon ages found in the Volta basin making it a plausible source for some of the zircon from that sample. The contribution of Volta basin sediments is most likely minor in the sample from Birim river that was analysed in this thesis (ASGH 029D); where these two zircon grains are the only ones that have ages not coinciding with Birimian rocks.

6.2 Juvenile nature of the Birimian terrain

Zircon grains that have ε_{Hf} close to the mantle reservoir at the time of crystallisation, and therefore model ages similar to their crystallisation ages, are thought to have crystallised from a juvenile magma without substantial contribution from an older crustal component. In previous studies of Hf-model ages in zircon, it has been noted that over 100 million years commonly separates zircon model ages and their crystallisation ages (Kemp et al. 2006; Pietranik et al. 2008; Wang et al. 2009; 2011; Lancaster et al. 2011). The residence time recorded in zircon has been linked to the assumption that most zircon bearing magmas do not form in a single step (Wang et al. 2009). Partial melting of the mantle most likely yields mafic, silica-undersaturated magmas (Rudnick 1995 and references therein), in which zircon is not likely to form (Hoskin & Schaltegger 2003). However, the length of the calculated residence time depends on the estimated nature of the reservoir from which the juvenile magma is assumed to have separated from. Commonly, model ages are calculated with reference to depleted mantle (DM) values (Kemp et al. 2006; Pietranik et al. 2008; Wang et al. 2009; Lancaster et al. 2011). Subduction zones are presumably an important site for additions of volume to the crust (Hawkesworth & Kemp 2006) and therefore a new evolutionary curve with present day $\varepsilon_{Hf} = 13.2 \pm 1.1$ was proposed based on data from modern island arcs (Dhuime et al. 2011a). The new curve has somewhat lower ε_{Hf} at present than has been suggested for the DM (Vervoort & Blichert-Toft 1999; Griffin et al. 2002; Hawkesworth et al. 2010).

A second evaluation of modern island arc rocks indicates that they are more heterogeneous than the error of ±1.1 ε-units indicates (Iizuka et al. 2013). An upper limit of ε_{Hf} = 17.2 and a lower limit of ε_{Hf} = 4.5 with an average of ε_{Hf} = 13.3 was suggested by Iizuka et al. (2013), where the average value falls close to the value estimated by Dhuime et al. (2011a). However, despite their effort not to use modern island arc rocks from areas where crustal contamination is thought to be plausible, the low value of the lower limit from Iizuka et al. (2013) is affected by several analyses having unusually low ε_{Hf} for juvenile magmas. This might indicate significant contribution from an older, crustal source. A way to avoid this is to assume that the lower limit deviates from the average value to the same extent as the upper limit. This results in an ε_{Hf} value of 13.3±3.9 that is projected to 0.0±0.0 at 4560 Ma to form a new depleted compositional band, defined as new crust (NC).

A majority of all zircon presented here fall within error from the NC when extrapolating the errors suggested by Iizuka et al. (2013) from present day values to ε_{Hf} = 0.0±0.0 at 4560 Ma (Fig. 18). If assuming that the lower error of Iizuka et al. (2013) is an overestimate and adjust it so that it equals the upper error, majority of zircons fall slightly below the juvenile field (Fig. 18) but nevertheless fall relatively close to it indicating a minor contribution from a reworked crust in the magmas, which supports the previously suggested juvenile nature of the Birimian bedrock (Boher et al. 1992; Taylor et al. 1992; Doumbia et al. 1998; Gasquet et al. 2003).

The zircon population from the Birim river stands out by having both the oldest crystallisation and model ages. The zircon grains that belong to the larger subgroup from the Kibi-Winneba belt and crystallised at ~2.22 Ga, have a similar or slightly older residence time than zircon grains from other populations. This indicates that they crystallised from relatively juvenile magmas. A few zircon grains from the smaller and younger subgroup that crystallised at ~2.15 Ga, have however distinctly lower ε_{Hf}(<0) and a residence time longer than 500 Ma. These low ε_{Hf} and long residence times indicates reworking of old, Archean crust. Archaean (2620-2600 Ma) Nd-model ages were reported from ~2.17 Ga Winneba granitoids west of Accra in southern Ghana (Taylor et al. 1992). The model ages of those ~2.17 Ga granitoids are in agreement with the model ages presented here for the Kibi-Winneba belt. Furthermore, a tonalite and a granite from the Suhum basin, which is located southeast of the Birim river sampling site, have model ages of around 2.8 Ga and 2.3 Ga respectively, where the older model ages belong to the younger intrusion.

Zircon with Hf-model ages older than 2500 Ma have mantle-like or mildly lowered $\delta^{18}O$. They range from having igneous zoning, indicating an undisturbed, magmatic origin, to being unzoned. The preserved igneous zoning along with concordant U-Pb ages and Th/U>0.1 indicates that the zircon grains record their original, igneous isotope signature. The data implies that the Kibi-Winneba belt initially grew through emplacement of juvenile magmas without major influences of older components and therefore in some distance from an Archaean crust. Rocks that crystallised at ~2.15 Ga and record contribution from an ancient Archaean crust, which seemingly did not contribute to magmas in the other belts and basins.

6.3 Influences of old Archaean component or juvenile crust?

Oxygen isotope ratios can be a helpful tool in identifying supracrustal components in magmas where deviations from the mantle values are thought to be indicative of influences of a recycled or a reworked component. The difference between a recycled and a reworked component is that a recycled component is transported to the mantle and can later become a part of the crust again, while a reworked component is only transferred and mixed within the crust but does not enter the mantle (Table 1) (Hawkesworth et al. 2010). A mixing model was used to estimate the potential contribution of the reworked or recycled material in the magma based on $\delta^{18}O$ and ε_{Hf}. The model is based on several assumptions and is therefore not meant to give precise results but to indicate the extent of mixing and possible nature of the components contributing to the magma.

Various end components were used to see which one would fit best to the data. No Archaean crust, that could give an idea of the nature of a possible ancient reworked component, is present in the eastern Man Shield. The Archaean component is therefore assumed to have an ε_{Hf} value of -10 at 2150 Ma based on the lowest ε_{Hf} values in zircon from Birim river and a granite and a tonalite from the Suhum basin (Anders Scherstén, unpublished data). Two O-isotope ratios are assumed for the ancient component. These represent a crust that has preserved its mantle-like oxygen isotope ratio ($\delta^{18}O$ = 5.7‰) and a sedimentary component with an average $\delta^{18}O$ value of sediments ($\delta^{18}O$ = 14‰) (Simon & Lécuyer 2005). No attempt is made to correct for the difference between whole rock and zircon $\delta^{18}O$. Zircon tends to record a slightly lower $\delta^{18}O$ than the magma which it crystallised from, where the difference between zircon and whole rock samples is fairly small in mafic magmas (~0.4‰) but increases in more evolved magmas (Valley et al. 2005). Mixing with sediments that have undergone relatively rapid recycling was also considered, represented by components with $\delta^{18}O$ = 14‰ and ε_{Hf} between 0 and 6. The juvenile end component is assumed to have ε_{Hf} = 7.0 at 2150 Ma based on NC values (Dhuime et al. 2011a) and $\delta^{18}O$ = 5.7‰ (Simon & Lécuyer 2005). Ratios between concentrations of Hf and O in crustal (MC - Mixed Crust) and juvenile (JC - Juvenile Crust) sources is assumed to be C_{JC}/C_{MC} = 0.4 for Hf and C_{JC}/C_{MC} = 1.0 for O based crustal and mantle compositions

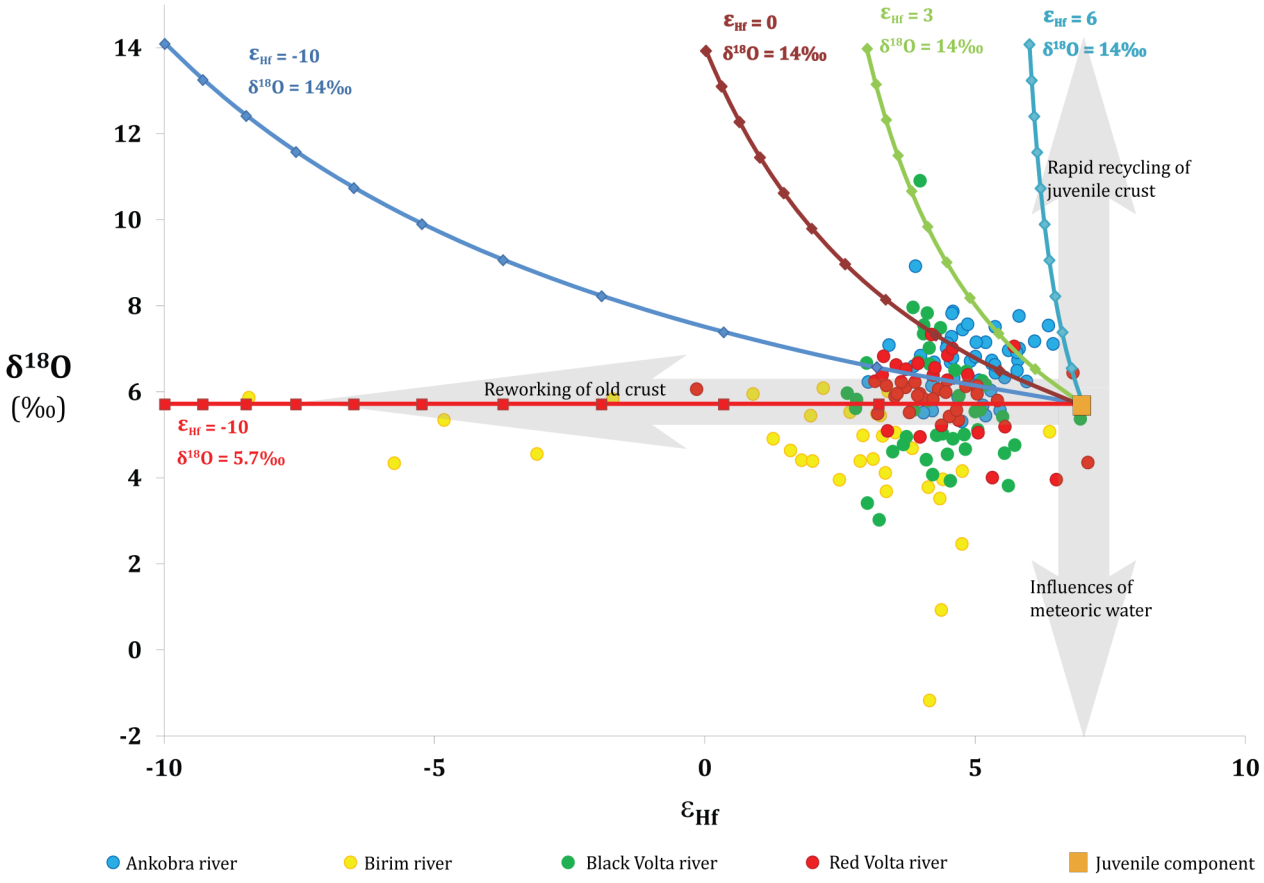

Fig. 20. Mixing model describing a mixing between a juvenile component (orange square) with ε_{Hf} = 7.0 at 2150 Ma and $\delta^{18}O$ = 5.7‰, and altering crustal components. Crustal components with ε_{Hf} between -10 and 6 were used in the model, representing ancient and juvenile crustal components. Two oxygen isotope ratios were used, representing crust with mantle-like $\delta^{18}O$ (5.7‰) and the average values of sediments (14‰) (Simon & Lécuyer 2005). Ticks represent 10% mixing. Meteoric water is the most probable source for low $\delta^{18}O$. Reworking of ancient crust results in zircon with low ε_{Hf}, while rapid reworking or recycling of juvenile crust leads to zircon with juvenile ε_{Hf} and elevated $\delta^{18}O$. The model suggests minor contribution from older crustal components in the Palaeoproterozoic, Birimian bedrock, with the contribution of an older component being less than 10% for the majority of the zircon. Few zircon grains from the Birim river (yellow) are an exception of this and form a mixing line between ancient and juvenile components. Zircon from the Ankobra river (blue) tend to be characterised by juvenile ε_{Hf} but heavy $\delta^{18}O$, indicating that the rocks of the Kumasi basin were in particular affected by rapid reworking of juvenile crust.

from Rudnick & Gao (2003) and Salters & Stracke (2004). The juvenile magma is assumed to be formed through 10% batch melting of a mantle peridotite.

Most of the zircon plot close to the juvenile component (Fig. 20) indicating little influence of an ancient crust, with generally less than 10% contribution. A few zircon from the Birim river are an exception of this and form a mixing line between a juvenile and an ancient component. Lack of significantly elevated oxygen isotope values in the Birim river sample indicates reworking of Archaean crust that has not undergone low temperature alteration. This crust presumably was mixed with a juvenile component that had a mantle-like $\delta^{18}O$, assuming closed system behaviour of the zircon after crystallisation.

A high $\delta^{18}O$ value in association with juvenile ε_{Hf} is observed in some zircon, particularly from the Ankobra river population. This can be retrieved through mixing of juvenile, mantle derived magma and juvenile supracrustal component that has undergone low temperature alteration and rapid reworking.

Early phases (e.g. olivine and pyroxene) in Phanerozoic island arc magmas tend to have mantle-like $\delta^{18}O$ but some deviate slightly from the mantle value, while whole rock samples often show higher values and can range up to 14‰ (Vroon et al. 2001; Eiler et al. 2000; Santo & Peccerillo 2008; Singer et al. 1992; Davidson 1985; Ito et al. 2003). Values retrieved from olivine and pyroxenes are thought to be better representatives of the original $\delta^{18}O$ of the magma since they are less susceptible to low temperature alteration than whole rock samples. However these mafic minerals belong to the less evolved magmas and therefore they might fail to record a rise in $\delta^{18}O$ asso-

ciated with fractional crystallisation (Eiler et al. 2000).

The deviations from mantle values recorded in modern island arc rocks has been explained by the involvement of high $\delta^{18}O$ hydrous fluids that are released from the subducting oceanic crust, addition of a melt fraction of the upper part of the subducted crust to the juvenile magma or assimilation of the overlying arc crust (Eiler et al. 2000; Vroon et al. 2001; Ito et al. 2003). Modelling indicates that the contribution of high $\delta^{18}O$ subducted crustal component to the magma commonly does not exceed 5% (Eiler et al. 2000; Ito et al. 2003; Vroon et al. 2001), but assimilation of the overlying crust can be much more extensive and is thought to be the reason for high $\delta^{18}O$ magmas of the Banda Arc (Vroon et al. 2001).

The model indicates that up to 30% contribution of a crustal component is needed to account for the observed $\delta^{18}O$ in most of the zircon that are enriched in ^{18}O, assuming a $\delta^{18}O$ of 14‰ of the crustal component (Fig. 20). This high degree of crustal contribution can not be explained solely by crustal contamination in the mantle, as indicated by the conditions at modern day island arcs. Assimilation of the host rock or underplating and assimilation of a juvenile oceanic crust and sediments, as has been proposed to be the case for juvenile, high $\delta^{18}O$ zircon of the Suludal arc (Roberts et al. 2013), might however be a plausible cause.

Oxygen isotope signatures of the detrital zircon presented here might furthermore be indicative of a maturing arc system. The proportion of zircon with $\delta^{18}O$>6.5‰ increases with younger crystallisation ages and a calculated 10 Ma running average indicates a continuous increase in the $\delta^{18}O$, from close to mantle values at ~2.20 Ga to 7.6‰ at ~2.10 Ga, without significant increase in contribution form an ancient crust. Older zircon grains are therefore presumably derived from juvenile, mantle derived magmas with little input from crustal components while the most probable explanation for the heavy oxygen signature in some of the younger zircon, is increased reworking of juvenile crust and sediments. This process of reworking forms a crust with an oxygen isotopic signature more similar to the average continental crust (Simon & Lécuyer 2005).

6.4 Low $\delta^{18}O$ zircon

Zircon with $\delta^{18}O$ lower than mantle-like values (<5.0‰) make up 19% of the total zircon population. They are most frequent in the Birim river sample where 18 low $\delta^{18}O$ zircons were analysed, having oxygen isotope ratios as low as -1.2±0.2‰. Low $\delta^{18}O$ in Archaean and Proterozoic zircon has been interpreted as being derived from high-temperature, hydrothermal alteration of a crustal protolith (Hiess et al. 2011; Zheng et al. 2004), or that hydrothermal alteration affected the zircon after its crystallisation (Iizuka et al. 2013). Lower oceanic crust has also been suggested as a source for low $\delta^{18}O$ magmas, since as opposed to the upper oceanic crust that has undergone low-temperature alteration, the lower oceanic crust has experienced high-temperature alteration and commonly has a $\delta^{18}O$ between 0-6‰ (Eiler et al. 2001).

Th/U ratios along with discordance and texture of the zircon have been used to identify zircon grains that preserve their original isotopic ratios from those that might be hydrothermally altered (Hiess et al. 2011). In the data presented here, no correlation is found between $\delta^{18}O$ and Th/U. Most of the zircon have Th/U > 0.2, which indicates that they have igneous origin (Rubatto 2002). None of the low $\delta^{18}O$ zircon contains apparent metamict zones or discordance, which might facilitate disturbance of the oxygen isotopic system after the crystallisation of the zircon (Valley 2003). However, the majority of the low $\delta^{18}O$ zircon are unzoned, a feature that is not unknown but uncommon in igneous zircon (Corfu et al., 2003), and might be an indication of disturbance in the isotopic system.

Analyses on zircon from Birimian granites in southeastern Ghana suggest a partial reset of their U-Pb system during the Pan-African orogeny, giving a lower intercept age at ~0.5 Ga. Meanwhile the Ar-Ar system in biotite and hornblende of the same granites seems to have withstood the Pan-African orogen and commonly reveals plateau ages between 2.00 and 2.06 Ga (Anders Scherstén, unpublished data). This would indicate that the Pan-African orogeny at around 0.5 Ga ago was not a tectonothermal event that exceeded the closure temperature of biotite, but rather a hydrous event that affected the U-Pb system in zircon (personal communication, Anders Scherstén). Given that low $\delta^{18}O$ zircon are most common in the Birim river sample, which is located close to the Pan-African mobile belt, hydrothermal alteration linked to the Pan-African orogeny might have caused some disturbance in the oxygen system as well as the U-Pb system of the detrital zircon analysed here. When plotting the detrital zircon grains from the Birim river population on an Tera-Wasserburg diagram (Appendix III), the discordant zircon define a line that intersects the concordia at ~550 Ma, which correlates with the timing of the Pan-African orogeny (Attoh et al. 1997). Discordant detrital zircon grains can however not be used in this manner to determine a lower intercept age since they are presumably derived from different rocks and therefore not formed in equilibrium with one another.

A $\delta^{18}O$ of a zircon that was affected by a hydrothermal event soon after its formation, could change significantly even though the U-Pb system, which is time related, would still plot within error from the concordia. This might be the explanation for the observed depletion in ^{18}O of some of the zircon that is not correlated with discordant U-Pb ages, but it is undermined by the observation that those zircon have an igneous Th/U ratio and there is no correlation between the texture of the zircons and their $\delta^{18}O$.

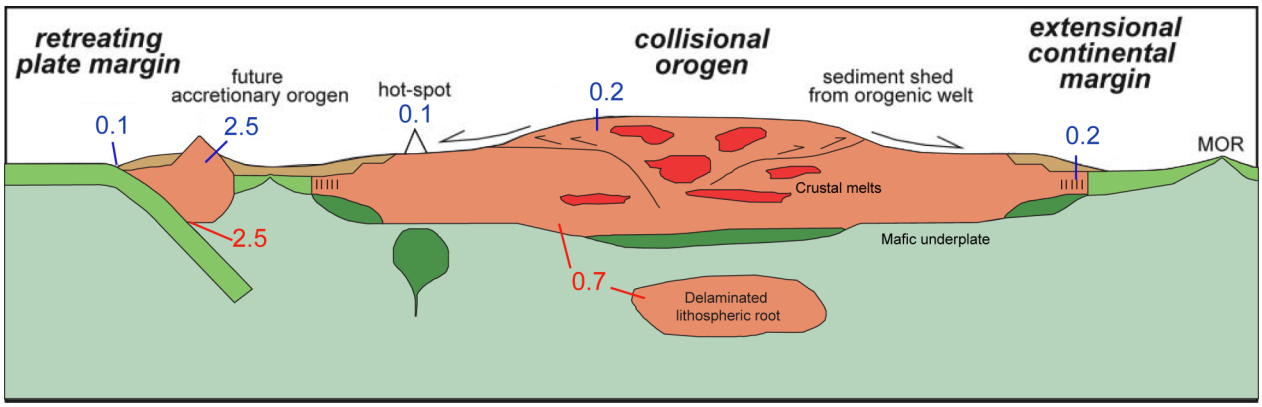

Fig. 21. Estimated addition (blue values) and removal (red values) of crustal volume based on Scholl & von Huene (2007, 2009). Values are given in km^3yr^{-1}. According to the estimated values, the volume of crust that is recycled to the mantle through sediment subduction, subduction erosion and delamination is on pair with the volume of juvenile magmas that is added to the crust. Figure redrawn from Hawkesworth et al. 2010.

6.5 Continental crustal growth

6.5.1 Generation of continental crust

Island arcs have been denoted as the main sites of addition of juvenile material to the crust. Estimates on the volume of magma that is added to the crust at modern day island arcs and the volume of crust that is recycled back into the mantle in the same tectonic setting, indicates that the net crustal growth rate is close to zero (Fig. 21) (Scholl & von Huene 2009) where some arcs have a positive net crustal growth rate while other arcs yield a loss of crust (Clift et al. 2009). Peaks in zircon crystallisation ages have been linked to episodic growth of crust due to periodicity in mantle plume activity caused by slab avalanches (Condie 1998) but the peaks also tend to correlate with supercontinent assemblies (Condie 1998; Campbell & Allen 2008). Continent-continent collisional margins are thought to be dominated by reworking of older crust and minor additions of juvenile material to the crust. However, this tectonic setting is presumably in favour of preservation of felsic crust leading to the zircon age peaks (Fig. 22) (Hawkesworth et al. 2009).

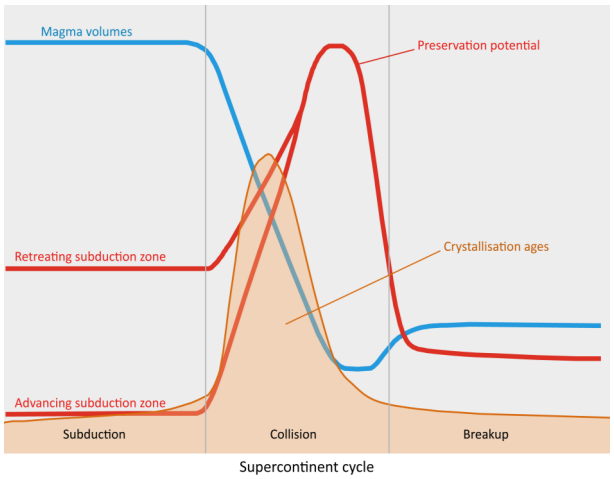

Fig. 22. The volume of preserved crust is not only dependent upon the volume of magma that is added to the crust (blue) but also the preservation potential of that crust (red). Even though the greatest volume of magma is added to the crust at subduction zones, the preservation potential of the crust formed in advancing subduction zones is presumably low, leading to a little preservation. During continental collision, less volume of juvenile magma is added to the crustthan in subduction zones. A better preservation potential of the crust in collision zones might lead to that greater volumes of crust is preserved. This might have led to the observed peaks in zircon crystallisation ages that are linked to supercontinent assemblies. Figure redrawn from Hawkesworth et al. 2009.

Zircon crystallisation ages do not necessarily have to represent times of addition of material to the crust. Igneous material that remains in a closed system and is repeatedly re-meleted, can yield zircon grains of different crystallisation ages but with a similar model age. These zircon grains tend to preserve their mantle-like oxygen isotope ratio (Kemp et al. 2006). They are derived from a single component and their model age should therefore in principle be indicative of an event where material separated from the mantle and was added to the crust. However, when magma is formed through melting of mixed components, the melt and zircon grains crystallising from it, will record a model age that is an average value of all the components contributing to the magma (Arndt and Goldstein 1987). The model age does therefore not indicate the timing of when a component separated from the mantle. Heavy oxygen signature of a zircon (>6.5 ‰) implies that it crystallised from a magma that contained a significant amount of sedimentary components (Kemp et al. 2006). A model age of such a zircon is thus presumably derived from more than one component and not indicative of crustal growth, while zircon with mantle-like oxygen isotope ratio are more likely to have crystallised from magmas formed through melting of a single component. The zircon grains analysed in this thesis indicate an addition of juvenile material to the crust, between 2.5 and 2.2 Ga and its stabilization through subsequent generations of felsic magmas between 2.22 and 2.12 Ga. This is represented by the distribution of model ages and crystallisation ages of zircons having mantle-like $\delta^{18}O$.

An increased number of zircons with heavy $\delta^{18}O$ and a gradual increase in $\delta^{18}O$ throughout the growth of the Birimian crust (Fig. 19) indicates an increased influence of supracrustal components in the magmas. Zircons with $\delta^{18}O$>6.5‰ have model ages between 2.4 and 2.1 Ga, and contain a recycled component that increases the model age as compared to the juvenile component. If the sediment that led to the enrichment in ^{18}O of the magma is an erosional product of young, juvenile rocks as is indicated by the juvenile ε_{Hf} signature of the zircons from Ghana, their influence on the model age would be trivial resulting in only slightly older model ages than if they only contained a mantle derived component.

Evolutionary trends defined by mantle-like zircon from individual populations differ from one another, with all the trends being poorly defined (R^2=0.69 for Birim river and R^2=0.01-0.16 for the other four populations). Since no oxygen data is available for the Sihili river, all zircon grains were used to calculate the regression line for that population. Therefore the regression line is most likely based on a mixture of zircon with ε_{Hf} derived from a single component and mixed sources, which reduces its validity. For the other four populations, only zircon with mantle-like $\delta^{18}O$ were used to define the regression line.

For the Ankobra river, regression line with the best fit (R^2=0.01) lies nearly parallel to the NC evolutionary curve indicating continuous addition of juvenile magma to the crust (Fig. 18). Regression lines through the other four populations indicate a lowered ε_{Hf} with younger ages. For the population of Black Volta, Red Volta and Sihili rivers, the slope of the regression lines indicate reworking of a mafic protolith with $^{176}Lu/^{177}Hf$ between 0.021-0.019 that was extracted from the mantle at ~2.4 Ga (for comparison see light blue line on Fig. 18). As indicated by crystallisation ages of the detrital zircon populations, stabilitisation of the crustal protolith and formation of zircon bearing magmas started first within the catchment area of the Black Volta river at ~2.2 Ga, but peaked at ~2.14 Ga in all of the three catchment areas. Plutonic activity then continued within the catchment area of the Sihili river, yielding a second peak in crystallisation ages at ~2.1 Ga, which resulted in the longer average residence time recorded in the Sihili river population than in the Ankobra, Black Volta and Red Volta river populations. The trend represented by the Birim river sample yields a negative value for $^{176}Lu/^{177}Hf$. This cannot be explained by reworking of a single crustal protolith, but requires either mixing between components, or a Pb-loss of the zircon which is not supported by geochronological or geochemical data.

All the regression lines are however poorly defined. A more plausible explanation might therefore be that there were episodic events of additions of juvenile magmas to the crust, rather than continuous additions or a single event. The most depleted data in the current ε_{Hf} dataset can be described in terms of a surface that defines periods of juvenile magma input that mixes with an older component, and periods of predominantly reworking of preexisting crust (Fig. 23) (c.f. Pietranik et al. 2008; Næraa et al. 2012). The detrital zircon from Birim river in southeastern Ghana

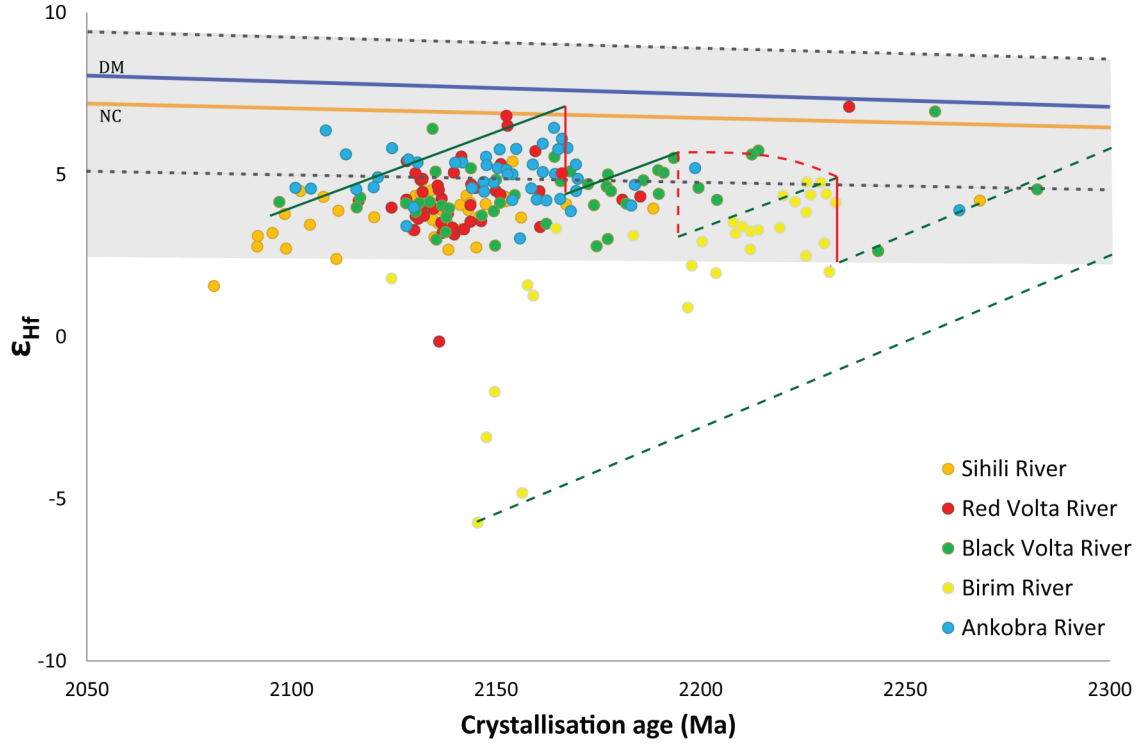

Fig. 22. Figure showing zircon crystallisation age and ε_{Hf} for detrital zircon within this study. Solid and stippled red lines and curve, define periods or events with juvenile magma input into the crust, while the green lines define periods that are dominated by crustal reworking. See text for discussion.

indicate involvement of an Archaean reworked component, and mixing between juvenile magmas and older reservoirs ~2230 Ma. A second juvenile addition event is noted at ~2200 Ma (Fig. 23). This event is not well defined, with relatively few data points, and might reflect semi-continuous juvenile magma input between 2230 Ma and 2200 Ma. Some of the most depleted zircon have crystallisation ages of ~2170 Ma and define the possibly third event. This event of addition of juvenile magmas is associated with reworking of Archaean crust in the southeast represented by zircon with low and negative ε_{Hf} (Birim river data and granites from southeast Ghana; Anders Scherstén, Personal communication).

Periods of juvenile input of magmas, represented by zircon with the most depleted ε_{Hf} values, are separated by periods of crustal reworking as indicated by the increasingly less depleted ε_{Hf} of the zircon between the periods of juvenile magma input (Fig. 23). This periodicity might be explained by retreating arcs as seen in the Cordilleras (DeCelles et al. 2009), as well as in the Archaean crust of southern West Greenland (Næraa et al. 2012). By analogy, the observed time - ε_{Hf} trends seen here could therefore indicate a variably retreating and advancing arc systems.

6.5.2 Preservation of the Birimian crust

It has been suggested that the Birimian is an example of a fast growing continental segment (e.g. Abouchami et al. 1990), which might have enhanced the preservation potential of the Birimian crust. To evaluate this, an attempt is made to estimate the growth rate of the Birimian crust. Based on previously reported geochemical data (Sylvester & Attoh 1992; Asiedu et al. 2004; Soumaila et al. 2004; Dampare et al. 2008), it is assumed that the Birimian grew in island arcs and its growth rate is compared to estimates of modern day island arcs. The area of the Palaeoproterozoic domain of the WAC was calculated by assuming its outlines as represented in Ennih & Liégeois (2008) and that the Taoudeni basin overlies Palaeoproterozoic rocks (Boher et al. 1992). According to these criteria the Palaeoproterozoic domain extends over ~3.2×10^6 km^2. Pasyanos & Nyblade (2007) used geophysical data to estimate the thickness of the crust in Africa, reaching a value of ~35 km for the WAC. According to these parameters the total volume of the preserved WAC Palaeoproterozoic domain is ~1.1×10^8 km^3. If assuming that the emplacement of the Palaeoproterozoic rocks took place over a period of 130 million years, based on ages compiled by Lompo (2009), then the net crustal growth rate is estimated to be ~0.9 km^3/yr. Although, the time period of Birimian crustal growth is perhaps overestimated. Especially if reworking of material that formed during the initial growth stages becomes more pronounced during the later stages (this

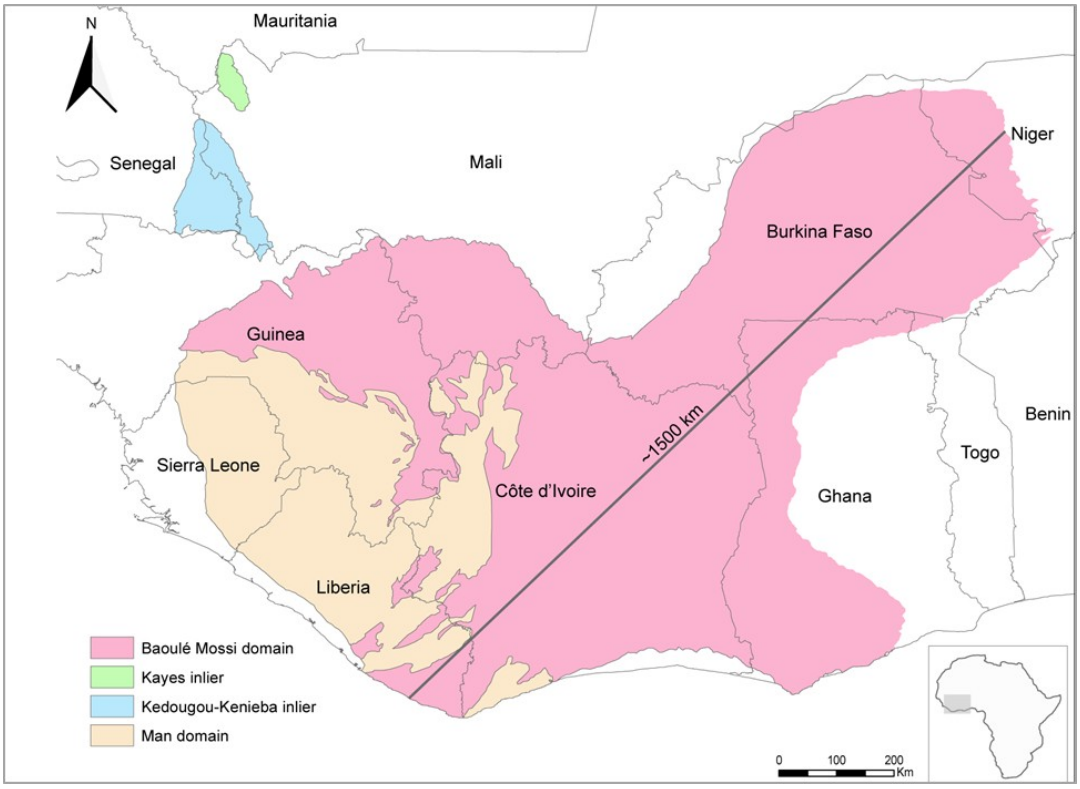

Fig. 24. Areal distribution of the Palaeoproterozoic Baoulé Mossi domain of the Man Shield is represented in pink. The arc length of an island arc, that presumably formed the Palaeoproterozoic bedrock, is estimated to be represented by the greatest length of the Baoulé Mossi domain that lies parallel to the volcanic belts in Ghana and Côte d'Ivoire. This distance is ~1500 km reaching from Liberia in southwest to Niger in northeast (Map made by Mikael Grenholm).

thesis). If a shorter time period of 100 Ma is assumed, the net growth rate increases to ~1.1 km^3/yr but is within the same order of magnitude as the estimated volume of magma (2.7 km^3/yr) that is being added to the crust at Phanerozoic subduction zones (Scholl & von Huene 2009). The calculations are however solely based on the volume of crust that has been preserved and does not take into account any volume that might have been eroded since the formation of the Birimian crust. Adding the volume of eroded crust would increase the calculated value to some extent but the rarity of high grade gneiss terranes might give some restrains on the magnitude of erosion indicating its limited effect.

Another way of expressing the production rate at subduction zones is to calculate the net crustal growth rate in relation to the arc length. The Palaeoproterozoic domain of the WAC is largely covered by Phaneorozoic sediments providing complications in estimating arc lengths. The Baoulé Mossi domain of the Man shield has better exposed sequences of volcanic belts and sedimentary basins that were used for guidance when calculating arc lengths. By assuming that the greatest length of the Baoulé Mossi domain that lies parallel to the volcanic belts of Ghana and Côte D'Ivoire represents the arc length, then it is estimated to be ~1500 km (Fig. 24). The Baoulé Mossi domain as represented in Baratoux et al. (2011) and Egal et al. (2002), extends over an area of ~$0.78 \cdot 10^6$ km^2, which results in a net production rate of ~140 km^3/Ma per km of arc length. This growth rate is high when compared to estimated values from active plate margins where the greatest net growth rate of ~98 km^3/Ma per km of arc length is estimated for Java (Clift et al. 2009). When considering the uncertainties associated with the estimates of arc length, the area of the Baoulé Mossi domain and the time span in which growth occurred, the growth rate of the Baoulé Mossi domain is probably within the same order of magnitude as the fastest growing arcs. The calculations do therefore not indicate that the Birimian terrane is an example of an extremely fast growing crustal segment.

If the Birimian is in fact an example of a fairly rapid but still not an unusually fast growing crust, it is likely that the tectonic setting in which the Birimian grew played a more important role in its preservation, than the rate of crust formation. At subduction zones, continental crust is mostly recycled to the upper mantle through sediment subduction and subduction erosion. In active margins, the net crustal growth ranges from negative (loss of crust) to up to ~100 km^3/Ma per km of arc length (Clift et al. 2009). There seems to be a correlation between the amount of sediments in the arc trench and the effectiveness of subduction erosion. Arcs that have the highest net crustal growth rate tend to have a forearc region of deformed, trench and oceanic sediments (Clift & Vannucchi 2004). If assuming that similar processes took place at subduction zones in the Palaeoproterozoic as in the Phanerozoic, the amount of preserved sediments in the Birimian crust might indicate an arc dominated by sediment accretion rather than subduction erosion. A retreating arc system might have further enhanced the preservation of the Birimian crust since rocks formed in a retreating arc

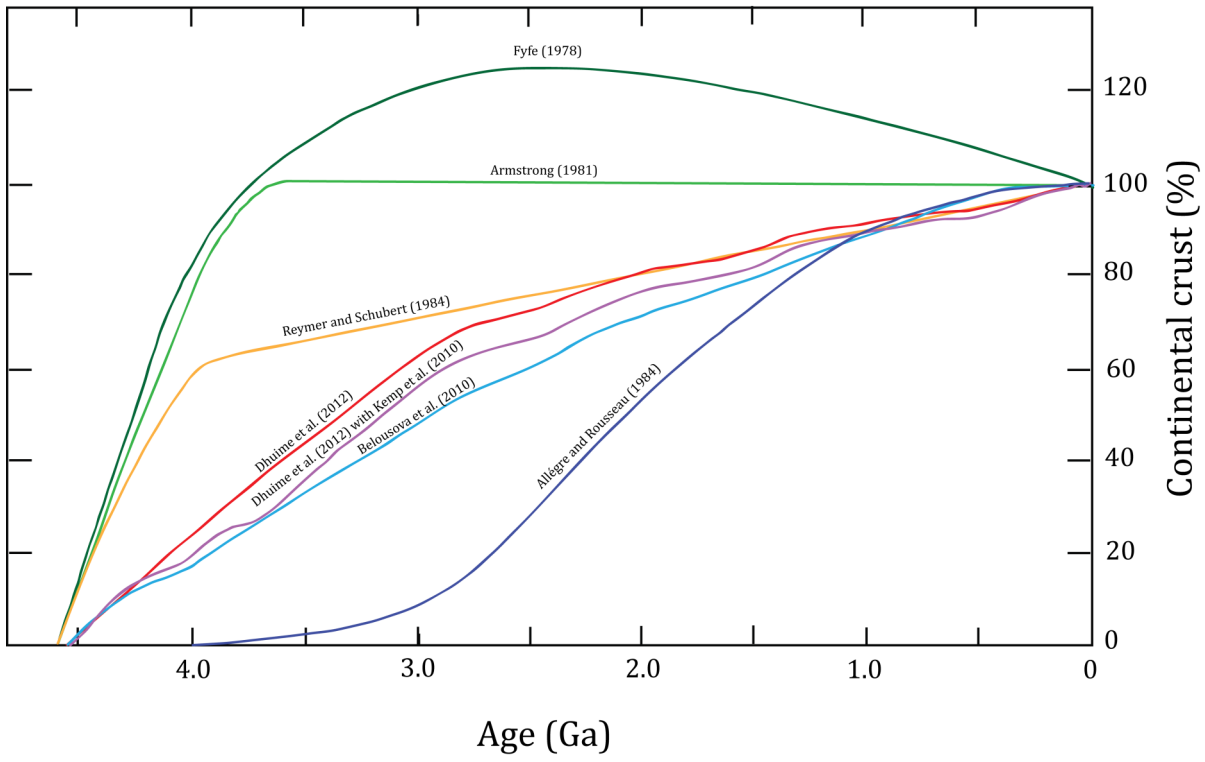

Fig. 25. Crustal growth curves as proposed by several models.

system tend to be better preserved than those formed in an advancing arc system (Fig. 22) (Collins 2002; Hawkesworth et al. 2009).

6.5.3 Crustal growth curves

Models indicating that the continental crust had reached or exceeded its current volume soon after the formation of the Earth were proposed by Armstrong (1981;1991) and Fyfe (1978) (Fig. 25). These have not received general acceptance and most models do suggest a more continuous continental crustal growth throughout the majority of Earth's history (e.g. Reymer & Schubert 1984; Allègre & Rousseau 1984).

Fairly recent progress in analytical techniques have resulted in an increased number of papers reporting U-Pb crystallisation ages of zircon and their Hf-model ages (e.g. Lackey et al. 2005; Kemp et al. 2006; Pietranik et al. 2008; Wang et al. 2009; 2011; Lancaster et al. 2011; Roberts et al. 2013). Several of these papers include oxygen isotope ratios of the zircon, to better constrain the contribution of different components to the magma from which the zircon crystallised. Combined U-Pb, Lu-Hf and O isotope analyses on zircon does not only provide information of when a zircon-bearing rock crystallised, but also when its source component initially separated from the mantle and was added to the crust. Zircon analyses can therefore be a useful tool to assess the evolution of crustal volume during the geological history. This has been utilized by Belousova et al. (2010) and Dhuime et al. (2012), both of which retrieved a crustal growth curve describing a faster growth in the Archaean than during the Proterozoic and Phanerozoic, with a more moderate crustal growth in the Archaean suggested by the model of Belousova et al. (2010) (Fig. 25).

In the model of Dhuime et al. (2012), $\delta^{18}O$ of zircon was used to determine whether the zircon grains crystallised from magma with mantle-like affinity or

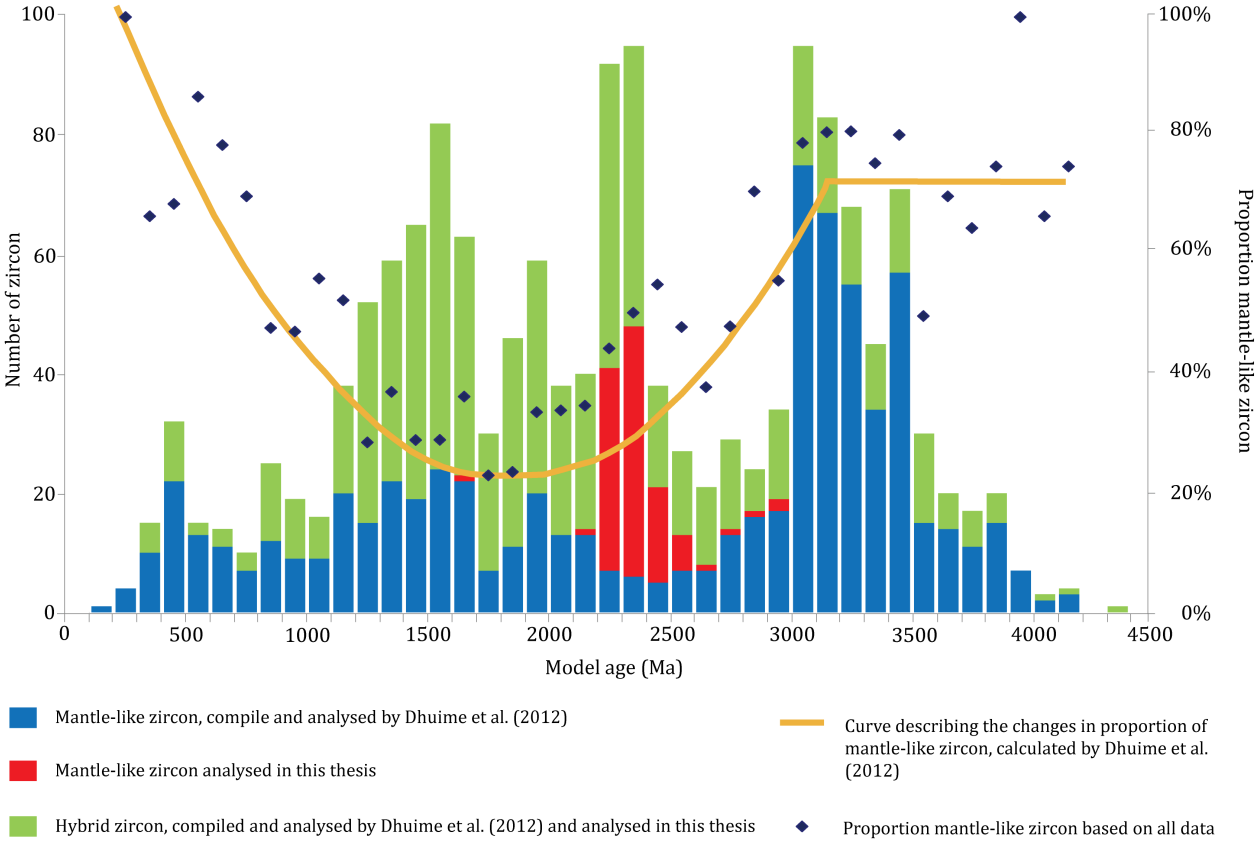

Fig. 26. The crustal growth model by Dhuime et al. (2012) is partially based on oxygen isotopes in detrital zircon. In the model, the zircon are divided into mantle-like zircon ($\delta^{18}O$ = 5.3±1.2) (blue) and hybrid zircon (green) and based on that, a curve describing changes in the proportion of mantle-like zircon throughout the geological history is retrieved (orange curve). The ratio is fairly stable at ~75% until ~3.0 Ga but then it starts to decrease, indicating a increased influence of reworking of the crust. Relatively few zircon from the database used by Dhuime et al. (2012) have model ages between 2200-2500 Ma, a time period which majority of the zircon analysed in this thesis (red) belongs to. Despite that the proportion of mantle-like zircon in the dataset from Ghana, is substantially higher (~60%) than is implied by the curve retrieved by Dhuime et al. (2012) for zircon with Hf-model ages between 2200-2500 Ma (~30%), adding the data from Ghana does not change the shape of the curve substantially. Comparison between the caluclated curve (orange) and the proportion of mantle-like zircon for every 100 Ma, based on data from Dhuime et al. (2012) and this thesis (blue diamonds), does though indicates that the curve might underrepresent the proportion of mantle-like zircon in the Proterozoic as most of the new calculated values plot above the curve. Figure modified from Dhuime et al. (2012).

from a hybrid magma containing recycled or reworked crustal components. The proportion of mantle-like zircon for every 100 Ma interval is plotted against the model ages, yielding two equations describing the change in the ratio between mantle-like and hybrid zircon from the Hadean to present. Up until ~3.0 Ga the proportion of mantle-like zircon remained stable at ~75% but then it started to decrease and reached minimum of ~20% at around 1900 Ma. The zircon from Ghana have model ages mainly falling between 2500 Ma and 2200 Ma, during a period of rather low proportion of mantle-like zircon formation (Dhuime et al. 2012) (Fig. 26). Even though the percentage of mantle -like zircon in the dataset from Ghana (~60%) is substantially higher than is represented for the same time period in the dataset of Dhuime et al. (2012), adding that data to the dataset does not have substantial influence on the shape of the curve. However, most of the percentages calculated using the combined dataset of Dhuime et al. (2012) and this thesis, plots above the curve defined by Dhuime et al. (2012). This indicates that the proportion of mantle-like zircon might be slightly underestimated in the model (Fig. 26).

In the second part of the model, an attempt is made to estimate the proportion of juvenile crust that is formed during each 100 Myr time interval, from 4.6 Ga to present. The estimate is based on Hf-model ages and crystallisation ages of detrital zircon, as well as on the previously determined equations that describe the change in proportion of mantle-like zircon throughout the geological history. Each 100 Myr time interval is given the same weight in the model, indicating that a constant volume of material is crystallised per 100 Myr throughout the geological record. The measured isotopes of the detrital zircon grains are used to determine whether that volume is represented by juvenile material, which is derived from the mantle, or if it is reworked older crust. Due to the assumptions that are made in the model, a 100 Myr time interval is assumed to be represented solely by juvenile magmatism if no zircon has a crystallisation age falling within that time period. This is the case for the first 700 million years, since no zircon from the dataset has a crystallisation age belonging to that time period.

Hadean and early Archaean crust constitutes a small fragment of the total continental crust on Earth. The oldest detrital zircon are dated from the Jack Hills (~4.4 Ga) (Cavosie et al., 2005), whilst the oldest crustal rocks from the Canadian shield (Bowring & Williams 1999; David et al. 2009) and Greenland (Nutman et al. 1996) are 3.8-4.0 Ga. The database that is used in the model of Dhumie et al. (2012) contains only a few zircon grains older than 3500 Ma, with the oldest zircon being dated to 3717 Ma. This leads to that each time interval prior to 3.8 Ga is described as a period of juvenile crust formation. The result is that nearly 35% of crust had been formed 3700 Ma ago according to the model. Kemp et al. (2010) analysed ~70 detrital zircon from the Jack Hills in Australia for U-Pb and Lu-Hf isotopes. Most of these zircon have crystallisation ages between 4.3 and 3.8 Ga. By adding data from Kemp et al. (2010) to the dataset of Dhuime et al. (2012), the curve alters and the percentage of crustal volume is brought down to ~25% at 3700 Ma (Fig. 25).

Even though the model of Dhuime et al. (2012) seems to be insusceptible towards additional data from the Protero- and Phanerozoic it is sensitive to addition of data from the Hadean and Archaean, both of which are represented by a limited number of grains in the zircon record. Increased data from the first 1000 Ma of the Earth could therefore alter the growth curve substantially, diminishing its plausibility at current state.

7 Conclusion

- The influence of Archaean crust is not apparent in zircon sampled from areas outside of the Kibi belt in southeastern Ghana. Detrital zircon from the other four populations have positive ε_{Hf} (0.9-7.1) indicating that they grew in juvenile magmas containing minor amounts of older crust.

- Crystallisation ages of zircon from the Kibi-Winneba belt (Birim river) in southeastern Ghana show a two peaked distribution. The earlier phase, ~2.22 Ga, is governed by juvenile zircon, while the ~2.15 Ga zircon have lower ε_{Hf} but mantle-like $\delta^{18}O$, indicating reworking of an older crust.

- Modelling based on ε_{Hf} and $\delta^{18}O$ indicates less than 10% contribution of recycled or reworked Archaean crust to most of the magma, which the zircon grew in. This excludes some of the zircon in the ~2.15 Ga subgroup of the Birim river population. These show a mixing trend between a juvenile component and an Archaean crustal component. Zircon grains with juvenile ε_{Hf} and elevated $\delta^{18}O$ make up a substantial part of the zircon populations, indicating rapid reworking of juvenile crust.

- Oxygen isotope ratios of the Black Volta, Red Volta and Ankobra river populations show an increased proportion of $\delta^{18}O>6.5‰$ zircon with younger ages. This is not observed in the Birim river population where all zircon have $\delta^{18}O<6.5‰$. The same trend of increased $\delta^{18}O$ with younger ages, is observed when a 10 Ma running mean is calculated for $\delta^{18}O$, which might indicate a maturing arc system.

- Adding the zircon data analysed in this thesis to a dataset that Dhuime et al. (2012) used to model the growth of the continental crust, indicates that the influence of reworked crust in

Proterozoic rocks might be slightly overestimated by the model.

- Despite the robustness of the model of Dhuime et al. (2012) when data containing zircon with crystallisation ages younger than ~3.7 Ga is added to the dataset, it is sensitive to addition of data containing zircon with crystallisation ages older than ~3.7 Ga. Since ~35% of the continental crust was already formed at 3.7 Ga, according to the model, it largely controls the overall shape of the curve. Increased data containing zircon with crystallisation ages >3.7 Ga could therefore substantially change the crustal growth model.

8 Acknowledgements

I would like to thank my supervisor Anders Scherstén for giving me the opportunity to work on this project, for all his support and guidance along the way, and for reviewing the manuscript and making suggestions on how to improve it. I would also like to thank Andreas Petersson for his help and discussions, as well as for his cooperation in reproducing the crustal growth model of Dhuime et al. (2012) and for providing me with the mixing model. I would like to thank Tony Kemp for his help and discussions when carrying out the Lu-Hf analysis, Mikael Grenholm for producing two of the maps that were used in this thesis, Tomas Næraa for useful comments on the manuscript, and Marín Ósk for being willing to listen to me whenever I needed to discuss my thoughts and ideas. Finally I would like to thank my family and friends for their support throughout my studies.

9 References

Abouchami, W., Boher, M., Michard, A. & Albaréde, F., 1990: A major 2.1-Ga event of mafic magmatism in west Africa: an early state of crustal accretion. *Journal of Geophysical Research 95*, 17605-17629.

Allègre, C.J. & Rousseau, D., 1984: The growth of the continent through geological time studied by Nd isotope analysis of shales. *Earth and Planetary Science Letters 67*, 19-34.

Amelin, Y., Lee, D.-C., Halliday, A.N. & Pidgeon, R.T., 1999: Nature of the Earth's earliest crust from hafnium isotopes in single detrital zircons. *Nature 399*, 252-255.

Armstrong, R.L., 1981: Radiogenic isotopes: the case for crustal recycling on a near-steady-state no-continental-growth Earth. *Philosophical Transactions of the Royal Society of London. Series A, Mathematical and Physical Sciences 301*, 443-472.

Armstrong, R.L., 1991: The persistent myth of crustal growth. *Australian Journal of Earth Sciences 38*, 613-630.

Arndt, N.T. & Goldstein, S.L., 1987: Use and abuse of crust-formation ages. *Geology 15*, 893-895.

Asiedu, D.K. et al., 2004: Geochemistry of Paleoproterozoic metasedimentary rocks from the Birim diamondiferous field, southern Ghana: implications for provenance and crustal evolution at the Archean-Proterozoic boundary. *Geochemical Journal 38*, 215-228.

Attoh, K., Dallmeyer, R.D. & Affaton, P., 1997: Chronology of nappe assembly in the Pan-African Dahomeyide orogen, West Africa: evidence from $^{40}Ar/^{39}Ar$ mineral ages. *Precambrian Research 82*, 153-171.

Baertschi, P., 1976: Absolute ^{18}O content of standard mean ocean water. *Earth and Planetary Science Letters 31*, 341-344.

Baratoux, L., Metelka, V., Naba. S., Jessell. M.W., Grégoire, M. & Ganne, J., 2011: Juvenile Paleoproterozoic crust evolution during the Eburnean orogeny (~2.2-2.0 Ga), western Burkina Faso. *Precambrian Research 191*, 18-45.

Belousova, E.A., Griffin, W.L., O'Reilly, S.Y. & Fisher, N.I., 2002: Igneous zircon: trace element composition as an indicator of source rock type. *Contribution to Mineralogy and Petrology 143*, 602-622.

Belousova, E.A., Kostitsyn, Y.A., Griffin, W.L., Begg, G.C., O'Reilly, S.Y. & Pearson, N.J., 2010: The growth of the continental crust: constraints from zircon Hf-isotope data. *Lithos 119*, 457-466.

Bindeman, I., 2008: Oxygen isotopes in mantle and crustal magmas as revealed by single crystal analysis. *Reviews in Mineralogy and Geochemistry 69*, 445-478.

Boher, M., Abouchami, W., Michard, A., Albarede, N, & Arndt, N.T., 1992: Crustal growth in West Africa at 2.1 Ga. *Journal of Geophysical Research 97*, 345-369.

Bouvier, A., Vervoort, J.D. & Patchett, P.J., 2008: The Lu-Hf and Sm-Nd isotopic composition of CHUR: constraints from unequilibrated chondrites and implication for the bulk composition of terrestrial planets. *Earth and Planetary Science Letters 273*, 48-57.

Bowring, S.A. & Williams, I.S., 1999: Priscoan (4.00-4.03 Ga) orthogneisses from northwestern Canada. *Contribution to Mineralogy and Petrology 134*, 3-16.

Campbell, I.H. & Allen, C.M., 2008: Formation of supercontinents linked to increases in atmospheric oxygen. *Nature Geoscience 1*, 554-558.

Cavosie, A.J., Valley, J.W. & Wilde, S.A., 2005: Magmatic $\delta^{18}O$ in 4400-3900 Ma detrital zircons: a record of the alteration and recycling of crust in the early Archean. *Earth and Planetary Science Letters 235*, 663-681.

Cherniak, D.J., Hervig, R., Koepke, J., Zhang, Y &

Zhao, D., 2010: Analytical methods in diffusion studies. *In* Y. Zhang & D.J. Cherniak (eds.): *Reviews in Mineralogy and Geochemistry 72*, 107-170. Mineralogical Society of America. Geochemical Society, Chantilly, Virginia.

Cherniak, D.J. & Watson, E.B., 2003: Diffusion in zircon. *In* J.M. Hanchar & P.W.O. Hoskin (eds.): *Reviews in mineralogy and geochemistry 53*, 113-143. Mineralogical Society of America, Washington.

Clift, P.D., Schouten, H. & Vannucchi, P., 2009: Arc-continent collisions, sediment recycling and the maintenance of the continental crust. *In* P.A. Cawood & A. Kröner (eds.): *Earth accretionary systems in space and time.* Geological Society, London, Special Publications 318, 75-103.

Clift, P. & Vannucchi, P., 2004: Controls on tectonic accretion versus erosion in subduction zones: implications for the origin and recycling of the continental crust. *Review of Geophysics 42*, doi: 10.1029/2003RG000127

Collins, W.J., 2002: Hot orogens, tectonic switching, and creation of continental crust. *Geology 30*, 535-538.

Condie, K.C., 1998: Episodic continental growth and supercontinents: a mantle avalanche connection? *Earth and Planetary Science Letters 163*, 97-108.

Corfu, F., Hanchar, J.M., Hoskin, P.W. & Kinny, P., 2003: Atlas of zircon textures. *In* J.M. Hanchar & P.W.O. Hoskin (eds.): *Reviews in mineralogy and geochemistry 53*, 469-500. Mineralogical Society of America, Washington.

Dampare, S.B., Shibata, T., Asiedu, D.K., Osae, S. & Banoeng-Yakubo, B., 2008: Geochemistry of Paleoproterozoic metavolcanic rocks from the southern Ashanti volcanic belt, Ghana: petrogenetic and tectonic setting implications. *Precambrian Research 162*, 403-423.

David, J., Godin, L., Stevenson, R., O´Neil, J. & Francis, D., 2009: U-Pb ages (3.8-2.7 Ga) and Nd isotope data from the newly identified Eoarchean Nuvvuagittuq supracrustal belt, Superior Craton, Canada. *Geological Society of America Bulletin, 121*, 150-163.

Davidson, J., 1985: Mechanisms of contamination in Lesser Antilles island arc magmas from radiogenic and oxygen isotope relationships. *Earth and Planetary Science Letters 72*, 163-174.

Davis, D.W., Hirdes, W., Schaltegger, U. & Nunoo, E.A., 1994: U-Pb age constraints on deposition and provenance of Birimian and gold-bearing Tarkwaian sediments in Ghana, West Africa. *Precambrian Research 67*, 89-107.

Davis, D.W., Williams, I.S. & Krogh, T.E., 2003: Historical development of zircon geochronology. *In* J.M. Hanchar & P.W.O. Hoskin (eds.): *Reviews in mineralogy and geochemistry 53*, 145-181. Mineralogical Society of America, Washington.

DeCelles, P.G., Ducea, M.N., Kapp, P. & Zandt, G, 2009: Cyclicity in Cordilleran orogenic systems. *Nature Geoscience 2*, 251-257.

Dhuime, B., Hawkesworth, C. & Cawood, P., 2011a: When continents formed. *Science 331*, 154-155.

Dhuime, B., Hawkesworth, C.J., Storey, C.D. & Cawood, P.A., 2011b: From sediments to their source rocks: Hf and Nd isotopes in recent river sediments. *Geology 39*, 407-410.

Dhuime, B., Hawkesworth, C.J., Cawood, P.A. & Storey, C.D., 2012: A change in the geodynamics of continental growth 3 billion years ago. *Science 335*, 1334-1336.

Doumbia, S., Pouclet, A., Kouamelan, A., Peucat, J.J., Vidal, M. & Delor, C., 1998: Petrogenesis of juvenile-type Birimian (Paleoproterozoic) granitoids in Central Côte-d'Ivoire, West Africa: geochemistry and geochronology. *Precambrian Research 87*, 33-63.

Egal, E., Thiéblemont, D., Lahondère, D., Guerrot, C., Costea, C.A., Iliescu, D., Delor, C., Goujou, J.-C., Lafon, J.M., Tegyey, M., Diaby, S. & Kolié, P., 2002: Late Eburnean granitization and tectonics along the western and northwestern margin of the Archean Kénéma-Man domain (Guinea, West African Craton). *Precambrian Research 117*, 57-84.

Eiler, J. M., 2001. Oxygen isotope variations of basaltic lavas and upper mantle rocks. *Reviews in Mineralogy and Geochemistry 43*, 319-364.

Eiler, J.M., Crawford, A., Elliott, T., Farley, K.A., Valley, J.W. & Stolper, E.M., 2000: Oxygen isotope geochemistry of oceanic-arc lavas. *Journal of Petrology 41*, 229-256.

Eisenlohr, B.N. & Hirdes, W., 1992: The structural development of the early Proterozoic Birimian and Tarkwaian rocks of southwest Ghana, West Africa. *Journal of African Earth Sciences 14*, 313-325.

Ennih, N. & Liégeois, J.-P., 2008: The boundaries of the West African craton, with special reference to the basement of the Moroccan metacratonic Anti-Atlas belt. *In* N. Ennih & J.-P. Ligeois (eds.): *The boundaries of the West African craton.* Geological Society, London, Special Publications 297, 1-17.

Fedo, C.M., Sircombe, K.N. & Rainbird, R.H., 2003: Detrital zircon analysis of the sedimentary record. *In* J.M. Hanchar & P.W.O. Hoskin (eds.): *Reviews in mineralogy and geochemistry 53*, 278-303. Mineralogical Society of America, Washington.

Feybesse, J.-L., Billa, M., Guerrot, C., Duguey, E., Lescuyer, J.-L., Milesi, J.-P. & Bouchot, V., 2006: The Paleoproterozoic Ghanian province: geodynamic model and ore controls, including regional stress modelling. *Precambrian Research 149*, 149-196.

Finch, R.J. & Hanchar, J.M., 2003: Structure and chemistry of zircon and zircon group minerals. *In* J.M. Hanchar & P.W.O. Hoskin (eds.): *Reviews in mineralogy and geochemistry 53*, 1-26. Mineralogical Society of America, Washington.

Fisher, C.M., Hanchar, J.M., Samson, S.D., Dhuime, B., Blichert-Torft, J., Vervoort, J.D. & Lam, R., 2011: Synthetic zircon doped with hafnium and rare earth elements: a reference material for in situ hafnium isotope analysis. *Chemical Geology 286*, 32-47.

Fujimaki, H., 1986: Partition coefficients of Hf, Zr, and REE between zircon, apatite, and liquid. *Contributions to Mineralogy and Petrology 94*, 42-45.

Fyfe, W.S., 1978: The evolution of the earth's crust - modern plate tectonics to ancient hot spot tectonics? *Chemical Geology 23*, 89-114.

Ganne, J., De Andrade, V, Weinberg, R.F., Vidal, O., Bubacq, B., Kagambega, N., Naba, S., Baratoux, L., Jessell, M. & Allion, J., 2012: Modern-style plate subduction preserved in the Palaeoproterozoic West African craton. *Nature 5*, 60-65.

Garçon, M., Chauvel, C. & Bureau, S., 2011: Beach placer, a proxy for the average Nd and Hf isotopic composition of a continental area. *Chemical Geology 287*, 182-192.

Gasquet, D., Barbey, P., Adou, M. & Paquette, J.L., 2003: Structure, Sr-Nd isotope geochemistry and zircon U-Pb geochronology of the granitoids of the Dabakala area (Côte d'Ivoire): evidence for a 2.3 Ga crustal growth event in the Palaeoproterozoic of West Africa? *Precambrian Research 127*, 329-254.

Gehrke, R.J., Casey, C. & Murray, R.K., 1990: Half-life of 176Lu. *Physical Review 41*, 2878-2882.

GERM, 2013. Geochemical Earth Reference Model. http://earthref.org/GERM

Griffin, W.L., Pearson, N.J., Belousova, E., Jackson, S.E., van Achterbergh, E., O´Reilly, S.Y. & Shee, S.R., 2000: The Hf isotope composition of cratonic mantle: LAM-MC-ICPMS analysis of zircon megacrysts in kimberlites. *Geochimica et Cosmochimica Acta 64*, 133-147.

Griffin, W.L., Wang, X., Jackson, S.E., Pearson, N.J., O´Reilly, S.Y., Xu, X. & Zhou, X., 2002: Zircon chemistry and magma mixing, SE China: in-situ analysis of Hf isotopes, Tonglu and Pingtan igneous complexes. *Lithos 61*, 237-269.

Grinyer, G.F., Waddington, J.C., Svensson, C.E., Austin, R.A.E., Ball, G.C., Hackman, G., O´Meara, J.M., Osborne, C., Sarazin, F., Scraggs, H.C. & Stöver, H.D.H., 2003: Half-life of 176Lu. *Physical Review C 67*, doi: 10.1103/PhysRevC.67.014302

Günther, D. & Heinrich, C.A., 1999: Enhanced sensitivity in laser ablation-ICP mass spectrometry using helium-argon mixtures as aerosol carrier. Journal *of Analytical Atomic Spectrometry 14*, 1363-1368.

Hanchar, J.M., Finch, R.J.. Hoskin, P.W.O., Watson, E.B., Cherniak, D.J. & Mariano, A.N., 2001: Rare earth elements in synthetic zircon: part 1. Synthesis, and rare earth element and phosphorus doping. *American Mineralogist 86*, 667-680.

Hanchar, J.M. & van Westrenen, W., 2007: Rare earth element behavior in zircon-melt systems. *Elements 3*, 37-42.

Harley, S.L. & Kelly, N.M., 2007: Zircon: Tiny but timely. *Elements 3*, 13-18.

Hawkesworth, C., Cawood, P., Kemp, T., Storey, C. & Dhuime, B., 2009: A matter of preservation. *Science 323*, 49-50.

Hawkesworth, C.J., Dhuime, B., Pietranik, A.B., Cawood, P.A., Kemp, A.I.S. & Storey, C.D., 2010: The generation and evolution of the continental crust. *Journal of the Geological Society, London 167*, 229-248.

Hawkesworth, C.J. & Kemp, A.I., 2006: The differentiation and rates of generation of the continental crust. *Chemical Geology 226*, 134-143.

Heaman, L.M., Bowins, R. & Crocket, J., 1990: The chemical composition of igneous zircon suites: implications for geochemical tracer studies. *Geochimica et Cosmochimica Acta 54*, 1597-1607.

Hiess, J., Bennett, V.C., Nutman, A.P. & Williams, I.S., 2011: Archaean fluid-assisted crustal cannibalism recorded by low $\delta^{18}O$ and negative $e_{Hf(T)}$ isotopic signatures of West Greenland granite zircon. *Contribution to Mineralogy and Petrology 161*, 1027-1050.

Hirdes, W. & Davis, D.W., 1998: First U-Pb zircon age extrusive volcanism in the Birimian Supergroup of Ghana, West Africa. *Journal of African Earth Sciences 27*, 291-294.

Hirdes, W., Davis, D.W. & Eisenlohr, B.N., 1992: Reassessment of Proterozoic granitoid ages in Ghana on the basis of U/Pb zircon and monazite dating. *Precambrian Research 56*, 89-96.

Hirdes, W., Davis, D.W., Lüdtke, G. & Konan, G., 1996: Two generations of Birimian (Paleoproterozoic) volcanic belts in northeastern Cote d'Ivoire (West Africa): consequences for the "Birimian controversy". *Precambrian Research 80*, 173-191.

Hoskin, P.W.O. & Ireland, T.R., 2000: Rare earth element chemistry of zircon and its use as a provenance indicator. *Geology 28*, 627-630.

Hoskin, P.W.O., Kinny, P.D., Wyborn, D. & Chappell, B.W., 2000: Identifying accessory mineral saturation during differentiation in granitoid magmas: an integrated approach. *Journal of Petrology 41*, 1365-1396.

Hoskin, P.W.O. & Schaltegger, U., 2003: The composition of zircon and igneous and metamorphic petrogenesis. *In* J.M. Hanchar & P.W.O. Hoskin (eds.): *Reviews in mineralogy and geochemistry 53*, 27-62. Mineralogical Society of America, Washington.

Iizuka, T., Campbell, I.H., Allen, C.M., Gill, J.B., Maruyama, S. & Makoka, F., 2013: Evolution of the African continental crust as recorded by U-Pb, Lu-Hf and O isotopes in detrital zircons from modern rivers. *Geochimica et Cosmochimica Acta 107*, 96-120.

Iizuka, T., Komiya, T., Rino, S., Maruyama, S. & Hirata, T., 2010: Detrital zircon evidence for Hf isotopic evolution of granitoid crust and continental growth. *Geochimica et Cosmochimica Acta 74*, 2450-2472.

Ireland, T.R. & Williams, I.S., 2003: Considerations in zircon geochronology by SIMS. *In* J.M. Hanchar & P.W.O. Hoskin (eds.): *Reviews in mineralogy and geochemistry 53*, 215-241. Mineralogical Society of America, Washington.

Ito, E., Stern, R. J. & Douthitt, C., 2003: Insights into operation of the subduction factory from the oxygen isotopic values of the southern Izu-Bonin-Mariana Arc. *The Island Arc 12*, 383-397.

John, T., Klemd, R., Hirdes, W. & Loh, G., 1999: The metamorphic evolution of the Paleoproterozoic (Birimian) volcanic Ashanti belt (Ghana, West Africa). *Precambrian Research 98*, 11-30.

Kalsbeek, F., Frei, D. & Affaton, P., 2008: Constraints on provenance, stratigraphic correlation and structural context of the Volta basin, Ghana, from detrital zircon geochronology: an Amazonian connection? *Sedimentary Geology 212*, 86-95.

Kemp, A.I.S., Hawkesworth, C.J., Paterson, B.A. & Kinny, P.D., 2006: Episodic growth of the Gondwana supercontinent from hafnium and oxygen isotopes in zircon. *Nature 439*, 580-583.

Kemp, A.I.S., Wilde, S.A., Hawkesworth, C.J., Coath, C.D., Nemchin, A., Pidgeon, R.T., Vervoort, J.D. and DuFrane, S.A., 2010: Hadean crustal evolution revisited: new constraints from Pb-Hf isotope systematics of the Jack Hills zircons. *Earth and Planetary Science Letters 296*, 45-56.

Klein, E.L., Moura, C.A.V. & Pinheiro, B.L.S., 2005: Paleoproterozoic crustal evolution of the Sao Luís Craton, Brazil: evidence from zircon geochronology and Sm-Nd isotopes. *Gondwana Research 8*, 177-186.

Kolesov, B.A., Geiger, C.A. & Armbruster, T., 2001. The dynamic properties of zircon studied by single-crystal X-ray diffraction and Raman spectroscopy. *European Journal of Mineralogy 13*, 939-948.

Kosler, J. & Sylvester, P.J., 2003: Present trends and the future of zircon in geochronology: laser ablation ICPMS. *In* J.M. Hanchar & P.W.O. Hoskin (eds.): *Reviews in mineralogy and geochemistry 53*, 243-275. Mineralogical Society of America, Washington.

Kramers, J., Frei, R., Newville, M., Kober, B. & Villa, I., 2009: On the valency state of radiogenic lead in zircon and its consequences. *Chemical Geology 261*, 4-11.

Lackey, J.S., Valley, J.M. & Saleeby, J.B., 2005: Supracrustal input to magmas in the deep crust of Sierra Nevada batholith: evidence from high-$\delta^{18}O$ zircon. *Earth and Planetary Science Letters 235*, 315-330.

Lancaster, P.J., Storey, C.D., Hawkesworth, C.J. & Dhuime, B., 2011: Understanding the roles of crustal growth and preservation in the detrital zircon record. *Earth and Planetary Science Letters 305*, 405-412.

Leube, A., Hirdes, W., Mauer, R. & Kesse, G.O., 1990: The early Proterozoic Birimian Supergroup of Ghana and some aspects of its associated gold mineralization. *Precambrian Research 46*, 139-165.

Lompo, M., 2009. Geodynamic evolution of the 2.25-2.0 Ga Paleoproterozoic magmatic rocks in the Man-Leo shield of the West African Craton. A model of subsidence of an oceanic plateau. *In* S.M. Reddy, R. Mazumder, D.A.D. Evans & A.S. Collins, (eds.): *Palaeoproterozoic supercontinents and global evolution.* Geological Society of London, Special Publication 323, 231-254.

Longerich, H.P. & Diegor, W., 2001: Introduction to mass spectrometry. *In* P. Sylvester, (ed.): *Laser-Ablation-ICPMS in the Earth Sciences. Principles and Applications.* Mineralogical Association of Canada, 1-20.

Ludwig, K.R., 2008: Isoplot 3.70. A geochronological toolkit for Microsoft Excel. *Berkeley Geochronology Center Special Publications 4.*

Mahood, G. & Hildreth, W., 1983: Large partition coefficients for trace elements in high-silica rhyolites. *Geochimica et Cosmochimica Acta 47*, 11-30.

Mezger, K. & Krogstad, E.J., 1997: Interpretation of discordant U-Pb zircon ages: an evaluation. *Journal of Metamorphic Geology 15*, 127-140.

Milési, J.-P., Ledru, P., Feybesse, J.-L., Dommanget, A. & Marcoux, E., 1992: Early Proterozoic ore deposits and tectonics of the Birimian orogenic belt. *West Africa. Precambrian Research 58*, 305-344.

Nir-El, Y. & Lavi, N., 1998: Measurement of the half-life of 176Lu. *Applied Radiation and Isotopes 49*, 1653-1655.

Nutman, A.P., McGregor, V.R., Friend, C.R.L., Bennett, V.C. & Kinny, P.D., 1996: The Itsaq Gneiss Complex of southern West Greenland; the world's most extensive record of early crustal evolution (3900-3600 Ma). *Precambrian Research 78*, 1-39.

Næraa, T., Scherstén, A., Rosing, M.T., Kemp, A.I.S., Kokfelt, T.F. & Whitehouse, M.J., 2012: Hafnium

isotope evidence for a transition in the dynamics of continental growth 3.2 Gyr ago. *Nature 485*, 627-630.

Oberthür, T., Vetter, U., Davis, D.W. & Amanor, J.A., 1998: Age constraints on gold mineralization and Paleoproterozoic crustal evolution in the Ashanti belt of southern Ghana. *Precambrian Research 89*, 129-143.

Page, F.Z., Ushikubo, T., Kia, N.T., Riciputi, L.R. & Valley, J.W., 2007: High-precision oxygen isotope analysis of picogram samples reveals 2 µm gradients and slow diffusion in zircon. *American Mineralogist 92*, 1772-1775.

Pasyanos, M.E. & Nyblade, A.A., 2007: A top to bottom lithospheric study of Africa and Arabia. *Tectonophysics 444*, 27-44.

Patchett, P.J. & Tatsumoto, M., 1980: A routine high-precision method for Lu-Hf isotope geochemistry and chronology. *Contributions to Mineralogy and Petrology 75*, 263-267.

Peck, W.H., Valley, J.W. & Graham, C.M., 2003: Slow oxygen diffusion rates in igneous zircons from metamorphic rocks. *American Mineralogist 88*, 1003-1014.

Pietranik, A.B., Hawkesworth, C.J., Storey, C.D., Kemp, A.I.S., Sircombe, K.N., Whitehouse, M.J. & Bleeker, W., 2008: Episodic, mafic crust formation from 4.5 to 2.8 Ga: new evidence from detrital zircons, Slave craton, Canada. *Geology 36*, 875-878.

Reymer, A. & Schubert, G., 1984: Phanerozoic addition rates to the continental crust and crustal growth. *Tectonics 3*, 63-77.

Roberts, N. M., Slagstad, T., Parrish, R.R., Norry, M.J., Marker, M. & Horstwood, M.S.A., 2013: Sedimentary recycling in arc magmas: geochemical and U-Pb-Hf-O constraints on the Mesoproterozoic Suldal Arc, SW Norway. *Contribution to Mineralogy and Petrology 165*, 507-523.

Rollinson, H. R., 1993: *Using geochemical data: evaluation, presentation, interpretation*. Pearson, 352 pp.

Rubatto, D., 2002: Zircon trace element geochemistry: partitioning with garnet and the link between U-Pb ages and metamorphism. *Chemical Geology 184*, 123-138.

Rudnick, R.L., 1995: Making continental crust. *Nature 378*, 571-578.

Rudnick, R.L. & Gao, S., 2003: Composition of the continental crust. *In* R.L. Rudnick, ed. *Tetrise on Geochemistry 3*, Elsevier, 1-64.

Salters, V.J., 1994: $^{176}Hf/^{177}Hf$ Determination in small samples by a high-temperature SIMS technique. *Analytical Chemistry 66*, 4186-4189.

Salters, V.J. & Stracke, A., 2004: Composition of the depleted mantle. *Geochemistry, Geophysics, Geosystems 5*, doi:10.1029/2003GC000597.

Santo, A.P. & Peccerillo, A., 2008: Oxygen isotopic variations in the clinopyroxene from the Filicudi volcanic rocks (Aeolian Islands, Italy): implications for open-system magma evolution. *The Open Mineralogy Journal 2*, 22-33.

Scherer, E., Münker, C. & Mezger, K., 2001: Calibration of the lutetium-hafnium clock. *Science 293*, 683-687.

Scholl, D.W. & von Huene, R., 2007: Crustal recycling at modern subduction zones applied to the past - issues of growth and preservation of continental basement crust, mantle geochemistry, and supercontinent reconstruction. *In* R.D. Hatcher, M.P. Carlson, J.H McBride & J.R.M. Catalán (eds.): *4-D Framework of continental crust*. Geolgoical Society of America Memoir 200, 9-32.

Scholl, D.W. & von Huene, R., 2009: Implications of estimated magmatic additions and recycling losses at the subduction zones of accretionary (non-collisional) and collisional (suturing) orogens. *In* P.A. Cawood & A. Kröner (eds.): *Earth accretionary systems in space and time.* Geological Society, London, Special Publications 318, 105-126.

Segal, I., Halicz, L. & Platzner, I.T., 2003: Accurate isotope ratio measurements of ytterbium by multiple collector inductively coupled plasma mass spectrometry applying erbium and hafnium in an improved double external normalization procedure. *Journal of Analytical Atomic Spectrometry 18*, 1217-1223.

Shannon, R.D., 1976: Revised effective ionic radii and systematic studies of interatomic distances in halides and chalcogenides. *Acta Crystallographica Section A 32*, 751-767.

Simon, L. & Lécuyer, C., 2005: Continental recycling: the oxygen isotope point of view. *Geochemistry, Geophysics, Geosystems 6*, doi:10.1029/-2005GC000958.

Singer, B.S., O'Neil, J.R. & Brophy, J.G., 1992: Oxygen isotope constraints on the petrogenesis of Aleutian arc magmas. *Geology 20*, 367-370.

Söderlund, U. & Johansson, L., 2002: A simple way to extract baddeleyite. *Geochemistry, Geophysics, Geosystems 3*, doi:10.1029/2001GC000212.

Söderlund, U., Patchett, P.J., Vervoort, J.D. & Isachsen, C.E., 2004: The ^{176}Lu decay constant determined by Lu-Hf and U-Pb isotope systematics of Precambrian mafic intrusions. *Earth and Planetary Science Letters 219*, 311-324.

Soumaila, A., Henry, P. & Rossy , M., 2004: Contexte de mise en place des roches basiques de la ceinture de roches vertes birimienne de Diagorou-Darbani (Liptako, Niger, Afrique de l'Ouest): plateau océanique ou environnement d'arc/bassin arriére-arc océanique. *Comptes Rendus Geoscience 336*, 1137-

1147.

Stacey, J.S. & Kramers, J.D., 1975: Approximation of terrestrial lead isotope evolution by a 2-stage model. *Earth and Planetary Science Letters 26*, 207-221.

Steiger, R.H. & Jäger, E., 1977: Subcommission on geochronology: convention of the use of decay constants in geo- and cosmochronology. *Earth and Planetary Science Letters 36*, 359-362.

Sylvester, P.J. & Attoh, K., 1992: Lithostratigraphy and composition of 2.1 Ga greenstone belts of the West African Craton and their bearing on crustal evolution and the Archean-Proterozoic boundary. *Journal of Geology 100*, 377-393.

Taylor, P.N., Moorbarth, S., Leube, A. & Hirdes, W., 1992: Early Proterozoic crustal evolution in the Birimian of Ghana: constraints from geochronology and isotope geochemistry. *Precambrian Research 56*, 97-111.

Tera, F. & Wasserburg, G.J., 1972: U-Th-Pb systematics in three Apollo 14 basalts and the problem of initial Pb in lunar rocks. *Earth and Planetary Science Letters 14*, 271-304.

Valley, J.W., 2003: Oxygen isotopes in zircon. *In* J.M. Hanchar & P.W.O. Hoskin (eds.): *Reviews in mineralogy and geochemistry 53*, 343-385. Mineralogical Society of America, Washington.

Valley, J.W., Chiarenzelli, J.R. & McLelland, J.M., 1994: Oxygen isotope geochemistry of zircon. *Earth and Planetary Science Letters 126*, 187-206.

Valley, J.W., Kinny, P.D., Schulze, D.J. & Spicuzza, M.J., 1998: Zircon megacrysts from kimberlite: oxygen isotope variability among mantle melts. *Contributions to mineralogy and petrology 133*, 1-11.

Valley, J.W., Lackey, J.S., Cavosie, A.J., Clechenko, C.C., Spicuzza, M.J., Basei, M.A.S., Bindeman, I., Ferreira, V.P., Sial, A.N., King, E.M., Peck, W.H, Sinha, A.K. & Wei, C.S., 2005: 4.4 billion years of crustal maturation: oxygen isotope ratios of magmatic zircon. *Contribution to Mineralogy and Petrology 150*, 561-580.

Vance, D. & Thrilwall, M., 2002: An assessment of mass discrimination in MC-ICPMS using Nd isotopes. *Chemical Geology 185*, 227-240.

Vermeesch, P., 2004: How may grains are needed for a provenance study? *Earth and Planetary Science Letters 224*, 441-451.

Vervoort, J.D. & Blichert-Toft, J., 1999: Evolution of the depleted mantle: Hf isotope evidence from juvenile rocks through time. *Geochimica et Cosmochimica Acta 63*, 533-556.

Vervoort, J.D., Patchett, P.J., Söderlund, U. & Baker, M., 2004: Isotopic composition of Yb and the determination of Lu concentrations and Lu/Hf ratios by isotope dilution using MC-ICPMS. *Geochemistry, Geophysics, Geosystems 5*, doi: 10.1029/2004GC000721.

Vroon, P.Z., Lowry, D, van Bergen, M.J., Boyce, A.J. & Mattey, D.P., 2001: Oxygen isotope systematics of the Banda Arc: low $\delta^{18}O$ despite involvement of subducted continental material in magma genesis. *Geochimica et Cosmochimica Acta 65*, 589-609.

Wang, C.Y., Campbell, I.H., Allen, C.M., Williams, I.S. & Eggins, S.M, 2009: Rate of growth of the preserved North American continental crust: evidence from Hf and O isotopes in Mississippi detrital zircons. *Geochimica et Cosmochimica Acta 73*, 712-728.

Wang, C.Y., Campbell, I.H., Stepanov, A.S., Allen, C.M. & Burtsev, I.N., 2011: Growth rate of the preserved continental crust: II. Constraints from Hf and O isotopes in detrital zircons from Greater Russian Rivers. *Geochimica et Cosmochimica Acta 75*, 1308-1345.

Watson, E.B. & Cherniak, D.J., 1997: Oxygen diffusion in zircon. *Earth and Planetary Science Letters 148*, 527-544.

Watson, E.B., Cherniak, D.J., Hanchar, J.M., Harrison, T.M. & Wark, D.A., 1997: The incorporation of Pb into zircon. *Chemical Geology 141*, 19-31.

Wetherill, G.W., 1956: Discordant uranium-lead ages, I. *Transaction, American Geophysical Union 37*, 320 -326.

Whitehouse, M.J. & Kamber, B.S., 2005: Assigning dates to thin gneissic veins in high-grade metamorphic terranes: a cautionary tale from Akilia, Southwest Greenland. *Journal of Petrology 46*, 291-318.

Whitehouse, M.J., Kamber, B.S. & Moorbath, S., 1999: Age significance of U-Th-Pb zircon data from early Archean rocks of west Greenland – a reassessment based on combined ion microprobe and imaging studies. *Chemical Geology 160*, 210-224.

Whitehouse, M.J. & Nemchin, A.A., 2009: High precision, high accuracy measurement of oxygen isotopes in a large lunar zircon by SIMS. *Chemical Geology 261*, 32-42.

Wiedenbeck, M., Hanchar, J.M, Peck, W.H., Sylvester, P., Valley, J., Whitehouse, M., Kronz, A., Morishita, Y., Nasdala, L., Fiebig, J., Franchi, I., Girard, J.-P., Greenwood, R.C., Hinton, R., Kita, N., Mason, P.R.D., Norman, M., Ogasawara, M., Piccoli, P.M., Rhede, D., Satoh, H., Schulz-Dobrick, B., Skår, O., Spicuzza, M.J., Terada, K., Tindle, A., Togashi, S., Vennemann, T., Xie, Q. & Zheng, Y.-F., 2004. Further characterisation of the 91500 zircon crystal. *Geostandards and Geoanalytical Research 28*, 9-39.

Wilde, S.A., Valley, J.W., Peck, W.H. & Graham, C.M., 2001: Evidence from detrital zircons for the existence of continental crust and oceans on the Earth 4.4 Gyr ago. *Nature 409*, 175-178.

Williams, I.S., 1998: U-Th-Pb Geochronology by ion microprobe. *In* M.A. McKibben, W.C. Shanks III & W.I. Ridley, (eds.). *Applications of microanalytical techniques to understanding mineralizing processes.* Reviews in Economic Geology 7, 1-35.

Winter, J.D., 2010: *Principles of Igneous and Metamorphic Petrology*, 2nd edition. Pearson Education, 720 pp.

Woodhead, J.D. & Hergt, J.M., 2005: A preliminary appraisal of seven natural zircon reference materials for in situ Hf isotope determination. *Geostandards and Geoanalytical Research 29*, 183-195.

Zheng, Y.-F., Wu, Y.-B., Chen, F.-K., Gong, B., Li, L. & Zhao, Z.-F., 2004: Zircon U-Pb and oxygen isotope evidence for a large-scale ^{18}O depletion event in igneous rocks during the Neoproterozoic. *Geochimica et Cosmochimica Acta 68*, 4145-4165.

Appendix I

1 U-Th-Pb zircon analyses

Secondary ion mass spectrometer (SIMS) U-Th -Pb analyses were carried out using a large geometry Cameca IMS1280 instrument at the Swedish Museum of Natural History. Instrument set up broadly follows that described by Whitehouse et al. (1999), Whitehouse & Kamber (2005) and references therein. An O_2^- primary beam with 23 kV incident energy (-13kV primary, +10 kV secondary) was used for sputtering. For this study, the primary beam was operated in aperture illumination (Köhler) mode yielding a ca. 15-20 µm spot. Presputtering with a 25 µm raster for 120 seconds, centring of the secondary ion beam in the 3000 µm field aperture (FA), mass calibration optimisation, and optimisation of the secondary beam energy distribution were performed automatically for each run, FA and energy adjustment using the $^{90}Zr_2{}^{16}O^+$ species at nominal mass 196. Mass calibration of all peaks in the mono-collection sequence was performed at the start of each session; within run mass calibration optimisation scanned only those peaks that yield consistently high signals from the zircon matrix, namely $^{90}Zr_2{}^{16}O^+$ (nominal mass 196), $^{94}Zr_2{}^{16}O^+$ (nominal mass 204), $^{177}HfO_2{}^+$ (nominal mass 209), $^{238}U^+$ and $^{238}U^{16}O_2{}^+$, with intermediate peaks adjusted by interpolation. A mass resolution (M/ΔM) of ca. 5400 was used to ensure adequate separation of Pb isotope peaks from nearby $HfSi^+$ species. Ion signals were detected using the axial ion-counting electron multiplier. All analyses were run in fully automated chain sequences.

Data reduction assumes a power law relationship between Pb^+/U^+ and $UO_2{}^+/U^+$ ratios with an empirically derived slope in order to calculate actual Pb/U ratios based on those in the 91500 standard. U concentrations and Th/U ratio are also referenced to the 91500 standard. Common Pb corrections are made only when ^{204}Pb counts statistically exceed average background and assume a $^{207}Pb/^{206}Pb$ ratio of 0.83 (equivalent to present day Stacey & Kramers (1975) model terrestrial Pb). Decay constants follow the recommendations of Steiger & Jäger (1977). All age calculations were done in Isoplot 3.70 (Ludwig 2008).

2 $\delta^{18}O$ analyses

Zircon oxygen isotopes were measured at the same spot sites as for U-Pb using a Cameca IMS1280 multi-collector ion microprobe at the Swedish Museum of Natural History. The instrument setup and analytical procedures followed closely those of Whitehouse & Nemchin (2009), using a ca. 2 nA Cs^+ primary ion beam together with a normal incidence low energy electron gun for charge compensation, medium field magnification (ca. 80x) and two Faraday detectors at a common mass resolution of ca. 2500. Measurements were performed in pre-programmed chain analysis mode with automatic field aperture and entrance slit centring on the ^{16}O signal. The magnetic field was locked using NMR regulation for the entire analytical session. Each data-acquisition run comprised a 20 x 20 µm pre-sputter to remove the Au layer followed by the centring steps and 64 seconds of data integration performed using a non-rastered, ca., 10 x 10 µm spot,. Every set of four to five unknowns was followed by two to five bracketing analyses on the Geostandards 91500 zircon. A $\delta^{18}O$ value of +9.86‰ (SMOW, Wiedenbeck et al. 2004) was assumed for the 91500 zircon in data normalisation and small linear-drift corrections were applied to each session.

3 Lu-Hf isotope analyses

Each analysis began with a run of a 30 second electronic baseline followed by an ablation period of 60 seconds involving 60 integration cycles of one second each. A laser pulse repetition rate of 4 Hz was used and the laser energy was held at ~6 J/cm^2 which equals an ablation rate of 0.06 µm per pulse for zircon (Anthony Kemp, personal communication). Helium carrier gas was used to transport the ablated particles from the sample chamber. It was combined with argon gas (flow rate ~0.8 l/min) and nitrogen (~0.005 l/min) further downstream before entering the argon plasma. Masses ^{171}Yb, ^{173}Yb, ^{175}Lu, ^{176}(Hf+Lu+Yb), ^{177}Hf, ^{178}Hf, ^{179}Hf and ^{180}(Hf+W+Ta) were measured simultaneously by Faradays detectors of the multi-collector detector unit. Isobaric interference of ^{176}Yb and ^{176}Lu on ^{176}Hf was calculated using the measured intensities of ^{171}Yb and ^{175}Lu along with known isotopic ratios of $^{176}Yb/^{171}Yb$ = 0.897145 (Segal et al. 2003) and $^{176}Lu/^{175}Lu$ = 0.02655 (Vervoort et al. 2004). Mass bias corrections were calculated using the exponential law. For calculations of β_{Hf}, measured intensities of ^{179}Hf and ^{177}Hf and a $^{179}Hf/^{177}Hf$ ratio of 0.7325 was used. β_{Yb} was calculated using measured intensities of ^{173}Yb and ^{171}Yb and a $^{176}Yb/^{171}Yb$ ratio of 1.130172 (Segal et al. 2003). Mass bias behaviour of Lu was assumed to be identical to Yb.

Three standards were used for quality control, FC-1, Mud tank zircon (Woodhead & Hergt 2005), and synthetic zircon (Fisher et al. 2011). In addition, the stable Hf isotope ratios, $^{178}Hf/^{177}Hf$ and ^{180}Hf $/^{177}Hf$, were monitored since these should be constant within error throughout the measurements. Analysed $^{176}Hf/^{177}Hf$ ratios of the unknown zircons were normalized based on comparison between the mean of analysed $^{176}Hf/^{177}Hf$ ratios of Mud tank zircon and its reported $^{176}Hf/^{177}Hf$ ratio of 0.282507 determined by solution analysis (Woodhead & Hergt 2005).

Calculations of ε_{Hf} were performed using $\lambda^{176}Lu = 1.867\text{x}10^{-11}$ yr^{-1} (Söderlund et al. 2004), $(^{176}Lu/^{177}Hf)_{CHUR}$ = 0.0336 and $(^{176}Hf/^{177}Hf)_{CHUR}$ = 0.282785 (Bouvier et al. 2008). Two stage model ages were calculated using new crust values of $^{176}Hf/^{177}Hf$=0.28315 and $^{176}Lu/^{177}Hf$ = 0.03795 (Dhuime et al. 2011a) and by assuming a $^{176}Lu/^{177}Hf$ of 0.015 for the crustal source.

Appendix II

Table 1: Compilation of U-Pb crystallisation ages, $\delta^{18}O$, ε_{Hf} and Hf-model ages of the analysed zircon.

Spot I.D	Sample	Structure	$^{207}Pb/^{206}Pb$ (Ma)		σ (Ma)	Disc. 2s (%)	$\delta^{18}O$ (‰)		abs (‰)	εHf_T		2σ	T_{NC} (Ma)	Comment
n3687-01	Ankobra river	weak z	2125	±	6		7.76	±	0.28	5.82	±	0.57	2204	
n3687-02	Ankobra river	weak z	2132	±	12									Lost
n3687-03	Ankobra river	unzoned	2164	±	12									Lost
n3687-04	Ankobra river	weak z	2150	±	11		7.15	±	0.27	5.20	±	0.60	2264	
n3687-05	Ankobra river	ign.zon	2160	±	4		6.29	±	0.29	4.23	±	0.63	2332	
n3687-06	Ankobra river	ign.zon	2183	±	97	-47								Discord.
n3687-07	Ankobra river	ign.zon	2155	±	9		6.74	±	0.28	5.79	±	0.72	2230	
n3687-08	Ankobra river	ign.zon	2157	±	14									Lost
n3687-09	Ankobra river	ign.zon	2154	±	8		5.56	±	0.26	4.21	±	0.44	2329	
n3687-10	Ankobra river	ign.zon	2148	±	11		6.33	±	0.27	5.55	±	0.63	2239	
n3687-11	Ankobra river	ign.zon	2161	±	6		6.27	±	0.31	5.08	±	0.49	2280	
n3687-12	Ankobra river	ign.zon	2121	±	7		6.72	±	0.28	4.92	±	0.51	2258	
n3687-13	Ankobra river	ign.zon	2183	±	8		5.52	±	0.26	4.05	±	0.40	2363	
n3687-14	Ankobra river	ign.zon	2148	±	8		6.03	±	0.27	5.29	±	0.48	2256	
n3687-15	Ankobra river	ign.zon	2156	±	5	1	6.23	±	0.27	3.03	±	0.56	2405	
n3687-16	Ankobra river	ign.zon	2200	±	6									Lost
n3687-17	Ankobra river	unzoned	2154	±	6									Lost
n3687-18	Ankobra river	ign.zon	2153	±	7		5.68	±	0.27	5.15	±	0.52	2269	
n3687-19	Ankobra river	ign.zon	2159	±	12	-6	6.66	±	0.28	5.31	±	0.65	2264	
n3687-20	Ankobra river	ign.zon	2101	±	8		7.87	±	0.29	4.59	±	0.35	2262	
n3687-21	Ankobra river	ign.zon	2149	±	6	1	5.31	±	0.30	4.76	±	0.53	2291	
n3687-22	Ankobra river	ign.zon	2154	±	6									Lost
n3687-23	Ankobra river	ign.zon	2120	±	5		6.32	±	0.30	4.61	±	0.45	2277	
n3687-24	Ankobra river	ign.zon	2161	±	10		6.24	±	0.27	5.95	±	0.43	2225	
n3687-25	Ankobra river	ign.zon	2154	±	7		6.15	±	0.32	5.01	±	0.55	2279	
n3687-26	Ankobra river	unzoned	2184	±	9		5.87	±	0.27	4.69	±	0.44	2323	
n3687-27	Ankobra river	ign.zon	2131	±	9		6.44	±	0.27	5.38	±	0.51	2237	
n3687-28	Ankobra river	weak zon	2166	±	9		6.69	±	0.28	4.25	±	0.39	2336	
n3687-29	Ankobra river	ign.zon	2113	±	7		6.97	±	0.29	5.62	±	0.48	2207	
n3687-30	Ankobra river	ign.zon	2116	±	7		6.69	±	0.28	4.55	±	0.56	2277	
n3687-31	Ankobra river	ign.zon	2147	±	7		7.45	±	0.33	4.77	±	0.62	2288	
n3687-32	Ankobra river	weak zon	2168	±	7		7.00	±	0.27	5.82	±	0.54	2239	
n3687-33	Ankobra river	ign.zon	2164	±	9		7.11	±	0.29	6.44	±	0.40	2196	
n3687-34	Ankobra river	ign.zon	2165	±	8		6.49	±	0.29	5.78	±	0.59	2239	
n3687-35	Ankobra river	ign.zon	2159	±	8	-2	7.82	±	0.29	4.58	±	0.59	2310	
n3687-36	Ankobra river	ign.zon	2142	±	12	-9								Lost
n3687-37	Ankobra river	ign.zon	2199	±	9		5.44	±	0.27	5.20	±	0.61	2303	
n3687-38	Ankobra river	ign.zon	2142	±	7		7.51	±	0.29	5.38	±	0.38	2246	
n3687-39	Ankobra river	weak zon	2108	±	8		7.54	±	0.29	6.36	±	0.52	2156	
n3687-40	Ankobra river	weak zon	2153	±	7		6.82	±	0.28	5.01	±	0.45	2278	
n3687-41	Ankobra river	unzoned	2166	±	12		7.18	±	0.28	6.10	±	0.52	2220	

n3687-42	Ankobra river	ign.zon	2164	±	9	-1	7.15	±	0.27	5.02	±	0.57	2286	
n3687-43	Ankobra river	weak zon	2144	±	5		6.79	±	0.29	4.59	±	0.56	2297	
n3687-44	Ankobra river	unzoned	2105	±	11		7.28	±	0.27	4.57	±	0.58	2267	
n3687-45	Ankobra river	weak zon	2170	±	7		7.57	±	0.28	4.87	±	0.50	2301	
n3687-46	Ankobra river	unzoned	2170	±	9		6.73	±	0.28	5.31	±	0.40	2272	
n3687-47	Ankobra river	unzoned	2130	±	14		6.84	±	0.27	4.00	±	0.53	2323	
n3687-48	Ankobra river	weak zon	2162	±	4		6.14	±	0.28	4.20	±	0.46	2336	
n3687-49	Ankobra river	ign.zon	2151	±	13		6.92	±	0.31	5.77	±	0.58	2228	
n3687-50	Ankobra river	ign.zon	2140	±	6		6.62	±	0.28	5.37	±	0.62	2245	
n3687-51	Ankobra river	ign.zon	2168	±	11	-4	6.60	±	0.28	3.87	±	0.52	2362	
n3687-52	Ankobra river	unzoned	2170	±	8		7.12	±	0.31	4.49	±	0.58	2324	
n3687-53	Ankobra river	ign.zon	2120	±	40		6.37	±	0.29	3.51	±	1.32	2346	Precision
n3687-54	Ankobra river	ign.zon	1888	±	22	-19	9.14	±	0.29					Discord.
n3687-55	Ankobra river	weak zon	2128	±	11		7.08	±	0.29	3.41	±	0.57	2358	
n3687-56	Ankobra river	unzoned	2129	±	7		5.57	±	0.29	5.47	±	0.94	2229	
n3687-57	Ankobra river	ign.zon	2147	±	9	-1	7.02	±	0.28	4.48	±	0.49	2307	
n3687-58	Ankobra river	ign.zon	2263	±	12		8.92	±	0.31	3.90	±	0.39	2437	
n4086-01	Birim river	weak.zon	2150	±	5	-1	5.83	±	0.24	-1.70	±	0.59	2697	
n4086-02	Birim river	unzoned	2223	±	14		-1.18	±	0.22	4.16	±	0.58	2388	
n4086-03	Birim river	ign.zon	2078	±	8	-15	5.27	±	0.24					Discord.
n4086-04	Birim river	ign.zon	2198	±	6	-1	6.09	±	0.24	2.19	±	0.59	2491	
n4086-05	Birim river	ign.zon	2214	±	8		4.97	±	0.24	3.29	±	0.50	2435	
n4086-06	Birim river	ign.zon	2212	±	8		5.53	±	0.24	2.69	±	0.56	2472	
n4086-07	Birim river	unzoned	2227	±	7		0.93	±	0.34	4.38	±	0.58	2378	
n4086-08	Birim river	weak zon	2156	±	6	-3	5.35	±	0.22	-4.82	±	0.99	2897	
n4086-09	Birim river	unzoned	2230	±	9		4.39	±	0.24	2.88	±	1.75	2475	
n4086-10	Birim river	unzoned	2226	±	7		4.69	±	0.22	3.84	±	0.80	2410	
n4086-11	Birim river	ign.zon	2159	±	5	-13	4.42	±	0.25	2.04	±	0.71	2470	Discord.
n4086-12	Birim river	ign.zon	1900	±	10	-44	6.93	±	0.31					Discord.
n4086-13	Birim river	weak zon	2142	±	4	-11				0.26	±	1.21	2567	Discord.
n4086-14	Birim river	weak zon	2197	±	6	-7	5.95	±	0.23	0.90	±	0.60	2572	
n4086-15	Birim river	unzoned	2159	±	5	-6	4.91	±	0.23	1.27	±	1.27	2518	
n4086-16	Birim river	unzoned	2223	±	11		3.69	±	0.26					Popped out
n4086-17	Birim river	ign.zon	2140	±	12	-13	4.66	±	0.25	1.08	±	0.70	2514	Discord.
n4086-18	Birim river	weak zon	2208	±	6		5.05	±	0.25	3.53	±	0.74	2416	
n4086-19	Birim river	unzoned	2231	±	12		3.97	±	0.24	4.41	±	0.69	2379	
n4086-20	Birim river	unzoned	2226	±	10		4.16	±	0.27	4.77	±	0.90	2352	
n4086-21	Birim river	ign.zon	2165	±	6		4.11	±	0.21	3.34	±	1.18	2392	
n4086-22	Birim river	unzoned	2233	±	10		3.78	±	0.26	4.14	±	1.02	2398	
n4086-23	Birim river	unzoned	1494	±	6		5.07	±	0.25	6.38	±	0.83	1656	
n4086-24	Birim river	weak zon	2158	±	5		4.64	±	0.23	1.59	±	0.79	2497	
n4086-25	Birim river	weak zon	2184	±	6		4.44	±	0.25	3.12	±	1.03	2422	
n4086-26	Birim river	weak zon	2209	±	14	-2	5.49	±	0.23	3.19	±	0.31	2438	
n4086-27	Birim river	unzoned	2229	±	5		2.46	±	0.24	4.76	±	0.78	2356	
n4086-28	Birim river	weak zon	2200	±	8		4.99	±	0.22	2.93	±	0.56	2447	

n4086-29	Birim river	unzoned	2220	±	6		3.52	±	0.22	4.35	±	0.83	2374	
n4086-30	Birim river	unzoned	2124	±	30		4.41	±	0.24	1.80	±	0.78	2457	
n4086-31	Birim river	unzoned	2146	±	13		4.34	±	0.22	-5.74	±	0.56	2946	
n4086-32	Birim river	weak zon	2219	±	6	-2	3.68	±	0.25	3.36	±	0.69	2435	
n4086-33	Birim river	unzoned	2232	±	7		4.39	±	0.24	2.00	±	0.51	2531	
n4086-34	Birim river	unzoned	2226	±	10		3.95	±	0.21	2.49	±	0.86	2495	
n4086-35	Birim river	unzoned	2212	±	10	-5	5.45	±	0.24	3.25	±	0.74	2437	
n4086-36	Birim river	weak zon	2148	±	7		4.55	±	0.29	-3.10	±	0.69	2783	
n4086-37	Birim river	unzoned	1883	±	6		5.86	±	0.27	-8.43	±	0.99	2904	
n4086-38	Birim river	weak zon	2122	±	135		5.11	±	0.26					Precision
n4086-39	Birim river	ign.zon	2210	±	6		6.02	±	0.25	3.39	±	0.47	2426	
n4086-40	Birim river	unzoned	2204	±	10		5.44	±	0.24	1.96	±	0.54	2511	
n4081-01	Black Volta river	unzoned	2135	±	5		8.32	±	0.18	6.41	±	0.49	2174	
n4081-02	Black Volta river	unzoned	2116	±	9		10.91	±	0.19	3.99	±	0.46	2312	
n4081-03	Black Volta river	ign.zon	2082	±	78		7.36	±	0.23	3.24	±	0.59	2331	Precision
n4081-04	Black Volta river	unzoned	2097	±	8		7.02	±	0.24	4.15	±	0.52	2286	
n4081-05	Black Volta river	weak zon	2243	±	10		5.97	±	0.21	2.64	±	0.42	2500	
n4081-06	Black Volta river	unzoned	2190	±	10	-1	6.25	±	0.21	5.14	±	0.43	2300	
n4081-07	Black Volta river	unzoned	2191	±	18	-3	5.11	±	0.21	5.05	±	0.42	2306	
n4081-08	Black Volta river	unzoned	2130	±	9		7.96	±	0.25	3.86	±	0.46	2332	
n4081-09	Black Volta river	ign.zon	2151	±	7		5.79	±	0.20	4.12	±	0.52	2332	
n4081-09b	Black Volta river	unzoned	2174	±	8	-2	7.55	±	0.22	4.06	±	0.69	2355	
n4081-10	Black Volta river	ign.zon	2131	±	6		7.83	±	0.18	4.12	±	0.57	2316	
n4081-11	Black Volta river	weak zon	2150	±	7		5.82	±	0.19	2.81	±	0.43	2414	
n4081-12	Black Volta river	unzoned	2150	±	11		6.47	±	0.22	4.84	±	0.53	2286	
n4081-13	Black Volta river	unzoned	2137	±	10		7.35	±	0.24	4.05	±	0.45	2325	
n4081-14	Black Volta river	unzoned	2177	±	9		3.41	±	0.25	3.01	±	0.47	2423	
n4081-15	Black Volta river	unzoned	2164	±	6		4.57	±	0.20	5.55	±	0.47	2253	
n4081-16	Black Volta river	weak zon	2177	±	15		5.54	±	0.19	5.00	±	0.58	2298	
n4081-17	Black Volta river	ign.zon	2186	±	13	-2	4.67	±	0.24	4.82	±	0.60	2316	
n4081-18	Black Volta river	ign.zon	2139	±	9	-2	6.69	±	0.20	3.96	±	0.43	2333	
n4081-19	Black Volta river	ign.zon	2177	±	10		6.50	±	0.18	4.63	±	0.41	2321	
n4081-20	Black Volta river	ign.zon	2175	±	6		5.62	±	0.21	2.79	±	0.49	2435	
n4081-21	Black Volta river	unzoned	2137	±	11		7.71	±	0.23	9.60	±	0.91	1975	Drift in signal (Lu-Hf)
n4081-22	Black Volta river	unzoned	2135	±	13		6.14	±	0.19	5.09	±	0.39	2258	
n4081-23	Black Volta river	unzoned	2166	±	10		5.01	±	0.22	4.80	±	0.56	2301	
n4081-24	Black Volta river	weak zon	2182	±	9		4.42	±	0.26	4.10	±	0.37	2359	
n4081-25	Black Volta river	ign.zon	2190	±	10	-5	5.02	±	0.19	4.40	±	0.59	2346	
n4081-26	Black Volta river	unzoned	2144	±	8		6.17	±	0.17	5.20	±	0.43	2259	
n4081-27	Black Volta river	unzoned	2147	±	9	-27	1.19	±	0.23					Discord.
n4081-28	Black Volta river	unzoned	2149	±	8		5.58	±	0.22	3.87	±	0.52	2347	
n4081-29	Black Volta river	unzoned	2117	±	7	-1	4.99	±	0.21	4.29	±	0.38	2294	
n4081-30	Black Volta river	unzoned	2178	±	9		4.54	±	0.22	4.49	±	0.42	2331	
n4081-31	Black Volta river	unzoned	2168	±	11		5.58	±	0.23	5.10	±	0.60	2285	
n4081-32	Black Volta river	weak zon	2134	±	11		6.64	±	0.18	4.16	±	0.53	2316	
n4081-33	Black Volta river	ign.zon	2173	±	12		5.91	±	0.22	4.71	±	0.34	2313	

n4081-34	Black Volta river	ign.zon	2204	±	7		4.07	±	0.18	4.22	±	0.32	2369	
n4081-35	Black Volta river	unzoned	2193	±	20		5.42	±	0.22	5.51	±	0.34	2279	
n4081-36	Black Volta river	weak zon	2147	±	7		4.96	±	0.18	3.74	±	0.32	2353	
n4081-37	Black Volta river	ign.zon	2138	±	7		3.02	±	0.16	3.23	±	0.34	2378	
n4081-38	Black Volta river	unzoned	2162	±	8		4.61	±	0.24	3.48	±	0.40	2382	
n4081-39	Black Volta river	weak zon	2138	±	10		4.78	±	0.22	3.68	±	0.61	2350	
n4081-40	Black Volta river	weak zon	2200	±	26		4.91	±	0.25	4.59	±	0.43	2342	
n4081-41	Black Volta river	unzoned	2499	±	15	-13	5.28	±	0.30					Discord.
n4081-42	Black Volta river	ign.zon	2257	±	10	-2	5.37	±	0.29	6.95	±	0.45	2240	
n4081-43	Black Volta river	unzoned	2282	±	6		3.93	±	0.26	4.55	±	0.40	2412	
n4081-44	Black Volta river	ign.zon	2214	±	5		4.76	±	0.26	5.74	±	0.58	2281	
n4081-45	Black Volta river	weak zon	2135	±	9		6.67	±	0.27	3.00	±	0.60	2391	
n4081-46	Black Volta river	unzoned	2213	±	7		3.82	±	0.25	5.62	±	0.64	2288	
n4081-47	Black Volta river	unzoned	2128	±	15		6.56	±	0.30	4.12	±	0.49	2314	
n4081-48	Black Volta river	ign.zon	2155	±	7		7.49	±	0.29	4.36	±	0.58	2320	
n4081-49	Black Volta river	weak zon	2425	±	10	-12	5.32	±	0.29					Discord.
n4081-50	Black Volta river	ign.zon	2291	±	13	-26	-0.26	±	0.30					Discord.
n4081-50b	Black Volta river	ign.zon	2381	±	8	-20								Discord.
n4082-01	Red Volta river	ign.zon	2153	±	17	-2	6.44	±	0.27	6.82	±	0.49	2164	
n4082-02	Red Volta river	ign.zon	2128	±	6	-1	5.79	±	0.25	5.42	±	0.66	2232	
n4082-03	Red Volta river	unzoned	2149	±	10									Lost
n4082-04	Red Volta river	unzoned	2114	±	21		5.60	±	0.29					Drift in signal
n4082-05	Red Volta river	unzoned	2142	±	9		5.19	±	0.28	5.56	±	0.56	2234	
n4082-06	Red Volta river	unzoned	2140	±	13		5.05	±	0.29	5.06	±	0.46	2264	
n4082-07	Red Volta river	weak zon	2150	±	11		6.85	±	0.30	4.50	±	0.46	2308	
n4082-08	Red Volta river	weak zon	2160	±	11		7.05	±	0.27	5.73	±	0.42	2238	
n4082-09	Red Volta river	weak zon	2138	±	7		5.52	±	0.26	3.79	±	0.63	2343	
n4082-10	Red Volta river	unzoned	2124	±	7		4.95	±	0.27	3.98	±	0.40	2319	
n4082-11	Red Volta river	ign.zon	2137	±	7		5.49	±	0.31	3.20	±	0.56	2379	
n4082-12	Red Volta river		2129	±	9		6.78	±	0.31					Lost
n4082-13	Red Volta river	ign.zon	2116	±	12	-2	7.33	±	0.28	4.20	±	0.57	2300	
n4082-14	Red Volta river	unzoned	2140	±	6		6.24	±	0.26	3.15	±	0.67	2384	
n4082-15	Red Volta river	unzoned	2144	±	11		5.34	±	0.28	4.70	±	0.59	2290	
n4082-16	Red Volta river	unzoned	2132	±	6		5.95	±	0.29	3.98	±	0.47	2326	
n4082-17	Red Volta river	ign.zon	2145	±	10	-1	7.00	±	0.28	4.59	±	0.50	2298	
n4082-18	Red Volta river	ign.zon	2181	±	8	-2	6.39	±	0.25	4.23	±	0.60	2350	
n4082-19	Red Volta river	unzoned	2153	±	10		3.96	±	0.25	6.51	±	0.58	2183	
n4082-20	Red Volta river	ign.zon	2161	±	11		5.09	±	0.28	3.38	±	0.46	2387	
n4082-21	Red Volta river	ign.zon	2144	±	9		5.83	±	0.28	4.06	±	0.66	2331	
n4082-22	Red Volta river	ign.zon	2139	±	6		6.15	±	0.27	3.36	±	0.61	2371	
n4082-23	Red Volta river	ign.zon	2137	±	9		5.90	±	0.31	3.52	±	0.56	2359	
n4082-24	Red Volta river	weak zon	2151	±	6		5.22	±	0.31	4.38	±	0.50	2316	
n4082-25	Red Volta river	unzoned	2130	±	11		6.40	±	0.28	3.29	±	0.55	2368	
n4082-26	Red Volta river	unzoned	2161	±	10		6.27	±	0.29	4.49	±	0.40	2317	
n4082-27	Red Volta river	weak zon	2137	±	7		6.56	±	0.28	4.26	±	0.56	2312	
n4082-28	Red Volta river	unzoned	2136	±	6	1	5.43	±	0.25	4.53	±	0.65	2295	

n4082-29	Red Volta river	unzoned	2185	±	11		6.06	±	0.31	4.33	±	0.66	2347	
n4082-30	Red Volta river	ign.zon	2132	±	6		6.13	±	0.25	4.83	±	0.35	2272	
n4082-31	Red Volta river	unzoned	2136	±	6		6.06	±	0.25	-0.15	±	0.54	2589	
n4082-32	Red Volta river	weak zon	2132	±	6		6.39	±	0.31	4.87	±	0.89	2270	
n4082-33	Red Volta river	unzoned	2136	±	6		5.57	±	0.29	4.66	±	0.54	2286	
n4082-34	Red Volta river	unzoned	2130	±	8		6.11	±	0.28	3.72	±	0.57	2341	
n4082-35	Red Volta river	unzoned	2131	±	19		6.23	±	0.27	3.64	±	0.36	2347	
n4082-36	Red Volta river	unzoned	2132	±	6		5.99	±	0.26	4.46	±	0.44	2296	
n4082-37	Red Volta river	unzoned	2130	±	8		5.91	±	0.26	3.94	±	0.63	2327	
n4082-38	Red Volta river	ign.zon	2130	±	6		6.13	±	0.26	5.04	±	0.45	2257	
n4082-39	Red Volta river	unzoned	2135	±	10		6.66	±	0.27	3.95	±	0.45	2330	
n4082-40	Red Volta river	weak zon	2200	±	314		6.03	±	0.26	6.06	±	0.47	2250	Precision
n4082-41	Red Volta river	unzoned	2151	±	8		4.01	±	0.26	5.32	±	0.58	2257	
n4082-42	Red Volta river	unzoned	2365	±	17	-10	6.34	±	0.28					
n4082-43	Red Volta river	ign.zon	2142	±	6		6.82	±	0.26	3.31	±	0.75	2376	
n4082-44	Red Volta river	ign.zon	2236	±	16	-5	4.36	±	0.31	7.09	±	0.58	2214	
n4082-45	Red Volta river	ign.zon	2144	±	6		6.62	±	0.27	3.55	±	0.61	2363	
n4082-46	Red Volta river	ign.zon	2132	±	7		6.53	±	0.27	3.73	±	0.69	2342	
n4082-47	Red Volta river	ign.zon	2777	±	55	-21	6.27	±	0.28					Discord.
n4082-48	Red Volta river	ign.zon	2212	±	4	-9	5.31	±	0.28					
n4082-49	Red Volta river	ign.zon	2128	±	7	1	5.83	±	0.31	4.23	±	0.63	2307	
n4082-50	Red Volta river	ign.zon	2146	±	7		5.96	±	0.25	3.56	±	0.51	2364	
n4082-51	Red Volta river	unzoned	2131	±	8		6.22	±	0.26	3.89	±	0.41	2331	
n4082-52	Red Volta river	unzoned	2166	±	7		5.95	±	0.27	5.04	±	0.57	2287	
n4083-01	Sihili river	ign.zon	2141	±	10	-15								Discord.
n4083-02	Sihili river	ign.zon	2138	±	5			±		3.50	±	0.48	2361	
n4083-03	Sihili river	weak zon	2132	±	12			±		4.35	±	0.59	2303	
n4083-04	Sihili river	unzoned	2086	±	13									Lost
n4083-05	Sihili river	ign.zon	2130	±	6			±		4.34	±	0.58	2301	
n4083-06	Sihili river	ign.zon	2136	±	9			±		3.51	±	0.72	2359	
n4083-07	Sihili river	unzoned	2132	±	8	-3		±		4.40	±	0.85	2299	
n4083-08	Sihili river	unzoned	2099	±	10			±		2.72	±	0.38	2379	
n4083-09	Sihili river	weakzon	2143	±	7			±		3.91	±	0.48	2339	
n4083-10	Sihili river	ign.zon	2143	±	5			±		4.36	±	0.43	2311	
n4083-11	Sihili river	unzoned	2156	±	16			±		3.68	±	0.59	2364	
n4083-12	Sihili river	ign.zon	2152	±	5			±		4.32	±	0.87	2321	
n4083-13	Sihili river	ign.zon	2148	±	8	-1		±		4.09	±	0.69	2332	
n4083-14	Sihili river	weak zon	2133	±	7			±		3.75	±	0.38	2342	
n4083-15	Sihili river	unzoned	2095	±	6			±		3.20	±	0.54	2345	
n4083-16	Sihili river	ign.zon	2092	±	7			±		3.11	±	0.76	2349	
n4083-17	Sihili river	ign.zon	2130	±	7			±		3.29	±	0.48	2367	
n4083-18	Sihili river	unzoned	2105	±	4			±		3.46	±	0.86	2337	
n4083-19	Sihili river	ign.zon	2141	±	7			±		3.31	±	0.73	2375	
n4083-20	Sihili river	ign.zon	2141	±	8	-15								Discord.
n4083-21	Sihili river	weak zon	2131	±	8	-5		±		3.76	±	0.59	2339	
n4083-22	Sihili river	unzoned	2152	±	8	-3		±		4.18	±	0.62	2329	

n4083-23	Sihili river	ign.zon	2092	±	24		±	2.78	±	0.43	2369		
n4083-24	Sihili river	unzoned	2135	±	7		±	3.07	±	0.40	2386		
n4083-25	Sihili river	unzoned	2111	±	14		±	2.40	±	0.51	2409		
n4083-26	Sihili river	weak zon	2134	±	6		±	4.06	±	0.61	2322		
n4083-27	Sihili river	unzoned	2154	±	6		±	5.40	±	0.54	2254		
n4083-28	Sihili river	unzoned	2271	±	82		±	6.64	±	0.66	2271		Precision
n4083-29	Sihili river	weak zon	2188	±	9	1	±	3.95	±	0.78	2373		
n4083-30	Sihili river	unzoned	2167	±	14		±	4.08	±	0.66	2348		
n4083-31	Sihili river	unzoned	2132	±	10		±	3.84	±	0.43	2335		
n4083-32	Sihili river	unzoned	2141	±	8		±	4.06	±	0.65	2328		
n4083-33	Sihili river	unzoned	2136	±	7		±	3.91	±	0.58	2334		
n4083-34	Sihili river	unzoned	2120	±	10		±	3.69	±	0.63	2334		
n4083-35	Sihili river	unzoned	2102	±	8		±	4.49	±	0.46	2269		
n4083-36	Sihili river	unzoned	2268	±	10		±	4.20	±	0.95	2422		
n4083-37	Sihili river	ign.zon	2144	±	7		±	4.13	±	0.76	2326		
n4083-38	Sihili river	ign.zon	2135	±	33	-1	±	3.46	±	0.65	2361		Precision
n4083-39	Sihili river	ign.zon	2098	±	7		±	3.78	±	0.78	2310		
n4083-40	Sihili river	unzoned	2108	±	8		±	4.31	±	1.29	2286		
n4083-41	Sihili river	weak zon	2136	±	11		±	4.66	±	0.73	2286		
n4083-42	Sihili river	unzoned	2149	±	7								Lost
n4083-43	Sihili river	ign.zon	2145	±	7		±	2.75	±	0.54	2414		
n4083-44a	Sihili river	unzoned	2133	±	28		±	3.77	±	0.72	2340		
n4083-44b	Sihili river	unzoned	2114	±	10	-12							Discord.
n4083-45	Sihili river	ign.zon	2081	±	16	-9	±	1.56	±	0.72	2437		
n4083-46	Sihili river	unzoned	2171	±	133	-8							Precision
n4083-47	Sihili river	ign.zon	2138	±	13		±	2.68	±	0.79	2412		
n4083-48	Sihili river	weak zon	2139	±	14	-23							Discord.
n4083-49	Sihili river	ign.zon	2133	±	47	-3	±	3.12	±	0.93	2381		Precision
n4083-50	Sihili river	ign.zon	2146	±	6	-2	±	3.70	±	0.41	2355		
n4083-51a	Sihili river	weak zon	2111	±	8	-3	±	3.88	±	0.63	2316		
n4083-51b	Sihili river	weak zon	2131	±	45	-17							Discord.
n4083-52	Sihili river	ign.zon	2132	±	9	-4	±	4.79	±	0.43	2275		
n4083-53	Sihili river	ign.zon	2135	±	6		±	3.60	±	0.69	2352		
n4083-54	Sihili river	ign.zon	2134	±	7	-8	±	4.52	±	0.60	2293		

[Ψ] U-Pb ages were calculated according to recommendations of Steiger and Jäger (1977) using Isoplot 3.70 (Ludwig 2008)

[¥] $\delta^{18}O$ was calculated compared to the Standard Mean Ocean Water (SMOW) .

[§] Isobaric interference and mass bias corrections were done using values from Segal et al. (2003) for $^{173}Yb/^{171}Yb = 1.130172$ and $^{176}Yb/^{171}Yb = 0.897145$, and a value from Vervoort et al. (2004) for $^{176}Lu/^{175}Lu = 0.02655$. Mass bias behaviour of Lu was assumed to be identical to Yb. Calculations on ε_{Hf} were done using $\lambda^{176}Lu = 1.867x10^{-11}$ yr^{-1} (Söderlund et al. 2004), $(^{176}Lu/^{177}Hf)_{CHUR} = 0.0336$ and $(^{176}Hf/^{177}Hf)_{CHUR} = 0.282785$ (Bouvier et al. 2008) according to the following equation:

[φ] Two stage Hf-model ages were calculated using NC values of $^{176}Hf/^{177}Hf = 0.28315$ and $^{176}Lu/^{177}Hf=0.03795$ (Dhuime et al. 2011a) and by assuming a $^{176}Lu/^{177}Hf$ of 0.015 for the crustal source.

Appendix III

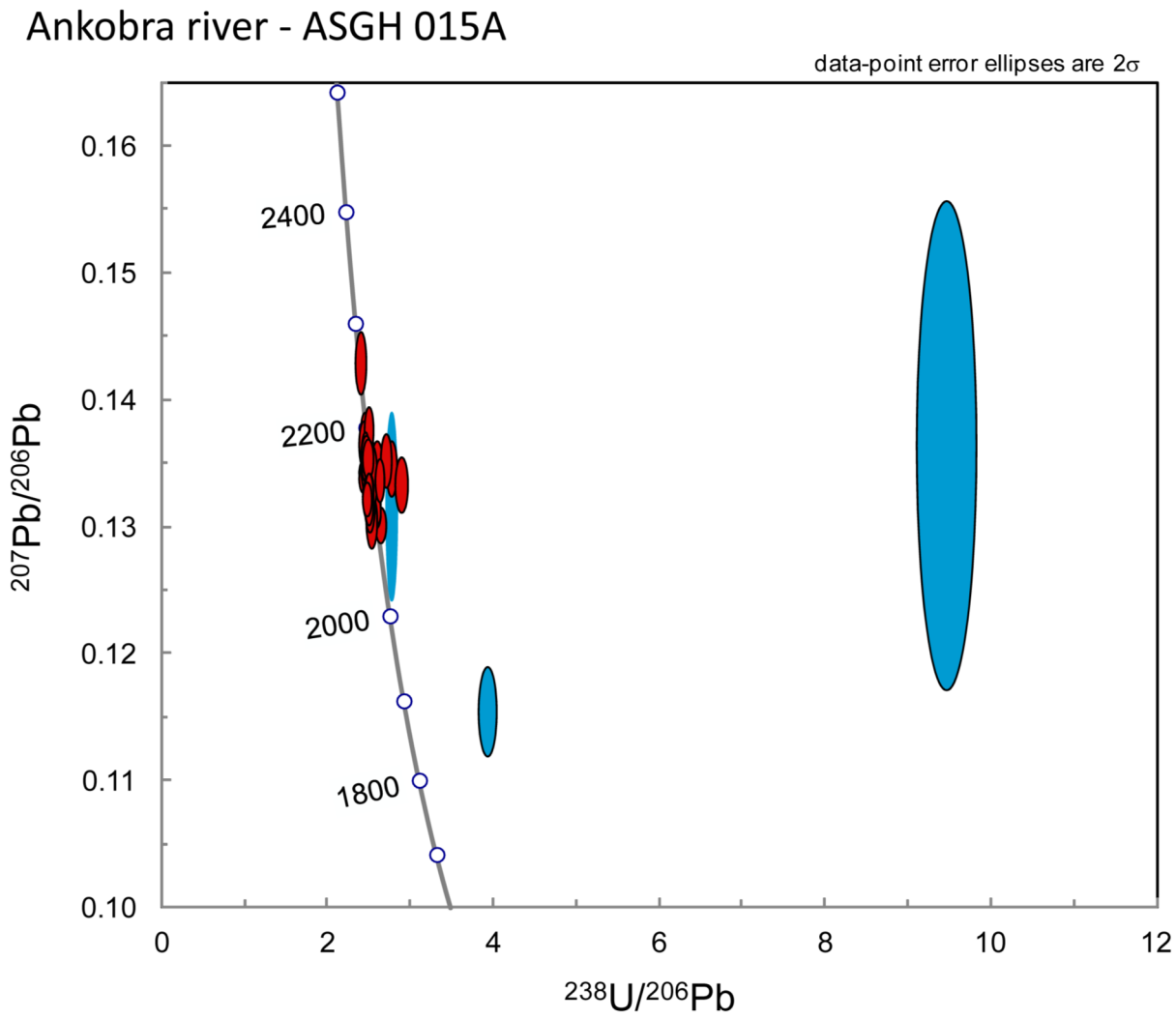

Fig. A.3.1. Tera-Wasserburg diagram showing all zircon from the Ankobra river population. Zircon represented by the blue ellipsoids were omitted due to lack of precision (>30 Ma) or discordance over 10%. Plot created using Isoplot 4.15 (Ludwig, 2008).

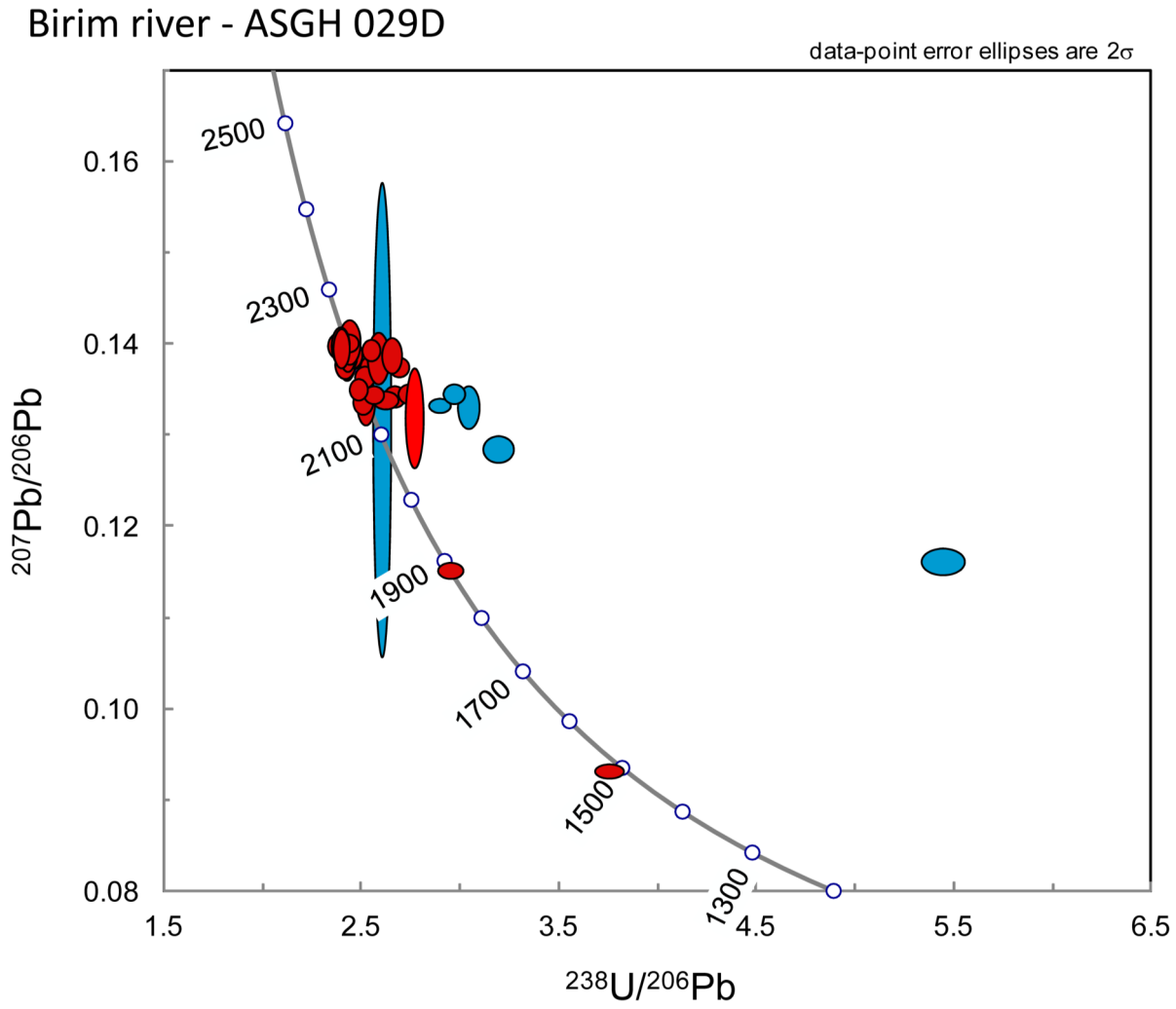

Fig. A.3.2 Tera-Wasserburg diagram showing all zircon from the Birim river population. Zircon represented by the blue ellipsoids were omitted due to lack of precision (>30 Ma) or discordance over 10%. Plot created using Isoplot 4.15 (Ludwig, 2008).

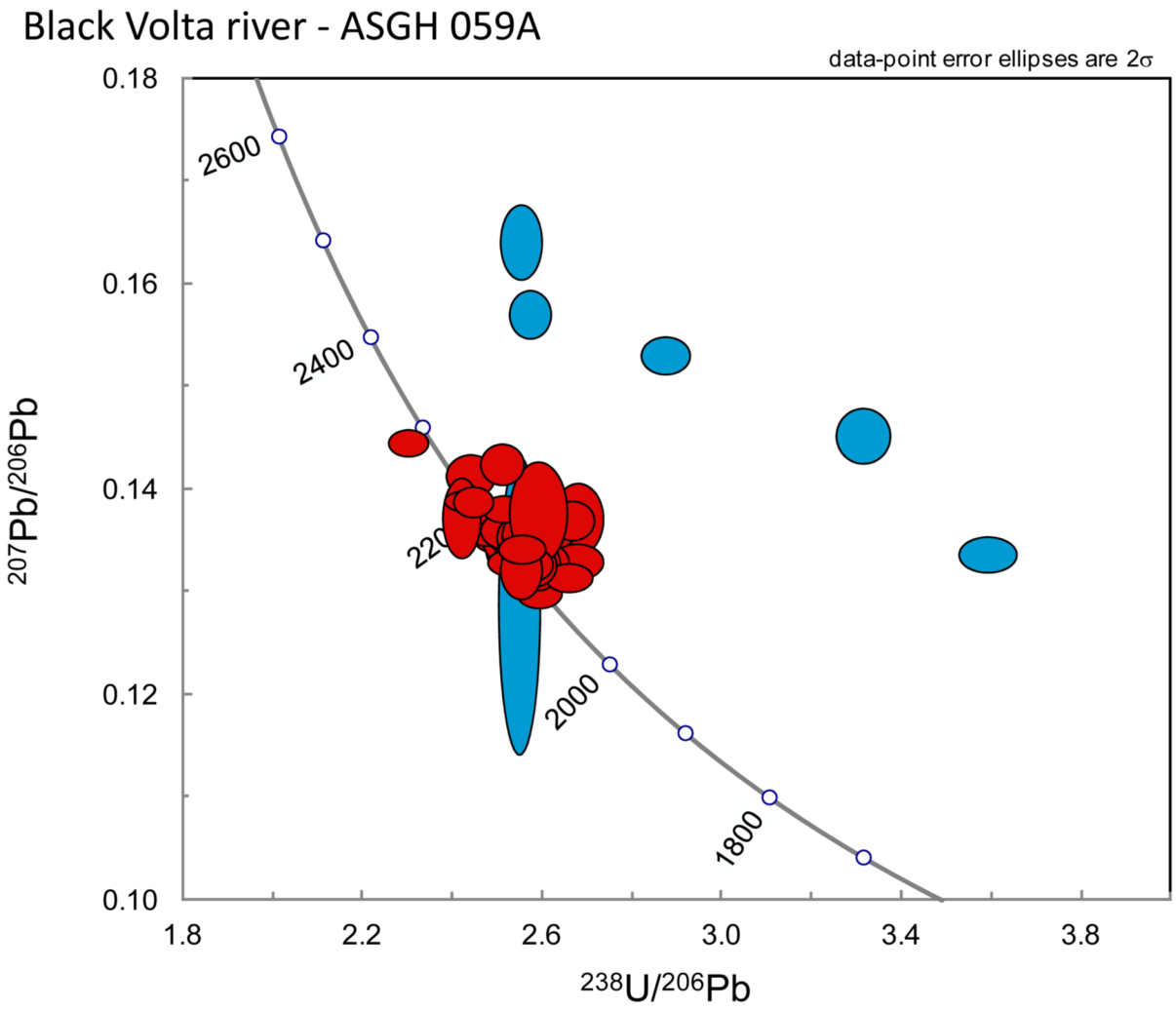

Fig. A.3.3. Tera-Wasserburg diagram showing all zircon from the Black Volta river population. Zircon represented by the blue ellipsoids were omitted due to lack of precision (>30 Ma) or discordance over 10%. Plot created using Isoplot 4.15 (Ludwig, 2008).

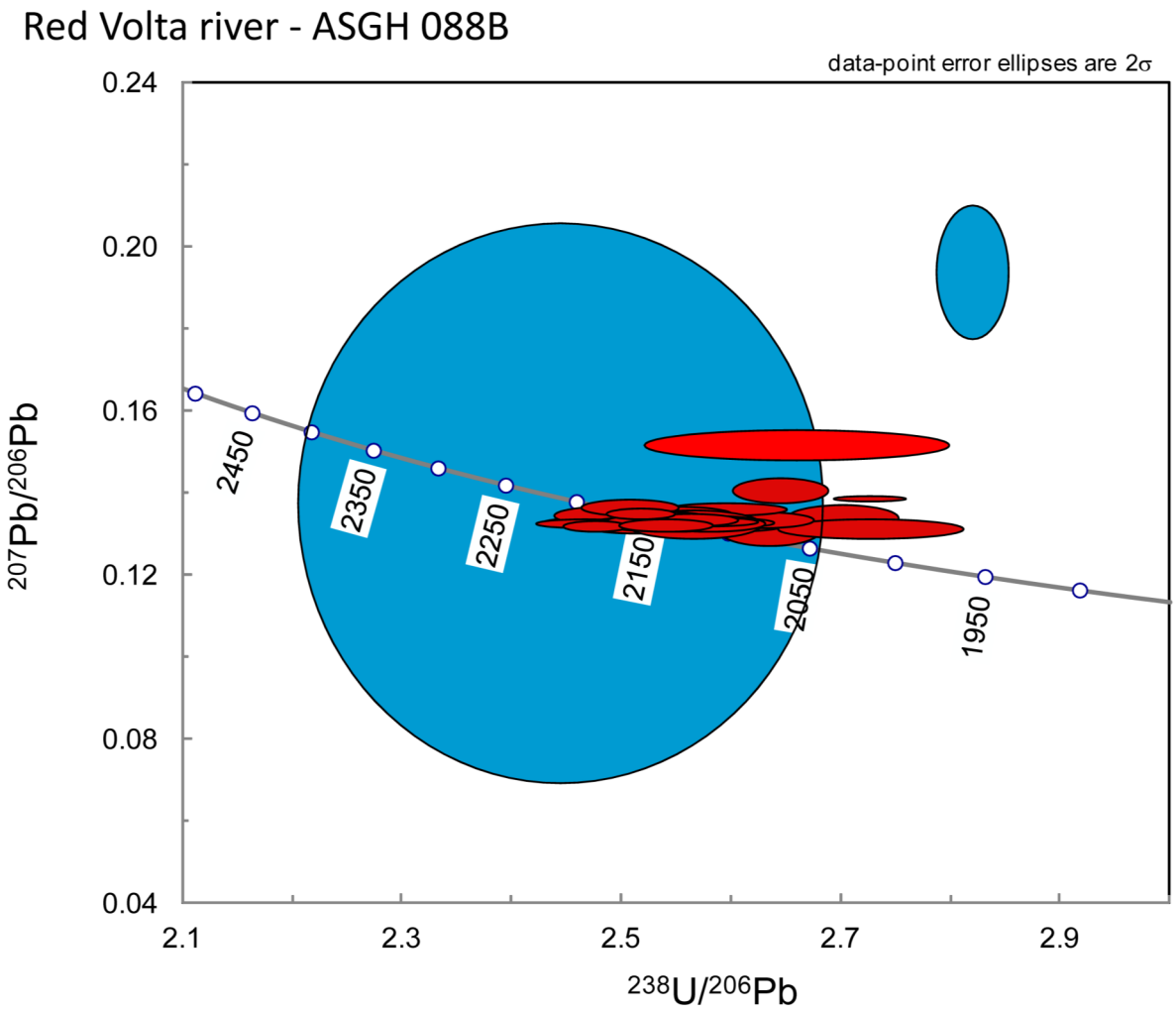

Fig. A.3.4. Tera-Wasserburg diagram showing all zircon from the Red Volta river population. Zircon represented by the blue ellipsoids were omitted due to lack of precision (>30 Ma) or discordance over 10%. Plot created using Isoplot 4.15 (Ludwig, 2008).

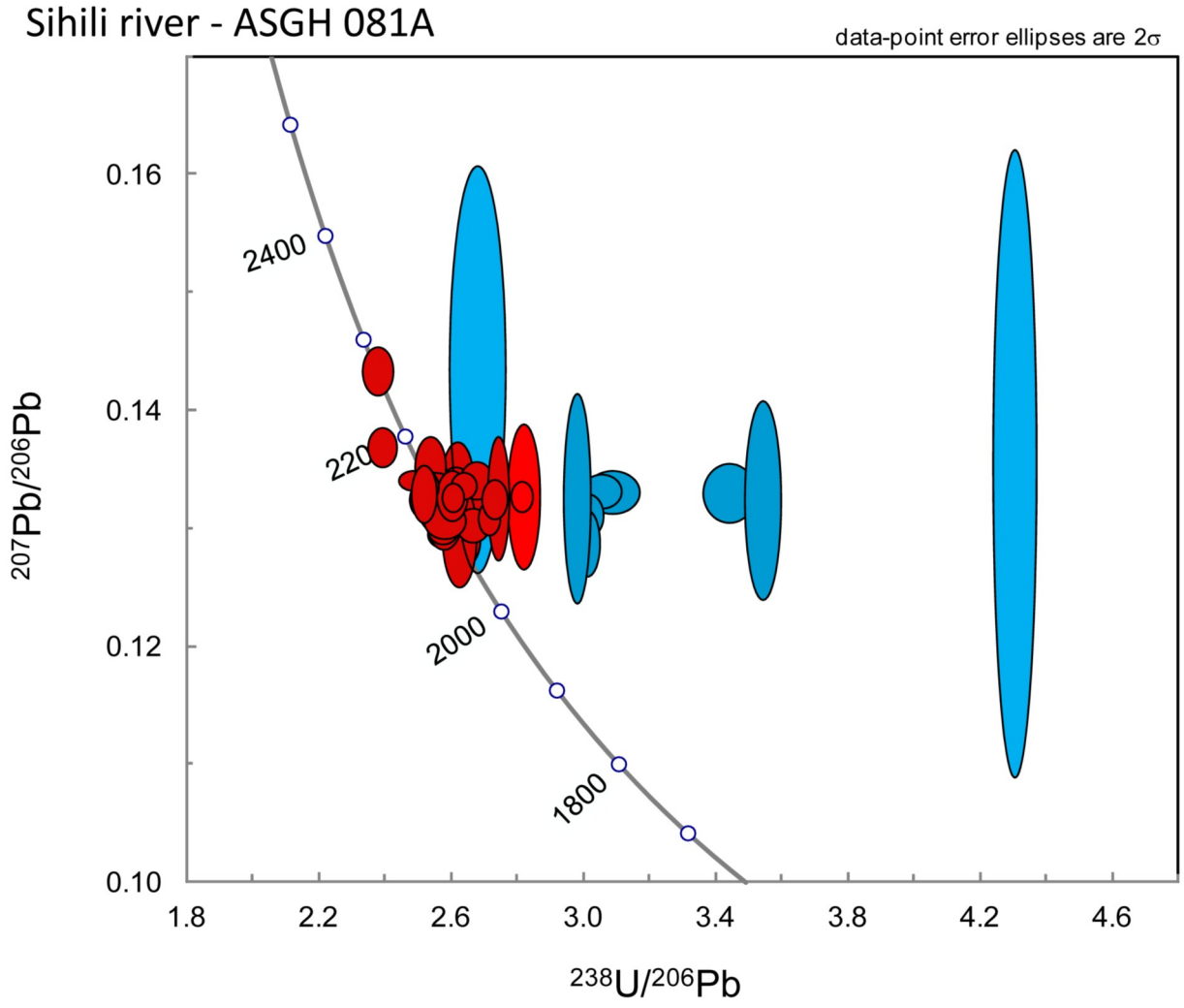

Fig. A.3.5. Tera-Wasserburg diagram showing all zircon from the Sihili river population. Zircon represented by the blue ellipsoids were omitted due to lack of precision (>30 Ma) or discordance over 10%. Plot created using Isoplot 4.15 (Ludwig, 2008).

Tidigare skrifter i serien "Examensarbeten i Geologi vid Lunds universitet":

324. Lundgren, Linda, 2012: Variation in rock quality between metamorphic domains in the lower levels of the Eastern Segment, Sveconorwegian Province. (45 hp)
325. Härling, Jesper, 2012: The fossil wonders of the Silurian Eramosa Lagerstätte of Canada: the jawed polychaete faunas. (15 hp)
326. Qvarnström, Martin, 2012: An interpretation of oncoid mass-occurrence during the Late Silurian Lau Event, Gotland, Sweden. (15 hp)
327. Ulmius, Jan, 2013: P-T evolution of paragneisses and amphibolites from Romeleåsen, Scania, southernmost Sweden. (45 hp)
328. Hultin Eriksson, Elin, 2013: Resistivitetsmätningar för avgränsning av lakvattenplym från Kejsarkullens deponis infiltrationsområde. (15 hp)
329. Mozafari Amiri, Nasim, 2013: Field relations, petrography and 40Ar/39Ar cooling ages of hornblende in a part of the eclogite-bearing domain, Sveconorwegian Orogen. (45 hp)
330. Saeed, Muhammad, 2013: Sedimentology and palynofacies analysis of Jurassic rocks Eriksdal, Skåne, Sweden. (45 hp)
331. Khan, Mansoor, 2013: Relation between sediment flux variation and land use patterns along the Swedish Baltic Sea coast. (45 hp)
332. Bernhardson, Martin, 2013: Ice advance-retreat sediment successions along the Logata River, Taymyr Peninsula, Arctic Siberia. (45 hp)
333. Shrestha, Rajendra, 2013: Optically Stimulated Luminescence (OSL) dating of aeolian sediments of Skåne, south Sweden. (45 hp)
334. Fullerton, Wayne, 2013: The Kalgoorlie Gold: A review of factors of formation for a giant gold deposit. (15 hp)
335. Hansson, Anton, 2013: A dendroclimatic study at Store Mosse, South Sweden – climatic and hydrologic impacts on recent Scots Pine (*Pinus sylvestris*) growth dynamics. (45 hp)
336. Nilsson, Lawrence, 2013: The alteration mineralogy of Svartliden, Sweden. (30 hp)
337. Bou-Rabee, Donna, 2013: Investigations of a stalactite from Al Hota cave in Oman and its implications for palaeoclimatic reconstructions. (45 hp)
338. Florén, Sara, 2013: Geologisk guide till Söderåsen – 17 geologiskt intressanta platser att besöka. (15 hp)
339. Kullberg, Sara, 2013: Asbestkontamination av dricksvatten och associerade risker. (15 hp)
340. Kihlén, Robin, 2013: Geofysiska resistivitetsmätingar i Sjöcrona Park, Helsingborg, undersökning av områdets geologiska egenskaper samt 3D modellering i GeoScene3D. (15 hp)
341. Linders, Wictor, 2013: Geofysiska IP-undersökningar och 3D-modellering av geofysiska samt geotekniska resultat i GeoScene3D, Sjöcrona Park, Helsingborg, Sverige. (15 hp)
342. Sidenmark, Jessica, 2013: A reconnaissance study of Rävliden VHMS-deposit, northern Sweden. (15 hp)
343. Adamsson, Linda, 2013: Peat stratigraphical study of hydrological conditions at Stass Mosse, southern Sweden, and the relation to Holocene bog-pine growth. (45 hp)
344. Gunterberg, Linnéa, 2013: Oil occurrences in crystalline basement rocks, southern Norway – comparison with deeply weathered basement rocks in southern Sweden. (15 hp)
345. Peterffy, Olof, 2013: Evidence of epibenthic microbial mats in Early Jurassic (Sinemurian) tidal deposits, Kulla Gunnarstorp, southern Sweden. (15 hp)
346. Sigeman, Hanna, 2013: Early life and its implications for astrobiology – a case study from Bitter Springs Chert, Australia. (15 hp)
347. Glommé, Alexandra, 2013: Texturella studier och analyser av baddeleyitomvandlingar i zirkon, exempel från sydöstra Ghana. (15 hp)
348. Brådenmark, Niklas, 2013: Alunskiffer på Öland – stratigrafi, utbredning, mäktigheter samt kemiska och fysikaliska egenskaper. (15 hp)
349. Jalnefur Andersson, Evelina, 2013: En MIFO fas 1-inventering av fyra potentiellt förorenade områden i Jönköpings län. (15 hp)
350. Eklöv Pettersson, Anna, 2013: Monazit i Obbhult-komplexet: en pilotstudie. (15 hp)

351. Acevedo Suez, Fernando, 2013: The reliability of the first generation infrared refractometers. (15 hp)
352. Murase, Takemi, 2013: Närkes alunskiffer – utbredning, beskaffenhet och oljeinnehåll. (15 hp)
353. Sjöstedt, Tony, 2013: Geoenergi – utvärdering baserad på ekonomiska och drifttekniska resultat av ett passivt geoenergisystem med värmeuttag ur berg i bostadsrättsföreningen Mandolinen i Lund. (15 hp)
354. Sigfúsdóttir, Thorbjörg, 2013: A sedimentological and stratigraphical study of Veiki moraine in northernmost Sweden. (45 hp)
355. Månsson, Anna, 2013: Hydrogeologisk kartering av Hultan, Sjöbo kommun. (15 hp)
356. Larsson, Emilie, 2013: Identifying the Cretaceous–Paleogene boundary in North Dakota, USA, using portable XRF. (15 hp)
357. Anagnostakis, Stavros, 2013: Upper Cretaceous coprolites from the Münster Basin (northwestern Germany) – a glimpse into the diet of extinct animals. (45 hp)
358. Olsson, Andreas, 2013: Monazite in metasediments from Stensjöstrand: A pilot study. (15 hp)
359. Westman, Malin, 2013: Betydelsen av raka borrhål för större geoenergisystem. (15 hp)
360. Åkesson, Christine, 2013: Pollen analytical and landscape reconstruction study at Lake Storsjön, southern Sweden, over the last 2000 years. (45 hp)
361. Andolfsson, Thomas, 2013: Analyses of thermal conductivity from mineral composition and analyses by use of Thermal Conductivity Scanner: A study of thermal properties in Scanian rock types. (45 hp)
362. Engström, Simon, 2013: Vad kan inneslutningar i zirkon berätta om Varbergscharnockiten, SV Sverige. (15 hp)
363. Jönsson, Ellen, 2013: Bevarat maginnehåll hos mosasaurier. (15 hp)
364. Cederberg, Julia, 2013: U-Pb baddeleyite dating of the Pará de Minas dyke swarm in the São Francisco craton (Brazil) – three generations in a single swarm. (45 hp)
365. Björk, Andreas, 2013: Mineralogisk och malmpetrografisk studie av disseminerade sulfider i rika och fattiga prover från Kleva. (15 hp)
366. Karlsson, Michelle, 2013: En MIFO fas 1-inventering av förorenade områden: Kvarnar med kvicksilverbetning Jönköpings län. (15 hp)
367. Michalchuk, Stephen P., 2013: The Säm fold structure: characterization of folding and metamorphism in a part of the eclogite-granulite region, Sveconorwegian orogen. (45 hp)
368. Praszkier, Aron, 2013: First evidence of Late Cretaceous decapod crustaceans from Åsen, southern Sweden. (15 hp)
369. Alexson, Johanna, 2013: Artificial groundwater recharge – is it possible in Mozambique? (15 hp)
370. Ehlorsson, Ludvig, 2013: Hydrogeologisk kartering av grundvattenmagasinet Åsumsfältet, Sjöbo. (15 hp)
371. Santsalo, Liina, 2013: The Jurassic extinction events and its relation to CO2 levels in the atmosphere: a case study on Early Jurassic fossil leaves. (15 hp)
372. Svantesson, Fredrik, 2013: Alunskiffern i Östergötland – utbredning, mäktigheter, stratigrafi och egenskaper. (15 hp)
373. Iqbal, Faisal Javed, 2013: Paleoecology and sedimentology of the Upper Cretaceous (Campanian), marine strata at Åsen, Kristianstad Basin, Southern Sweden, Scania. (45 hp)
374. Kristinsdóttir, Bára Dröfn, 2013: U-Pb, O and Lu-Hf isotope ratios of detrital zircon from Ghana, West-African Craton – Formation of juvenile, Palaeoproterozoic crust. (45 hp)

LUNDS UNIVERSITET

Geologiska institutionen
Lunds universitet
Sölvegatan 12, 223 62 Lund